JOURNAL OF APPLIED PHYSICS

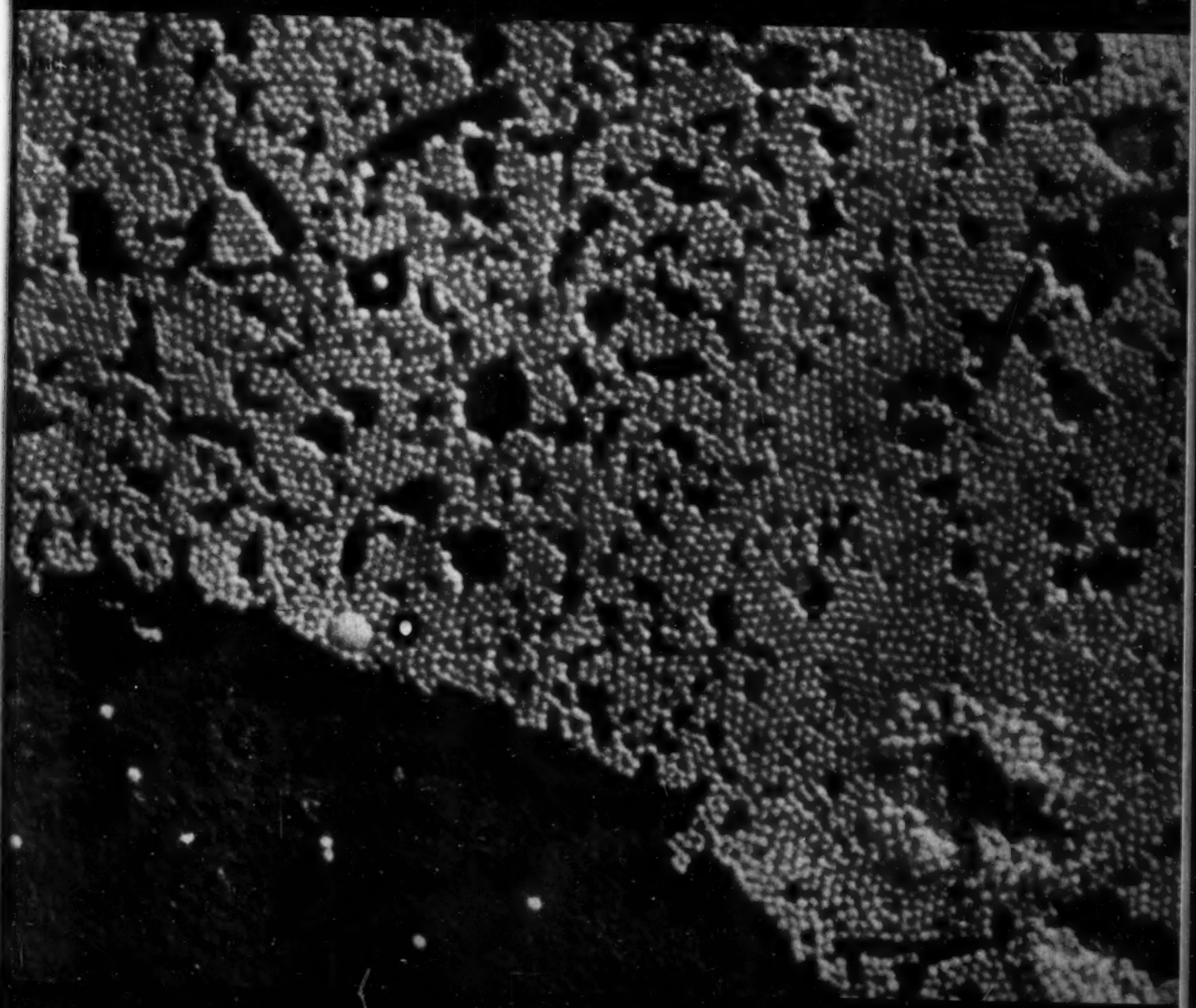

JOURNAL OF APPLIED PHYSICS

Vol. 17, No. 1 JANUARY, 1946

In This Issue

		Page
Reconversion of the *Journal of Applied Physics*		1
Atomic Engineering?	THEODORE VON KÁRMÁN	2
Contributed Original Research		
Interchange of Energy between an Electron Beam and an Oscillating Electric Field	JESS MARCUM	4
On the Improvement of Resolution in Electron Diffraction Cameras	JAMES HILLIER AND R. F. BAKER	12
Applications of Metallic Shadow-Casting to Microscopy	ROBLEY C. WILLIAMS AND RALPH W. G. WYCKOFF	23
Electrical Resistance of Iron Wires and Permalloy Strips at Radiofrequencies	ALVA W. SMITH, J. H. GREGORY, AND J. T. LYNN	33
Liquid Rise in a Capillary Tube	WESLEY E. BRITTIN	37
Shunt and Series Sections of Transmission Line for Impedance Matching	C. T. TAI	44
On the Proportion of Crystalline and Amorphous Components in Stretched Vulcanized Rubber	A. J. WILDSCHUT	51
Letters to the Editor:		
On Plane Rotations in *n* Dimensions	PETER T. LANDSBERG	60
Letter to the Editor	GERALD PICKETT	61
On a Novel Form of Refrigerator	JENNY E. ROSENTHAL	62
Elastic Limit for Dynamic Loading	V. BARGMANN AND H. F. LUDLOFF	63
Erratum: Secondary Electron Emission of Pyrex Glass	C. W. MUELLER	62
Electron Microscope Society of America. Third Annual Meeting		66
In Every Issue		
Here and There		64
New Booklets		65
Recent Applications of Physics		xiv
Index to Advertisers		xxvi

BOARD OF EDITORS

ELMER HUTCHISSON, *Editor*

Associate Editors

R. BOWLING BARNES
OTTO BEECK
W. F. BUSSE
S. H. CALDWELL
CLARK GOODMAN
SELIG HECHT
W. JAMES LYONS
PAUL E. SABINE
FREDERICK SEITZ
J. R. TOWNSEND

Publication of the American Institute of Physics

ADMINISTRATIVE STAFF

HENRY A. BARTON, *Director*

MARGARET S. GRIFFIN *Publications Manager*

THEODORE VORBURGER, *Business Manager*

JOHN T. TATE, *Adviser on Publications*

GOVERNING BOARD

PAUL E. KLOPSTEG, *Chairman*

WALLACE WATERFALL, *Secretary*

GEORGE B. PEGRAM, *Treasurer*

T. D. COPE
R. B. DOW
L. A. DUBRIDGE
FLOYD A. FIRESTONE
HARVEY FLETCHER
R. C. GIBBS
K. S. GIBSON
HERMANN MARK
A. G. WORTHING
JOHN T. TATE
L. W. TAYLOR
N. W. TAYLOR
WALLACE WATERFALL

The JOURNAL OF APPLIED PHYSICS, published monthly at Prince and Lemon Sts., Lancaster, Pa., is devoted to physics in its role as the science basic to other natural sciences and to the arts and industries. Previous to 1937 this publication was known as PHYSICS. The JOURNAL OF APPLIED PHYSICS publishes editorials, news of physicists, and reviews, as well as technical papers of applied physics.

Manuscripts should be submitted to Elmer Hutchisson, Editor, Case School of Applied Science, Cleveland 6, Ohio.

Subscriptions and orders for back numbers should be addressed to Prince and Lemon Streets, Lancaster, Pa. or to the American Institute of Physics, 57 East 55 Street, New York 22, N. Y.

Subscription Price

	U. S. AND CANADA	ELSEWHERE
To members of scientific societies	$5.00	$5.70
To all others	7.00	7.70

Back Number Prices

Complete set: Vol. 1, July, 1931–Vol. 16, 1945—$101.50
Yearly back number rate: $7.70
Single copies: $0.70 each.

Changes of address and proofs should be addressed to the Publications Manager.

Advertising rates supplied on request. Orders, advertising copy, and cuts should be sent to the American Institute of Physics.

Entered as second class matter January 22, 1937, at the Post Office at Lancaster, Pennsylvania, under the Act of March 3, 1879
Accepted for mailing at the special rate of postage provided for in the Act of February 28, 1925, authorized May 2, 1932.

Copyright 1946, by the American Institute of Physics.

Journal of Applied Physics

Volume 17, Number 1 **January, 1946**

Reconversion of the *Journal of Applied Physics*

GRADUALLY the *Journal of Applied Physics* is recovering some of its prewar characteristics. During the past few years paper restrictions were particularly acute because of the large increase in circulation which occurred after the paper quota for the *Journal* was set. In fact, had it not been for the generous cooperation of the editors of *The Review of Scientific Instruments* and the *Journal of Chemical Physics* in sharing their paper quotas, several numbers of this *Journal* could not have appeared. However, the size of the past few issues shows that that difficulty is now over, and in this issue we are permitted once more to return to a high quality coated paper stock.

New problems are on the horizon. The number of papers submitted is large and shows signs of increasing. These papers are generally of high quality and cover a wide range as far as subject matter is concerned. If the number of papers increases at a faster rate than the circulation, the Editor may be forced to choose between outstanding papers in Field A as opposed to outstanding papers in Field B. Or he may find it necessary to accept good research contributions at the expense of review or summary articles. Indications of reader preference on these matters would be as welcome as they are scarce.

Many of the engineering societies are in the process of examining their reader interest rather closely to assist in setting definite limits to the fields which they are to cover and to reduce overlapping with other societies. These studies are of considerable interest to this Editor because of the close relation between applied physics and engineering. It is helpful, in visualizing the publishing activities in America of the entire field of technical and engineering knowledge, to make use of a polar chart in which basic physics is at the center. The major subdivisions of physics, such as mechanics, thermodynamics, acoustics, optics, electrostatics, electrodynamics, may be thought of as occupying particular sectors. Thus, reading out radially in any one sector, for example that devoted to mechanics, one would start with fundamentals in mechanics, contributions to which are usually published in *The Physical Review*. Then one would pass through a region covered by the *Journal of Applied Physics* or the *Journal of Applied Mechanics*. Out still farther one would find subject matter covered by *Mechanical Engineering*, the official publication of the A.S.M.E. The polar chart has the advantage that the sector widens out as the variety of applications increases. In the outer regions we would find mechanics divided into many subjects, such as machinery, automotive engineering, aeronautical engineering, and so forth. Still farther out, perhaps, would be fields covered by trade publications.

In a chart of the type here visualized, the region to be covered by the *Journal of Applied Physics* seems rather naturally to be an annulus surrounding basic physics. In some sectors this annulus becomes very narrow, and in others it must be quite broad, to cover the gap between fundamental physics and engineering. It seems quite clear that one important function of the *Journal* is to provide a publishing medium in those sectors where this gap is broad. Gradually as applications develop, specialized journals will necessarily begin to take over. However, as new fundamental knowledge develops, new sectors will open for the *Journal of Applied Physics*. Thus, the emphasis in the *Journal* is very likely to change as time goes on, but it will always be just outside that covered by those journals concerned with developments in fundamental or "pure" physics.

Atomic Engineering?*

THEODORE VON KÁRMÁN
California Institute of Technology, Pasadena, California

IT has happened now for the third time in our lifetime ("our" referring to the elders of the engineering profession) that new avenues of engineering activities of tremendous importance have been opened by physicists, and the engineering profession has found itself unprepared to challenge the task.

In 1887 the physicist Heinrich Hertz discovered "wireless telegraphy." In fact, he experimentally confirmed the existence of electromagnetic waves which anybody may easily read in Maxwell's equations of the electromagnetic field, i.e., anybody who can read equations at all. It took several decades for radio engineering to become a branch of the engineering profession and for adequate measures to be taken to incorporate the fundamentals of field theory into the engineering curriculum.

The discovery of electromagnetic waves of long wave-length was followed very soon by the discovery of x-rays, i.e., electromagnetic waves of very short length of a frequency far beyond the spectrum of visible light. It has to be said to the credit of the engineering profession that it took advantage of x-ray techniques in various industrial fields, and the design and construction of x-ray apparatus were recognized as an important branch of engineering.

Similarly, the infra-red technique, i.e., the technique of waves longer than those of visible light but very much shorter than radio waves, was justly considered as an engineering problem.

However, in the period between the two world wars, physicists made great efforts to narrow the gap between radio and infra-red waves. They succeeded in producing microwaves which made possible the marvelous technique now commonly designated as the art of radar. The physical facts were known a long time before the beginning of the recent war. However, during the war, physicists, by their superior knowledge of electronics, i.e., the mechanics of electric particles, were able to solve the engineering problems of producing and directing microwaves. I will not contest the fact that a great many American engineers were sufficiently familiar with electronics; many made important discoveries and contributions to electronic devices. But somehow our engineering education does not encourage the idea of the unlimited horizon, when fundamental thinking in novel fields is required.

And now it seems we are at the threshold of the new atomic age. I do not know whether or not this is true, but certainly we shall have "atomic engineering" in the fields of power and transportation. Are we prepared for the problems involved?

The first application of atomic engineering was directed by military engineers; plants and many gadgets were probably designed and constructed by engineers. However, not only the discovery of the fundamental facts but also the methods of application were suggested, worked out, and tested by physicists. I concede that security regulations and personal relations in the "nuclear clan" played a great part in the choice of collaborators. However, I raise the question, do we give today to the future engineer enough fundamental knowledge in basic questions of the structure of matter, the nature of energy, the relation between matter and energy, so that he will be able to think intelligently in the new field, to have good engineering judgment on possibilities and methods? Is he better equipped than anybody else who reads a few popular articles in the *New York Times* or in the *Saturday Evening Post?* Is there something wrong in our engineering education? I am afraid there is.

First, I believe we have a tendency to restrict our teaching to scientific knowledge which has immediate applications. We often forget that almost every new physical or chemical discovery *might* have engineering application. After all, engineering is the conquest of nature, i.e., matter and energy, for human comfort, and therefore an engineer cannot know too much about the inner structure of the matter against whose whimsical moods he struggles and the laws

* Reprinted by permission from *Mechanical Engineering*, October, 1945.

of energy which he wants to exploit and harness.

Second, we underestimate the interest of our students in "natural philosophy." We are reluctant to present the fundamentals of physics and chemistry as a living science full of question marks and changing concepts. We believe we ought to introduce the findings of research only after the unshakable truth has been established. We tend to stick to classical concepts. I found, while teaching mechanics of continuous media, elasticity, and fluid dynamics, that my students listened eagerly as I told them something about atomic structure of the materials and kinetic theory of gases. I wonder how many engineering students obtain a picture of entropy, chemical reaction, and the like, from a modern point of view. And why should ordinary combustion be an engineering topic, and nuclear reaction a mystery of modern alchemy?

Third, we overestimate the importance of transfer of experience to coming engineering generations in comparison with a training aimed at true understanding of the happenings of nature. We try to train engineers so that the employer can use them almost immediately after graduation from school. One of my former students was employed as an instructor in a well-known engineering school. He suggested some changes in the hydraulics curriculum in the direction of modern fluid dynamics. His superior asked him the use of teaching the findings of research men who, he conceded, found interesting results in hydrodynamics. None of these men, he said, would be able to design a sewage pipe system. No doubt he was right in this statement of fact, but he was wrong in his conclusion. Fortunately, the more intelligent employers are beginning to realize that immediate usefulness is not the most important criterion of a novice engineer. They appreciate sound fundamental understanding and do not want the school to train for them the type of practical engineer, who—according to the *bon mot* of a prominent Englishman, himself an engineer—perpetuates the errors of his predecessors.

Fourth, I certainly do not wish to make of every engineer a scientist, or, God forbid, a nuclear physicist. However, we shall try to give him an education which shall enable him to follow the progress of science, as, I believe, every medical doctor should have sufficient education to follow the development of biology which has produced in our time almost as spectacular discoveries as physical science. At the institution at which I have been teaching in the last fifteen years, science and engineering students have essentially common curricula the first two years. The physics student continues after that to move on a relatively high intellectual level of understanding natural phenomena from a scientific point of view. I have often wondered why the engineering student has to make a steep dive into an atmosphere in which the beam on three supports is considered a most difficult problem and the exact clear principles of mechanics and thermodynamics are replaced by semi-scientific, semi-popular "ersatz" truths.

I am convinced that the knowledge of the deepest origins and also the limitations of the principles do not handicap a person in their practical application; as a matter of fact, real knowledge makes the application easier and safer. And after all, physics students are not any more intelligent than engineering students.

I have digressed from the subject indicated by the title. From the little I know and the little I have read on the subject, I really believe that the problems involved in the development of atomic power for stationary and transportation purposes are primarily of the nature of engineering and especially applied mechanics. In other words, the picture of the nuclear processes obtained by the physicists contains so much of the truth, if such thing as truth exists, that from now on systematic observation and computation must lead to practical solutions. Certainly intriguing engineering problems, like the development of materials resistant to extreme temperatures and extreme corrosion, and difficult applications of our knowledge in diffusion and heat transfer, will be involved. However, it may sound paradoxical, but it seems to me that the processes involved in atomic engineering are less complex than, for example, the processes of combustion of conventional solid and liquid fuels; less complex in the sense that simple considerations and theoretical computations may give closer approximations to reality than in the case of molecular reactions. What can appeal more to a scientific engineer?

Contributed Original Research

Interchange of Energy between an Electron Beam and an Oscillating Electric Field

JESS MARCUM*
Westinghouse Research Laboratories, East Pittsburgh, Pennsylvania
(Received October 25, 1945)

Relations between various parameters are obtained which describe the behavior of an accelerated electron beam which is caused to traverse an alternating electric field. In particular, a mechanicographical means for obtaining the gain or loss of energy is described. It is shown that under the most favorable conditions a maximum of 17 percent of the energy in the accelerated beam may be transferred to the alternating field. Application of these principles to a type of ultra-high frequency oscillator is treated.

INTRODUCTION

THIS report deals with a theoretical analysis of the conversion of kinetic energy of electrons into radio frequency energy of an oscillating electric field. In Fig. 1, a is a cathode maintained at a negative potential V_0 with respect to the plates b and c. In the region between b and c there is an oscillating electric field so the electric vector is uniform and equal to $E \sin \omega t$, being directed along the direction of motion of the electrons.

In the theory developed in this paper space charge is neglected, each electron is supposed to go all the way through without striking the grids, and non-uniformity of the electric field near the grids is neglected. In practice, the plates b and c may be built into a cavity resonator but this is not essential for the first part of the discussion which follows.

The problem of the energy exchange between an electron beam and an oscillating field disposed in this way relative to the beam has been treated analytically by Müller and Rostas.[1] But the analytical method which they use involves approximations which limit the range of results they can obtain.

In this report it is shown how the problem can be studied by means of a mechanical-graphical computing device which gives results of more generality than those found by Müller and Rostas.

METHOD OF SOLUTION

The equation of motion of an electron entering at phase δ is

$$\frac{d^2x}{dt^2}=\frac{eE}{m}\sin(\omega t+\delta), \tag{1}$$

where e is electronic charge, m is electronic mass, and E is the amplitude of the electric vector. The electrons all enter with velocity v_0 determined by the accelerating cathode potential V_0. Integrating (1) we find for the velocity v at later times

$$v=v_0-\frac{eE}{m\omega}[\cos(\omega t+\delta)-\cos\delta]. \tag{2}$$

A second integration gives the coordinate x as a

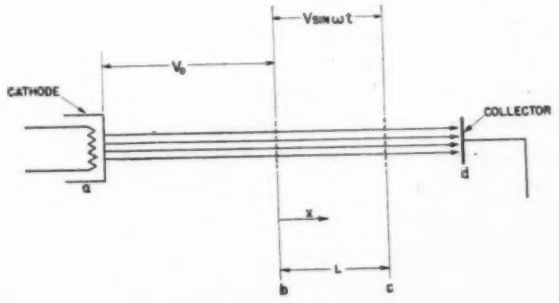

FIG. 1. Schematic diagram.

* On leave of absence from Westinghouse Research Laboratories. Present address, Princeton University, Princeton, N. J.

[1] J. J. Müller and E. Rostas," Un Generateur a Temps de Transit, Utilisant un Seul Resonateur de Volume," Helv. Phys. Acta **13**, 435 (1940).

function of the time,

$$x=v_0t-\frac{eE}{m\omega^2}[\sin(\omega t+\delta)-\omega t\cos\delta-\sin\delta]. \quad (3)$$

It is convenient to introduce certain dimensionless variables as follows,

$\eta=\dfrac{eE}{m\omega v_0}$ = ratio of momentum change produced by force eE in time $1/\omega$ to the initial momentum of the electron.

$\theta=\omega t+\delta$ = phase of oscillating field in "electrical radians."

$\alpha=\dfrac{\omega x}{2\pi v_0}$ = time measured in cycles of oscillation frequency to go the distance x when moving with the entrance velocity, v_0.

In terms of these quantities (2) and (3) become

$$v/v_0=1-\eta[\cos\theta-\cos\delta], \quad (2b)$$

$$2\pi\alpha=\theta-\delta-\eta[\sin\theta-\sin\delta+(\delta-\theta)\cos\delta]. \quad (3b)$$

If we could eliminate θ between these two equations, we could express (v/v_0) as a function of α, which is a measure of the distance gone in the oscillating field, and δ the phase of entry into the field, as well as η which is a measure of the amplitude of the oscillating field.

The ratio of the decrease in kinetic energy of an electron to its original energy is

$$\rho(\delta)=\frac{mv_0^2/2-mv^2/2}{mv_0^2/2}=1-\left(\frac{v}{v_0}\right)^2, \quad (4)$$

which, since v/v_0 is a function of η, δ, and α, becomes also a function of the same variables which will be designated

$$\rho(\delta,\eta,\alpha). \quad (5)$$

If the beam entering the grid at b is unmodulated, then equal numbers of electrons enter at all phases of the oscillating field and the average energy exchange of the electrons with the field is given by averaging $\rho(\delta,\eta,\alpha)$ over all phases δ in a cycle.

We denote this average, which depends parametrically on η and α by $\bar{\rho}(\eta,\alpha)$ in accord with the notation,

$$\bar{\rho}(\eta,\alpha)=\frac{1}{2\pi}\int_0^{2\pi}\rho(\delta,\eta,\alpha)d\delta. \quad (6)$$

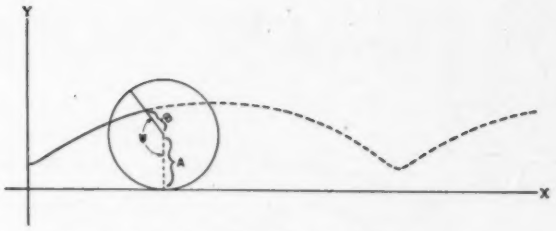

FIG. 2. Generation of a cycloid.

A positive value of $\bar{\rho}(\eta,\alpha)$ means that on the average the electrons lose energy to the oscillating field, and $\bar{\rho}(\eta,\alpha)$ gives the fraction of the beam energy that is given up to the electric field. In applying the formula for $\bar{\rho}(\eta,\alpha)$, the quantity α is to be calculated by using for x the distance of separation of the two grids b and c.

In actual fact, however, there is no exact analytical way to eliminate θ between the Eqs. (2b) and (3b) in order to carry out the calculation as formulated. Müller and Rostas give an approximate analytical calculation of the problems.

Equations (2b) and (3b) can be written in this form

$$v/v_0=(1+\eta\cos\delta)-\eta\cos\theta, \quad (2c)$$

$$2\pi\alpha=(1+\eta\cos\delta)\theta-\eta\sin\theta-[\delta(1+\eta\cos\delta)-\eta\sin\delta]. \quad (3c)$$

These equations are evidently the equations representing cycloids in a graph in which (v/v_0) is plotted as ordinate and $2\pi\alpha$ is plotted as abscissa. The standard equations for the cycloid generated by rolling a circle of radius A on the x axis with the tracing point at radius B from the center of the circle are,

$$\left.\begin{aligned}X&=A\psi-B\sin\psi\\Y&=A-B\cos\psi\end{aligned}\right\}. \quad (7)$$

Comparing with (2c) and (3c) we see that the relationship between (v/v_0) and $2\pi\alpha$ is given by a cycloid in which

$(1+\eta\cos\theta)$ = radius of rolling circle.

η = distance of tracing point from center.

θ = angle through which rolling circle is turned.

$[\delta(1+\eta\cos\theta)-\eta\sin\delta]$ = displacement of origin along x axis.

The relations are indicated in Fig. 2.

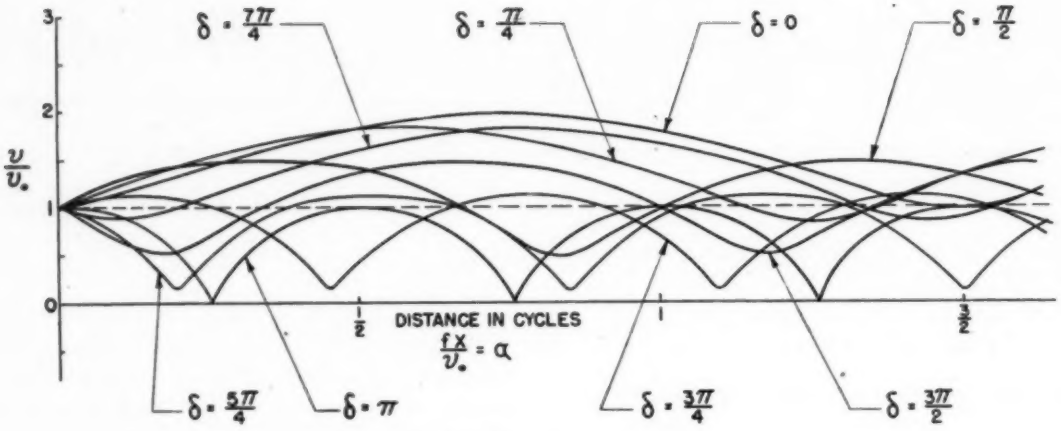

FIG. 3. Cycloidal graph for $\eta = 0.5$.

Because of this fact, a convenient means is available for getting at the velocity of the electrons as a function of distance gone in the oscillating field. It is easy to cut out wheels of the appropriate radii for a given value of η and different phases of entry δ and to roll out the corresponding cycloids. This is what was actually done to obtain the results presented in this paper. In practice, eight equally spaced values of δ throughout a cycle were used. The values of $\bar{\rho}$ were then calculated by averaging the energy exchange for these eight phases as an approximation to integration over all phases.

A section of a typical family of cycloids is shown in Fig. 3. These correspond to the eight different phases of entry in the special case $\eta = \frac{1}{2}$. It may be shown that we must have $\eta < 0.823$ in order that none of the electrons will be returned into the accelerating field. (See Appendix.) We do not consider any cases for which $\eta > 0.823$ in this paper. The calculations for this condition are considerably more involved.

SIMPLIFIED QUALITATIVE PICTURE

Since the main object of the study is to learn the conditions of operation under which $\bar{\rho}(\eta, \alpha)$ is as great as possible, it is desirable to give a rough consideration of the way in which the conversion efficiency depends on these two parameters. In order to make $\bar{\rho}$ as great as possible it would be desirable to have each electron leave the oscillating field when its velocity is least.

For a given value of η, the value of (v/v_0) in (2c) is clearly least when $\cos\theta = 1$, so the least value of v/v_0 is

$$\left(\frac{v}{v_0}\right)_{\min} = 1 - \eta(1 - \cos\delta). \tag{8}$$

If every electron could be made to leave the oscillating field with this speed ratio (which is not possible in fact), then we should have

$$\bar{\rho} = 1 - \frac{1}{2\pi}\int_0^{2\pi} [1 - \eta(1 - \cos\delta)]^2 d\delta = 2\eta - 3\eta^2/2, \tag{9}$$

which is therefore an absolute upper limit to the conversion efficiency. In Fig. 4 this upper limit is

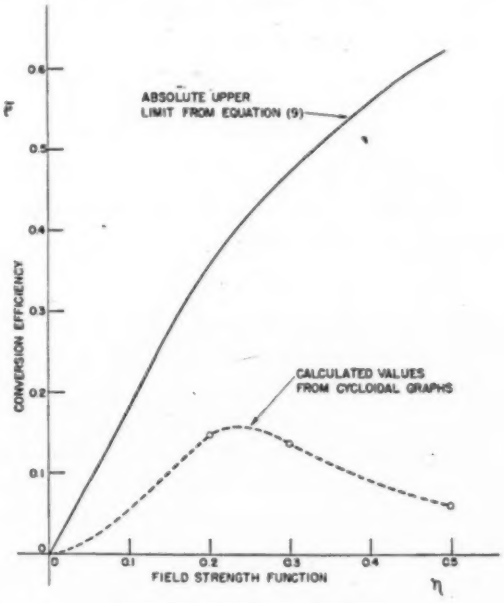

FIG. 4. Efficiency functions.

graphed as a function of η, together with the actual maximum conversion efficiencies (for best possible choice of α at each value of η) obtained from the cycloidal graphs.

We wish to consider further the most favorable values of η and α. The electrons entering at phase $\delta=0$ never have a velocity less than v_0 so they have a conversion efficiency ratio of 0.00 at best. In order to take them out of the field at a time when they have not actually gained energy from the oscillating field the distance x must be chosen to have the values $x=l$ where

$$\omega l/v_0=2\pi n_1(1+\eta), \tag{10}$$

where n_1 is any integer. The electrons which enter at phase $\delta=\pi$ may, for appropriate choice of $\omega l/v_0$, be made the most efficient at giving up energy to the field. From (2c) and (3c) it is seen that this appropriate choice for them is

$$\omega l/v_0=2\pi(n_2+\tfrac{1}{2})(1-\eta), \tag{11}$$

where n_2 is any integer.

We can get a rough formula for the best values of η by requiring (10) and (11) to be consistent, that is, that l be such that the "best" ($\delta=\pi$) and the "worst" ($\delta=0$) electrons leave when their energies are minimum. This gives

$$2\pi n_1(1+\eta)=2\pi(n_2+\tfrac{1}{2})(1-\eta),$$

or

$$\eta=\frac{2(n_2-n_1)+1}{2(n_2+n_1)+1}. \tag{12}$$

Although this is a very rough calculation,* the

n_2 \ n_1	1	2	3	4	5	6	7	8
1	η = .200 Q = 1.20							
2	.428 1.43	.111 2.22						
3		.272 2.54	.077 3.23					
4		.384 2.77	.200 3.60	.059 4.24				
5		.466 2.93	.294 3.89	.158 4.64	.048 5.24			
6			.363 4.10	.238 4.96	.130 5.65	.040 6.24		
7			.429 4.29	.304 5.22	.200 6.00	.111 6.67	.055 7.25	
8			.479 4.44	.360 5.44	.259 6.50	.172 7.05	.097 7.68	.031 8.25

FIG. 5. Approximate points for maximum conversion efficiency.

* It is possible to make similar calculations for a two-cavity klystron which give results in good agreement with the more exact theory.

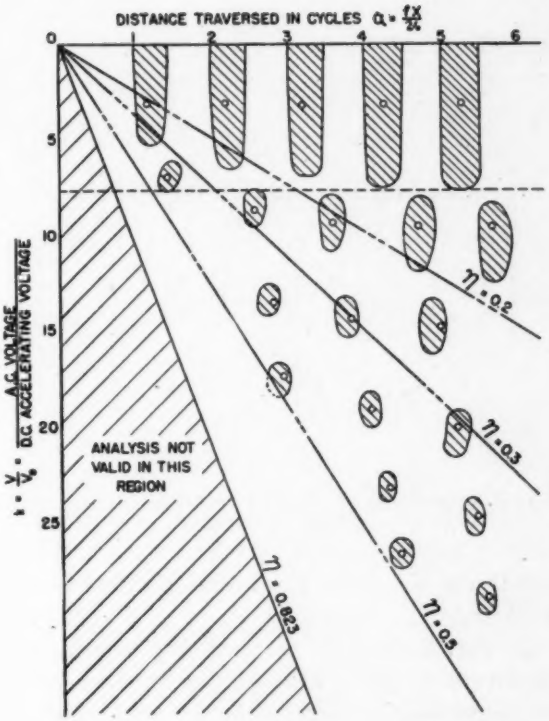

FIG. 6. Regions of positive and negative conversion efficiency.

more exact work with the cycloids bears out the expectation that this consideration should indicate the most favorable values of η. Going with each such value of η will be an appropriate value of α given by (10) or (11).

Each pair of values of n_1 and n_2 will be called a "mode" of operation. In Fig. 5 is a tabulation of the values of η (first line in box) and of α going with quite a range of modes leading to values of η in the range $0<\eta<\frac{1}{2}$.

Instead of characterizing the operating points by η and α it is convenient to use $k=4\pi\alpha\eta$ and treat the different operating conditions as defined by the value of k and α. It will be recalled that α is the number of cycles of oscillation required by an electron traveling with the entrance velocity to traverse the space between the grids. We have

$$k=4\pi\alpha\eta=\frac{eEl}{mv_0^2/2},$$

so the physical significance of k is that it is the ratio of the energy which an electron would gain in the field, if it were static, to its initial energy; k is also the ratio of the oscillating voltage

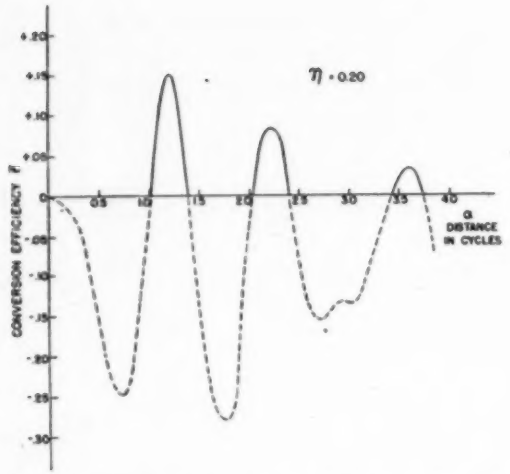

FIG. 7. Conversion efficiency as obtained from cycloidal graphs for $\eta = 0.20$.

amplitude $V = El$ to the initial cathode voltage $V_0 = mv_0^2/2e$.

In Fig. 6 the field of operating conditions is shown in a plot of k against α. The points corresponding to different modes listed in Fig. 5 are shown as "bull's-eyes." In the neighborhood of each bull's-eye is a shaded region. These indicate the fields of values within which $\bar{\rho}$ is positive, that is, in which the beam gives up energy to the oscillating field. The word "mode" is conveniently associated with a whole shaded region surrounding each bull's-eye.

In the regions that are not shaded in Fig. 6 the conversion ratio $\bar{\rho}$ is negative which means that on the average the electrons leave the oscillating field with more energy than they had on entering.

RESULTS OF CYCLOID GRAPHS

Actual values of $\bar{\rho}$ could be shown on an extended form of Fig. 6 in which the values of $\bar{\rho}$ are indicated by means of a contour map. The values of $\bar{\rho}$ are obtained from the cycloids for a number of values of η. The value of $\bar{\rho}$ is first computed for a number of successive values of α at constant η. On Fig. 6 this corresponds to a cross section along one of the diagonal lines as shown. Such a cross section of the $\bar{\rho}$ as a function of k and α surface is shown in Fig. 7. This shows $\bar{\rho}$ as a function of α for $\eta = 0.2$ as calculated from the cycloids.

The necessary wooden wheels were made and rolled and values calculated to construct similar curves for $\eta = 0.3$, 0.5, and 0.823 and the resulting curves for $\bar{\rho}$ as a function of α are shown in Figs. 8–10.

In Fig. 11 is shown a contour map indicating the dependence of $\bar{\rho}$ on k and α over a region corresponding to the upper left-hand corner of the larger region indicated in Fig. 6. In drawing this graph the data obtained by rolling out the cycloids were supplemented by calculations based on the analytical work of Müller and Rostas. It must be admitted that the exact extent of the region of positive $\bar{\rho}$ surrounding the bull's-eyes going with larger values of k is largely conjectural. By drawing the cycloids for more closely spaced values of η one could find these boundaries more accurately if any real interest attached to a knowledge of them.

It is interesting to consider qualitatively how it comes about that $\bar{\rho}$ is negative over so much more of the (k, α) plane in Fig. 6 than the part in which $\bar{\rho}$ is positive. This comes about partly because more than half of a cycloid lies above its middle. For example, an electron which enters at $\delta = \pi/2$ will have $v > v_0$ for more than half of the *distance* traversed on a long path even though its velocity varies sinusoidally with the time. A more important factor lies in the fact that the relative energy varies as $(v/v_0)^2$ and so parts of the curve above $v/v_0 = 1$ contribute more than parts below

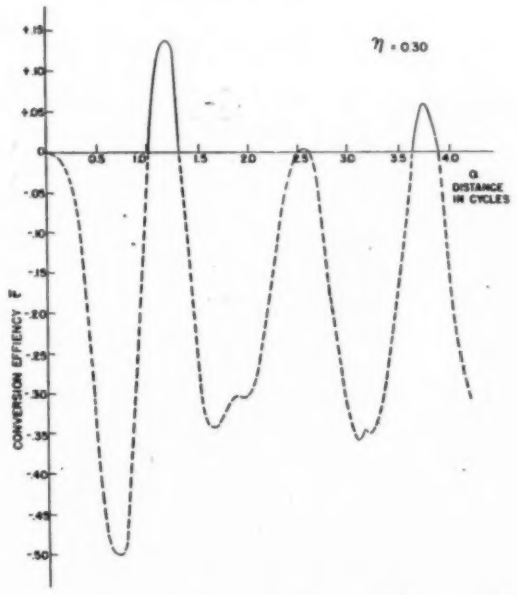

FIG. 8. Conversion efficiency as obtained from cycloidal graphs for $\eta = 0.3$.

by the same amount toward giving a negative value of $\bar{\rho}$.

APPLICATION TO A RESONANT CAVITY OSCILLATOR

Now that the α, k, $\bar{\rho}$ contour map has been obtained (at least over the limited range covered by Fig. 11), one will naturally ask to what practical use can it be put? We limit our discussion to one case, that of constructing an ultra-high frequency oscillator for use in the centimeter wave region. In this case, the planes b and c of Fig. 1 become part of the two opposite walls of a cavity resonator. Any resonator has a property of its dimensions and frequency termed the shunt resistance, S. This is such a quantity that $V^2/2S$, where V is the peak alternating voltage between two specified points of the resonator (usually the points at which the electron beam enters and leaves), gives the average power loss in the walls.

The problem is: Given a tube with a cavity of known resonant frequency f, shunt resistance S, beam current I_0, beam voltage V_0, where on the α, k, $\bar{\rho}$ map is the operating point? Provided no power is being taken from the resonator, the following is the condition for equilibrium

$$V_0 I_0 \bar{\rho} = V^2/2S \tag{13}$$

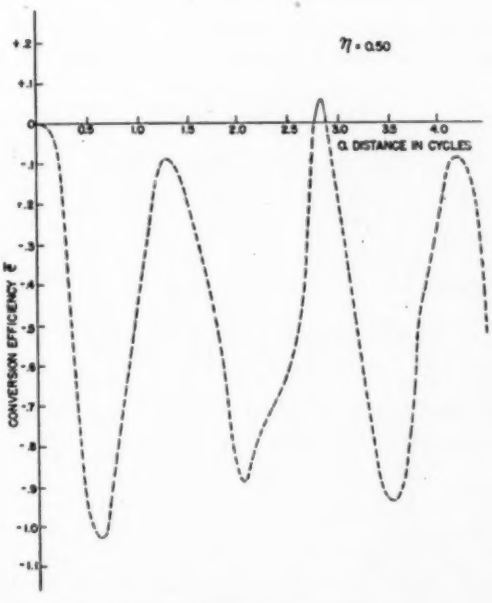

FIG. 9. Conversion efficiency as obtained from cycloidal graphs for $\eta = 0.5$.

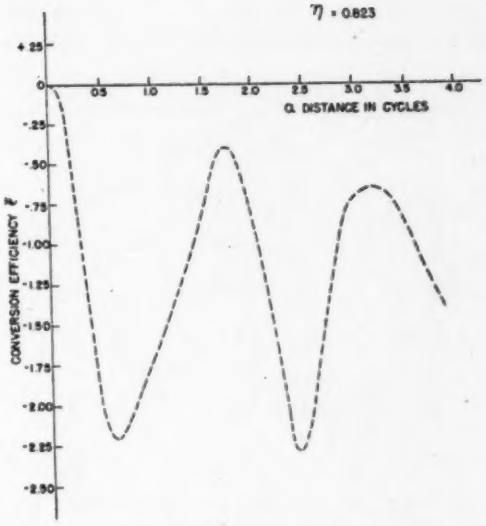

FIG. 10. Conversion efficiency as obtained from cycloidal graphs for $\eta = 0.823$.

which may be transformed to

$$\bar{\rho} = \frac{k^2}{2}\left(\frac{R_0}{S}\right), \tag{14}$$

where $R_0 = V_0/I_0$ is the "resistance" of the beam.

We may now draw a set of curves on the α, k, $\bar{\rho}$ contour map for various values of S/R_0 (the dotted curves on Fig. 11).

Suppose now a tube is in operation; the following quantities are known: f, V_0, I_0, and S. Compute S/R_0 and α. Drop down from the proper value of α on Fig. 11 to the appropriate S/R_0 curve. This is the operating point, and at once η, $\bar{\rho}$, and V are known. Thus, for any set of parameters, the operating conditions may be determined by use of Fig. 11 (or an expanded version).

A tacit assumption in the above reasoning should be pointed out. The frequency at which the tube oscillates has been assumed to be the same as the resonant frequency of the cavity. Actually, the beam current will contain a reactive component which is out of phase with the cavity voltage. This will cause the operating frequency of the tube to shift slightly so that the shunt impedance also contains a reactive component. The error in the efficiency as given in Fig. 11 due to this effect may be shown to be very small. The only point of practical interest attaching to this effect is that for every point on the α, k, $\bar{\rho}$ contour

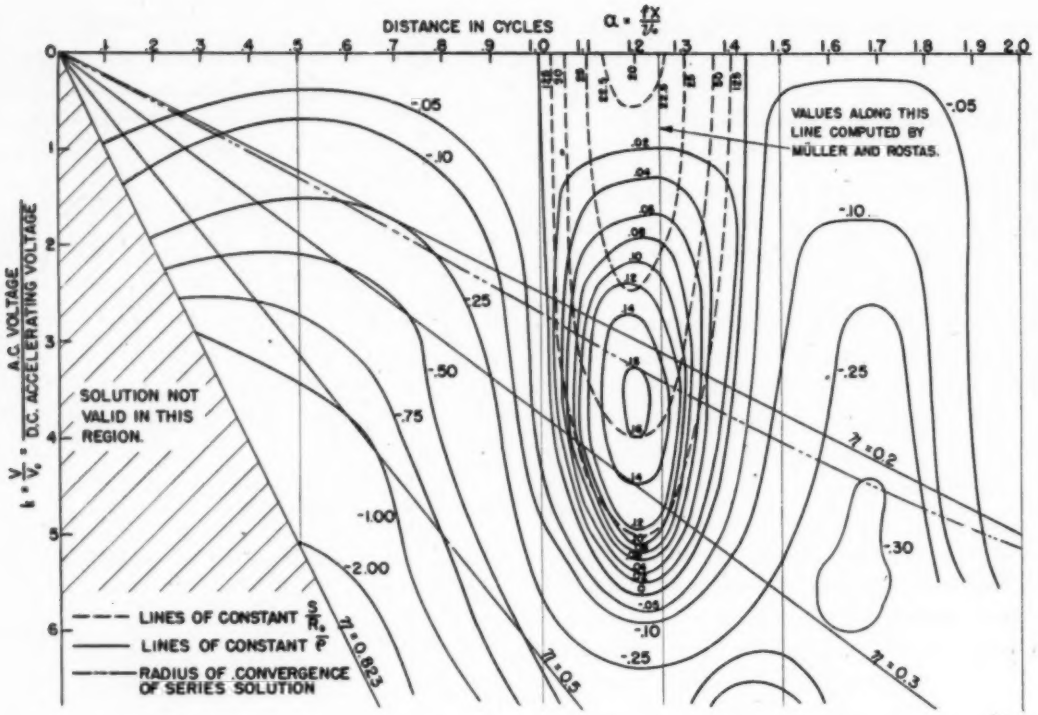
DISTANCE IN CYCLES
A.C. VOLTAGE / D.C. ACCELERATING VOLTAGE
SOLUTION NOT VALID IN THIS REGION.
VALUES ALONG THIS LINE COMPUTED BY MÜLLER AND ROSTAS.
LINES OF CONSTANT
LINES OF CONSTANT
RADIUS OF CONVERGENCE OF SERIES SOLUTION

FIG. 11. Complete operating characteristics for first mode and surroundings.

map there is a definite frequency of oscillation. In other words, a second set of frequency contours should be superimposed on Fig. 11 to give complete operating information. The calculation of these frequency contours is possible, but is not attempted here.

We note that S/R_0 must be at least 20, in the first mode, before oscillations are possible. This is in accord with a general principle of operation of velocity-modulated oscillators—for a given tube with a given accelerating voltage, oscillations will start only after the beam current reaches a finite value which is called the "starting current."

The value of R_0/S for starting is shown (see Appendix II) to be

$$\frac{R_0}{S}=-\frac{1}{2}\left(\frac{\sin 2\pi\alpha}{2\pi\alpha}-\frac{\sin^2\pi\alpha}{\pi^2\alpha^2}\right). \tag{15}$$

This gives the necessary value of S/R_0 for any α along the $k=0$ axis in order that oscillations will be possible. This information is shown in graphical form in Fig. 12. In effect, it gives the values of the S/R_0 curves of the α, k, $\bar{\rho}$ contour map along the $k=0$ axis.

After the necessary value of starting current is reached, oscillations will then build up in the first row of modes (Fig. 11) as the current is further increased. However, none but the first row of modes will be self-starting.

If one now desires to take out of the resonator a certain average power, P, it is only necessary to increase the beam current by an amount such that

$$P=V_0I_0\bar{\rho}-k^2V_0^2/2S,$$

where $\bar{\rho}$ is the conversion efficiency as determined from Fig. 11.

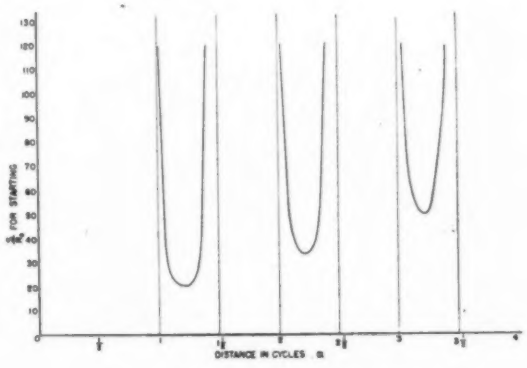

FIG. 12. Starting current function.

By use of a collector electrode on which is placed a voltage which will just stop the slowest electrons leaving the resonator, the efficiency may be increased. According to Müller and Rostas an increase of 7 percent is possible in the first mode.

APPENDIX I. LIMITATION ON EXTENT OF SOLUTION

To find the first electron to be thrown back into the accelerating field we put $\alpha=\partial\alpha/\partial\theta=0$ from (3b)

$$\frac{\partial\alpha}{\partial\theta}=1+\eta\cos\delta-\eta\cos\theta, \tag{16}$$

or

$$\eta=1/(\cos\theta-\cos\delta). \tag{17}$$

From (17) it is clear that the electron which enters at $\delta=\pi$ is the most likely one to be thrown back. For this electron

$$\eta=1/(1+\cos\theta). \tag{18}$$

We may solve for θ from this equation by putting $\alpha=0$ and $\delta=\pi$ in (3b) which gives

$$(1-\eta)(\theta-\pi)-\eta\sin\theta=0. \tag{19}$$

Eliminating η from (18) and (19) gives

$$\tan\theta=\theta-\pi. \tag{20}$$

The first root of this equation, and the only one with physical significance, is $\theta=-1.35$ radians. From (18) we get $\eta_{\max}=0.823$. For values of η greater than 0.823, some electrons will be thrown back into the accelerating field, and a more complex method of analysis is required. For values of η between 0.5 and 0.823, some electrons will have their direction of motion reversed while traversing the region of the alternating field, but none will be returned into the accelerating field.

APPENDIX II. EQUATION FOR STARTING CURRENT

We indicate here how Eq. (15) for the starting current function R_0/S may be derived. The problem is exactly the same as stated in Eq. (6), except we are now given the further assumption $\eta\ll1$. The integral in (6) may now be solved exactly if higher order terms in η are neglected.

The scheme is as follows

$$\bar{\rho}=\frac{1}{2\pi}\int_0^{2\pi}\left[1-\left(\frac{v}{v_0}\right)^2\right]d\delta, \tag{21}$$

which from (2b) becomes

$$\bar{\rho}=\frac{\eta}{2\pi}\int_0^{2\pi}[2(\cos\theta-\cos\delta)-\eta(\cos\theta-\cos\delta)^2]d\delta. \tag{22}$$

We must obtain θ as a function of δ from (3b). If $\eta\ll1$ as a first approximation

$$2\pi\alpha=\theta-\delta \quad \text{or} \quad \theta=2\pi\alpha+\delta. \tag{23}$$

If this value of θ is substituted in (22) we obtain

$$\bar{\rho}=-2\eta^2\sin^2\pi\alpha. \tag{24}$$

This answer, however, has no meaning because we have no information from (3b) regarding η. A more accurate value of θ is obtained from (3b) by substituting for θ from (23) in all terms except the first θ.

$$\theta=2\pi\alpha+\delta+\eta[\sin(2\pi\alpha+\delta)-\sin\delta-2\pi\alpha\cos\delta]. \tag{25}$$

When this value for θ is substituted in (22), the integration performed, and all terms in powers of η greater than the squared term dropped, the following formula is obtained for $\bar{\rho}$:

$$\bar{\rho}=2\eta^2(\pi\alpha\sin2\pi\alpha-2\sin^2\pi\alpha). \tag{26}$$

Making use of $\bar{\rho}=(k^2/2)(R_0/S)$ and $\eta=k/4\pi\alpha$,

$$\frac{R_0}{S}=\frac{1}{2}\left(\frac{\sin2\pi\alpha}{2\pi\alpha}-\frac{\sin^2\pi\alpha}{\pi^2\alpha^2}\right), \tag{27}$$

which is the same as (15). This agrees with the result obtained by Müller and Rostas by a different method.

On the Improvement of Resolution in Electron Diffraction Cameras

JAMES HILLIER AND R. F. BAKER
RCA Laboratories, Princeton, New Jersey

(Received September 6, 1945)

An electron optical system is described in which it is possible to obtain (1) high resolution electron diffraction patterns, (2) shadow electron microscope images, and (3) electron diffraction patterns of selected variable areas of the specimen. The change in mode of operation of the system is accomplished by electrical adjustments without changing the specimen position in any way. A number of phenomena related to the attainment of high resolution diffraction patterns are described. Pertinent details of the experimental apparatus are discussed and some representative results are shown.

IMMEDIATELY after the initial use of the electron diffraction camera as a means of demonstrating the wave properties of an electron beam its further use as a means of analysis was recognized; probably through analogy with the x-ray system. While the special properties of the electron beam have led to the application of the electron diffraction technique to a number of important academic problems concerning the structure of matter, the field of analysis by diffraction methods has continued to be dominated by the older and further developed x-ray diffraction technique. For some time it has been the opinion of the authors that there is no basic reason for this dominance and that if the instrumentation and technique of electron and x-ray methods had been developed equally the former would have definite advantages.

With the introduction of the electron diffraction adapter for the electron microscope[1] some of the advantages of using electronically regulated high voltage supplies and precision electron optics in electron diffraction were realized. However, while this adapter satisfies the desire of the electron microscopist to utilize further the possibilities of his instrument as an analytical tool and provides a means of obtaining high quality electron diffraction patterns, it does not represent, by any means, a complete exploitation of the high precision techniques now available to the electron optical designer.

The electron diffraction adapter has also emphasized an often overlooked but nevertheless important aspect of the electron diffraction method of analysis; namely, the careful correlation of the morphology of the specimen as observed in the light or electron microscope with the nature of the diffraction patterns obtained.

These are only a few of the considerations which have pointed to the necessity of a re-examination of the electron diffraction technique and to the development of a new instrument which will be described below.

[1] J. Hillier, R. F. Baker, and V. K. Zworykin, J. App. Phys. **13**, 571–577 (1942).

I. THE ELECTRON OPTICS OF THE ELECTRON DIFFRACTION CAMERA

Early electron diffraction cameras followed the

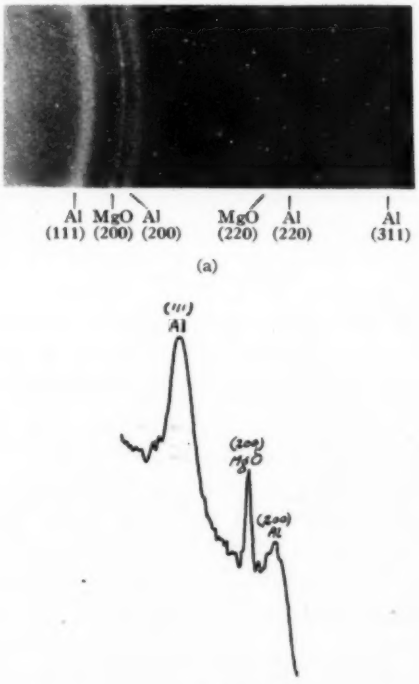

FIG. 1.* (a). An enlargement of a portion of an electron diffraction pattern of a specimen prepared by catching magnesium oxide smoke on a collodion membrane on which a thin aluminum film had been evaporated. This picture demonstrates the difference in natural line widths for different materials. (b). Microphotometer trace of part of the negative used in Fig. 1(a).

* *Note:* In order to obtain prints of diffraction patterns which were suitable for publication it was found necessary to print the pictures by varying the exposure radially. No interpretation should be made regarding the relative intensities of the lines.

same basic design as x-ray cameras, consisting essentially of an electron source, a collimating system arranged to produce a narrow beam of electrons, a specimen, a fluorescent screen, and some means of permanently recording the patterns. It was soon observed that the addition of a focusing lens either ahead of or behind the specimen greatly improved the sharpness of the rings obtained.[2] The resolving power of this improved type of camera was sufficient to demonstrate natural ring widths in the case of the most commonly used test specimens; namely, evaporated films of aluminum, silver, or gold. It is possible that this was an unfortunate circumstance as it did not provide adequate stimulus for the design of instruments possessing higher resolving power. It is now realized that these particular specimens are somewhat special, most specimens having natural ring widths as much as an order of magnitude smaller and requiring considerably greater resolving power than was obtainable in these earlier instruments. (See Fig. 1.)

It is difficult to assign a value of resolving power to an electron diffraction camera since the obtained resolution is a function of the ring diameter or in other words of the lattice spacing producing a particular spot or ring. If we assume

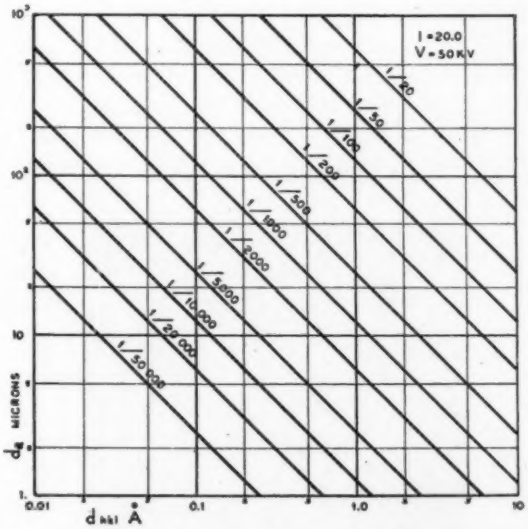

FIG. 2. Shows the maximum center spot size (d_d) which can be tolerated for a given desired resolving power (expressed as a fractional parameter on each curve) and lattice spacing (d_{hkl}).

[2] G. I. Finch and A. G. Quarrell, Proc. Roy. Soc. **A141**, 399 (1933); G. I. Finch, A. G. Quarrell, and H. Wilman, Trans. Faraday Soc. **31**, 1051 (1935); G. I. Finch and H. Wilman, Ergeb. d. exakt. Naturwiss. **16**, 353 (1937).

TABLE I.

$d_c = 0.01$ cm	$k = 10$ cm^{-2}
$m = 1$–2 (approximately)	$r = 0.025$ cm
$v = 20$ cm	$l = 20$ cm
$f_2 = 10$ cm	

that the focused electron beam at the position of the diffraction pattern consists of a circular disk of illumination of uniform intensity and of radius $d_d/2$, it can be shown that the minimum separation between distinguishable rings is $1.73d_d/2$.* This is assuming further that the rings have no natural width and that the lenses have no aberrations. Using Bragg's law and the geometry of the instrument and assuming that the angle of deflection is small and that there is no lens between the specimen and plate, we obtain an expression for the resolving power of an electron diffraction camera:

$$(\Delta d_{hkl}/d_{hkl}) = (-\Delta D/D) = 1.73 d_d d_{hkl}/2l\lambda, \quad (1)$$

where d_{hkl} is the lattice spacing, D the diameter of the corresponding ring, l the distance between the specimen and the photographic plate, and $\lambda = (150/V)^{\frac{1}{2}}$ is the wave-length associated with a beam of V electron volts energy. (See Fig. 2.) In this expression

$$(d_d/2) = (d_c \cdot m/2) + (v/f_2) k r^3 + S, \quad (2)$$

where d_c is the diameter of the electron source, m is the magnification of the lens system, v is the distance between the final lens and the photographic plate, f_2 is the focal length of the final lens, k is the spherical aberration constant of the final lens $f_2 = f_{20}(1 - kr^2)$, and r is the radius of the aperture used in the final lens. The added term S represents the change in spot-size due to the disturbance in the imaging system introduced by the presence of the specimen. This latter effect will be discussed further below. Table I is a typical set of practical values for the early single lens type of camera. In this case the first term of Eq. (2) is the most important except for specimens which charge badly. It amounts to 0.005 − 0.010 cm and leads to a limiting resolving power in the range 1/70 to 1/170 for $d_{hkl} = 1.5A$

* If, as is usually the case in electron diffraction patterns, the diameter of the ring is much greater than the spot-size, the radial intensity distribution in a ring obtained by uniformly distributing such spots around the circumference of the ring is given by $I_x = C\{(d_d/2)^2 - x^2\}^{\frac{1}{2}}$ where C is an instrumental constant and x is the distance from the center of the distribution measured in the radial direction. The half-value width (i.e., $1.73d_d/2$) of this distribution may be used as a measure of the resolving power providing the rings to be resolved are of equal intensity.

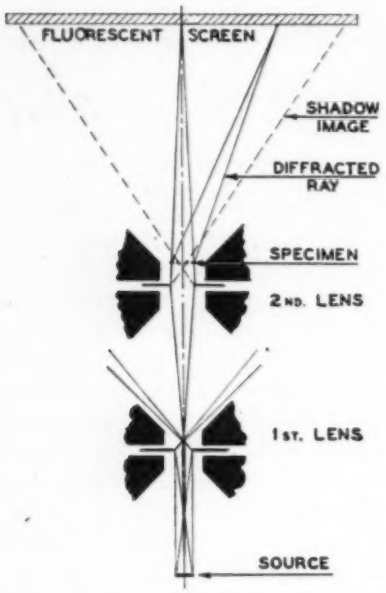

FIG. 3. Schematic diagram of the lens system in the new electron diffraction camera.

and $\lambda = 0.055A$. With the system to be described below, patterns have been obtained which require resolving powers better than 1/400 to separate rings and as good as 1/5000 to show the true intensity distribution in those rings, showing that the above resolving powers are inadequate for general work.

Figure 3 shows schematically the lens system of an electron diffraction camera in which a second lens has been added to reduce the size of the final spot. In this case

$$m = m_1 m_2 = 0.01 \times 2.5 = 0.025.$$

Here both the first and second terms of Eq. (2) are important making

$$(d_d/2) = 1.25 \times 10^{-4} + 3.1 \times 10^{-4} + S = 6.7 \times 10^{-4} + S \text{ cm}.$$

Under these conditions the instrument has a limiting resolving power of approximately 1/1000. By reducing the value of r to 0.0025 cm and the value of d_c to 0.0025 cm the resolving power can be made better than 1/10,000, a value which is seldom attained in practice due to the appreciable effects of the specimen on the focusing of the spot.

The arrangement of lenses shown in Fig. 3 is the same as that used in the shadow type microscope. This fact leads to the possibility of combining two types of instruments into a very useful analytical tool. The only change in this system necessary to convert it from a diffraction camera into an electron microscope is a reduction of the focal length of the second lens to place a highly reduced image of the electron source close to the plane of the specimen. In a practical instrument using magnetic lenses this means that it is only necessary to increase the current excitation of the second lens. In one arrangement which has been tried preset shunt resistors can be connected into the coil circuit of the second lens so that the mere snapping of a switch can change the instrument from one type of operation to the other. While the electron microscope images obtained in this manner are not of the high quality of those obtained with a conventional electron microscope, they are quite satisfactory for most purposes. (See Fig. 4.)

The resolving power of the instrument operated as a shadow type electron microscope is given by the expression

$$d_i = (d_k m_1 m_2'/2) + (l\lambda/m_i)^{\frac{1}{2}}, \qquad (3)$$

where m_2' is the adjusted value of the magnification of the second lens and m_i is the magnification (electronic) of the image of the specimen. In a practical case the focal length of the second lens is reduced from 10 cm to 0.2 cm (making $m_2' = 0.023$) which leads to a resolving power of the order of 200A providing that the electronic magnification of the system is maintained above 10,000×. The magnification may be controlled either by further slight adjustment of the power of the second lens or by mechanical translation of the specimen along the optic axis. In this type of electron microscope focusing is neither possible nor necessary; aberrations of the lens system do

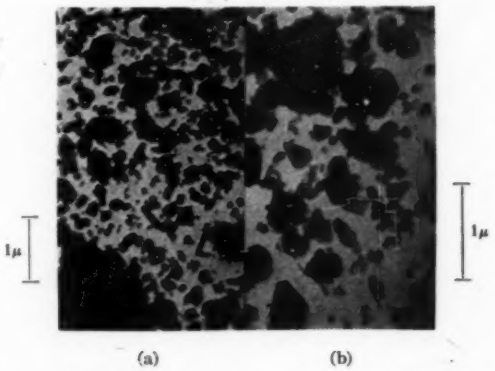

FIG. 4. Comparison between electron micrographs of a clay obtained with the shadow type electron microscope (a) and a conventional magnetic microscope (b). The pictures are not intended to represent the ultimate performance in either case. The shadow micrograph is an enlargement from that obtained in the sequence shown in Fig. 14.

not affect the sharpness of the image but enter as a distortion.

The two modes of operation of the lens system shown in Fig. 3, that is, as a high resolution electron diffraction camera and as a shadow type microscope operating at high magnification, represent the two possible extremes of adjustment. Intermediate to these extremes there is a very interesting continuous range of possible adjustments where the image field consists of a combination of an electron image and an electron diffraction pattern of the same specimen area. The individual diffraction spots are dark field images of the diffracting particles while the central spot is a bright field shadow image of the same particles. Both the diameter of the area of irradiation of the specimen (d_s) and the diameter of the defocused diffraction spot (d_d') vary continuously between these two extremes of adjustment according to the expressions:

$$d_s = 2r\left\{1 - \frac{l'}{v_2}\right\} + d_k m_1 m_2' \qquad (4)$$

and

$$d_d' = 2r\left\{\frac{(l+l')}{v_2} - 1\right\} + d_d, \qquad (5)$$

where $(1/v_2) = (1/f_2) + (1/u_2)$.

The symbols used are explained in Fig. 5 which is a series of ray diagrams showing the operation of the two lens system as an electron microscope, as an electron diffraction camera, and at an intermediate adjustment. The effect of the spherical aberration of the second lens is neglected in these formula. Using the parameters of the practical case these expressions have been

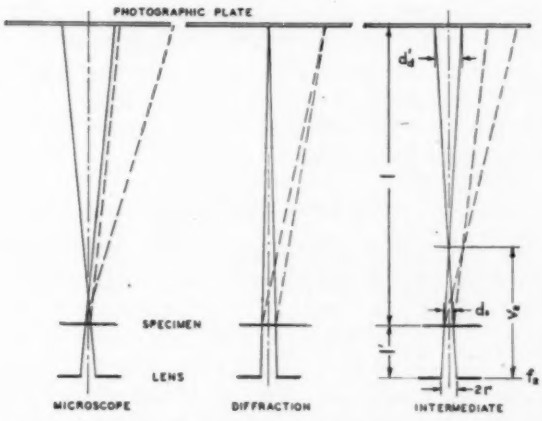

FIG. 5. A series of ray diagrams illustrating the operation of the new camera as a shadow microscope (a), electron diffraction camera (b), and an intermediate adjustment (c).

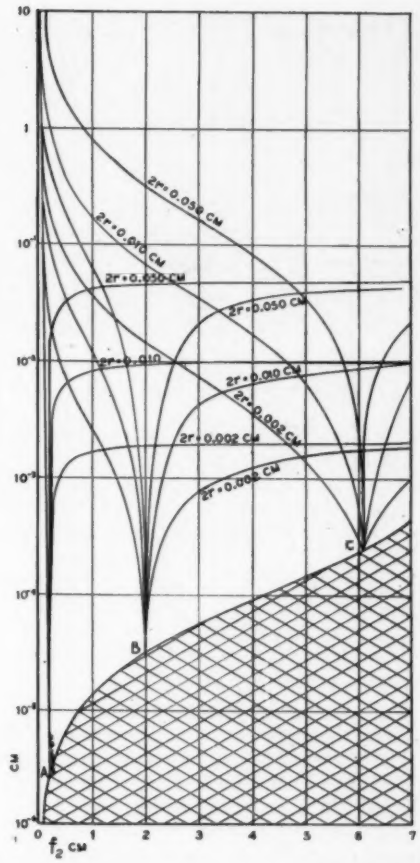

FIG. 6. A set of curves showing a relationship between the diameter of the beam at specified positions in the camera against the focal length of the final lens. The curve, *A*, *B*, *C*, gives the minimum beam cross section. The curves originating at *A* give the diameter of the area of bombardment of the specimen when situated 2 mm above the second lens. The curves originating at *B* give the same for the specimen position 2.6 cm from the second lens. Curves originating from *C* give the diameter of the central spot of the diffraction pattern at the plate position 20.0 cm from the second lens.

calculated for different size second lens apertures and plotted in Fig. 6. From this set of curves it is possible to read off the area of the specimen covered for different adjustments of second lens strength and the spot size (and therefore resolving power) obtained in the corresponding diffraction pattern. The base curve *ABC* gives the minimum spot size at any plane between the second lens and the photographic plate.

It is obvious that it is not possible to produce a focused electron diffraction pattern of a submicroscopic area of the specimen by electron optical means. It can be accomplished only insofar as the size of the aperture of the final lens can be reduced and insofar as the particular diffraction pattern

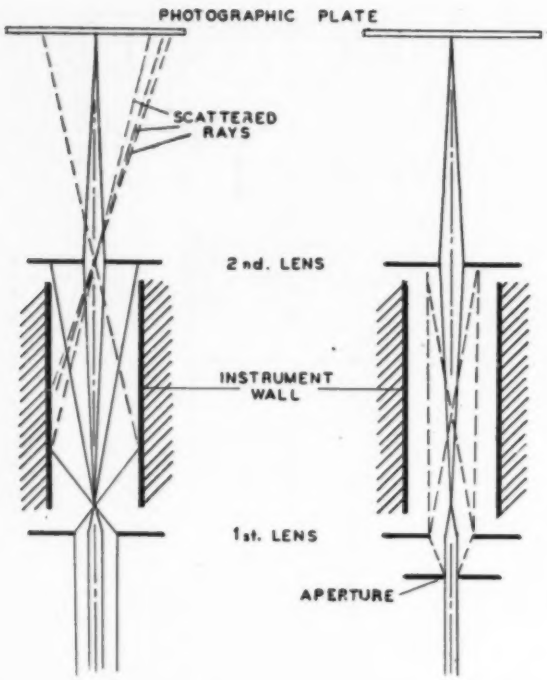

FIG. 7. Ray diagrams showing the origin of spurious patterns due to reflections from apertures and the walls of the system and their elimination by the proper placement of apertures.

encountered can tolerate the required defocusing. For instance, with a 0.002-cm aperture and the focal length of the second lens adjusted to make the image of the source coincide with the specimen plane (point *A* on Fig. 6) the diameter of the area of the specimen irradiated is approximately 230A but the spot diameter in the associated diffraction pattern is 0.2 cm leading to a resolving power of only 1/10 for a lattice spacing of 1.5A. This is hardly sufficient for critical work.

It is possible to reach an advantageous compromise by moving the specimen position further away from the second lens. Such a change is indicated by the series of curves leaving the point *B* on Fig. 6. In this case the specimen has been placed at a distance 2.6 cm from the second lens. The minimum diameter of the area of irradiation is then about 3000A but with the same aperture (i.e., 0.002 cm diam.) the spot diameter in the associated diffraction pattern is 0.015 cm leading to a resolving power of 1/100 for a spacing of 1.5A. This provides a fairly useful arrangement for point diffraction.

As will be seen from the results given below, the operation of this system over its entire range of adjustment is proving very interesting and fruitful and provides a good illustration of the flexibility of an electron optical system as an analytical tool.

II. ELECTRON DIFFRACTION TECHNIQUES

The establishment of a new instrument as a useful tool and the value of the results obtained from its application depend on the skill and ingenuity displayed both in the operation of the instrument and in the preparation of specimens. This is particularly true in the critical use of the x-ray and electron diffraction techniques. One aid in the attainment of skill in this regard is through an understanding of the possible pitfalls in the method. For this reason some of the difficulties encountered in the use of high resolution electron diffraction are discussed below. The inclusion of these difficulties is not intended as a criticism of the electronic method, it being possible to list equally important difficulties in the corresponding x-ray method.

(a) Vacuum

In electron diffraction work it is necessary to have an extremely good vacuum if dependable results are to be obtained. This is particularly so in the case of surface investigations where contaminants arising from the interaction between the electron beam and the residual vapors in the system are laid down at a rate which quickly masks the original surface. The contaminants are usually organic in nature originating from the materials used in connection with demountable joints, from improperly cleaned metal surfaces or from the oil of the diffusion pumps commonly used.

The full seriousness of this problem has only recently been realized and little has yet been done towards its solution. It is obvious that the problem of designing an instrument which is, at the same time, generally useful and free from all the possible sources of contamination, is an exceedingly difficult one.

(b) Lens Apertures

In an electron diffraction camera of the two-lens type considered above, the pencils of electrons which take part in the formation of the focused spot utilize the full open area of the second lens and hence suffer the corresponding amount of lens aberrations. It is not possible, in this case, to provide an *effective* limitation of the lens aperture, as is done in the electron microscope. Instead it is necessary to provide the lens

with an actual aperture of such diameter that a satisfactory compromise is reached between the intensity of the final spot and the increase in its diameter caused by the aberrations. The proper insertion of an aperture bearing absolutely no surface contamination requires considerable patience and skill.

The arrangement of the lenses leads to another technical difficulty. It involves a long focus lens fitted with a relatively small aperture which is, in effect, an ideal pinhole camera for electrons and will reproduce in the final image plane a faithful image of any part of the instrument between the final lens and the source and in the field of view of the final lens, from which electrons are scattered. This results in a number of spurious markings on the plane of the diffraction pattern. The spurious markings are particularly intense if the electron beam strikes an offending part of the instrument at grazing incidence. Figure 7(a) shows in ray-diagram form the origin of these spurious markings. (See Fig. 8a.) Such markings can be completely eliminated by the proper placement of apertures. In the case of the two lens system being considered it is necessary to place an aperture at the source-side focal point of the first lens. Its diameter must be sufficiently small to prevent electrons striking any part of the system between the first and second lenses except the aperture of the second lens. This is illustrated in Fig. 7(b). By this means no scattering can take place except at the edges of the apertures themselves. The scattering at the edge of the first aperture is focused on the second aperture and is stopped.

Scattering at the aperture of the final lens produces a different effect.* Here the aperture behaves as a secondary source of electrons, producing a shadow image of the entire specimen at low magnification. Figure 8(b) is an example of this type of defect. The use of a clean, conducting, and sharp-edged aperture will minimize this effect.

In considering spurious markings another phenomenon should be mentioned although it has no connection with the aperturing of the system. Occasionally a point of the specimen holder or even a point of the specimen itself which is not in the plane of the diffracting particles will reflect electrons very efficiently. Since such a reflection is the equivalent of a point source close to the specimen the conditions are similar to those of the shadow type microscope. In this case if the reflection occurs on the lens side of the specimen there will be superimposed on the diffraction a shadow image of part of the specimen. The field of view, intensity, and magnification of this image depend on the accidental placement and size of the reflecting particle relative to the specimen.

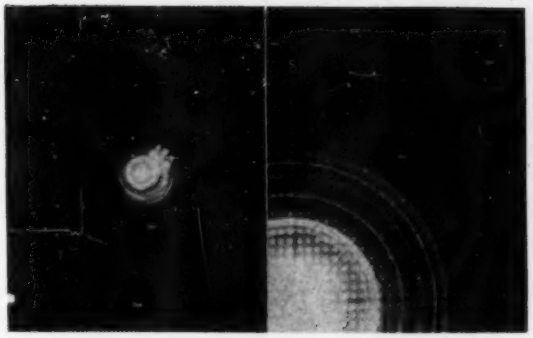

(a) (b)

FIG. 8. (a) An electron diffraction pattern of zinc oxide smoke on which can be seen spurious markings due to the reflection from the walls between the two lenses. (b) An electron diffraction pattern of zinc oxide on which is superimposed a low magnification of a shadow image of the supporting wire screen which arises as a result of scattering at the aperture of the final lens.

(c) Specimen

It is well known that most electron diffraction (and electron microscope) specimens acquire a charge as a result of the bombardment which they undergo. The magnitude of this charge and its distribution on the specimen vary widely according to the physical characteristics of the specimen and the technique of mounting. Except in extreme cases, the steady charged state of the specimen does not disturb the imaging process in the electron microscope. Here the deflection of the individual rays by the charge on the specimen is almost indistinguishable, as far as the microscope objective is concerned, from the scattering which takes place at the specimen and which is a necessary part of the imaging process. In the electron diffraction camera, however, it is not the specimen that is being imaged on the final screen but a distant electron source. Any focusing, deflection, or scattering of the electron beam which takes place at the specimen is not corrected by the lens system and appears as a defocusing, distortion, or diffusion, respectively, of the final spot. Observation of the spot on the fluorescent screen with a 60× magnifier will serve to convince the investigator of the importance of this

* The scattered electrons are affected only slightly by the field of the lens.

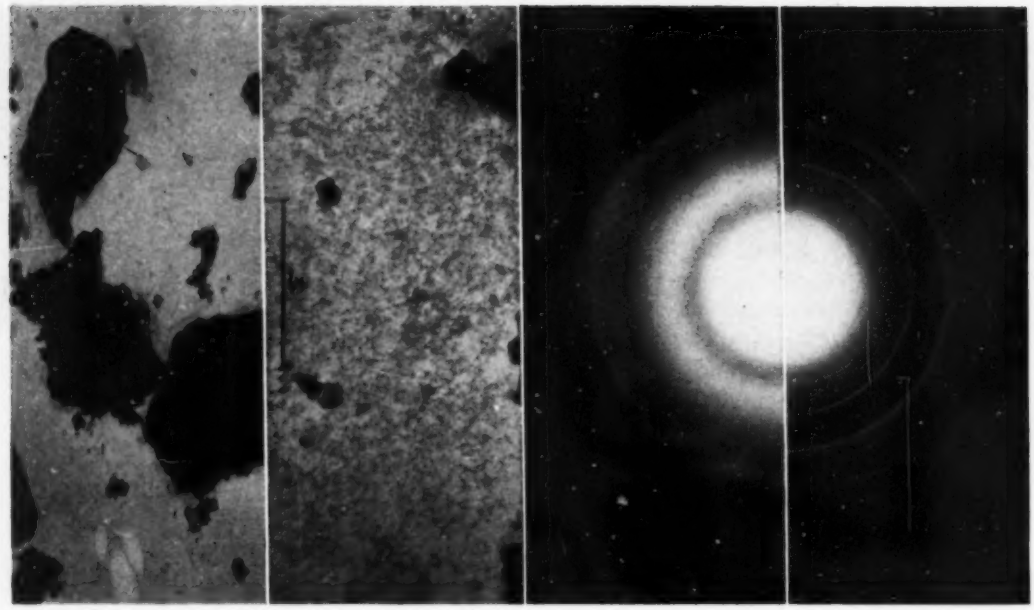

(a) (b) (c) (d)

FIG. 9. (a) An electron micrograph of an early dispersion of activated alumina. (b) An electron micrograph of a good dispersion of alumina. (c) An electron diffraction of the poor dispersion. (d) An electron diffraction pattern of the good dispersion of alumina.

effect and provide a means of determining its presence and magnitude.

The effect of charge on specimens for electron diffraction has long been recognized as a difficulty in the case of reflection work and methods of overcoming it have been developed. The authors wish to stress the fact that the effect is present in transmission work and is equally important if high resolution patterns are desired. The effect can be eliminated by the use of an auxiliary low voltage electron "spray." It has also been found that the inclusion of a conductor (connected to ground) in the irradiated area of the specimen will eliminate specimen charge. Proper specimen preparation is also instrumental in reducing the effects of charge.

A complete discussion of the techniques of preparation of the specimen for electron diffraction work is beyond the scope of this paper. However, the importance of the use of the electron microscope for the control of the specimen technique in the case of transmission and reflection diffraction work must be pointed out.

Many powder specimens of industrial importance have a particle size around 1μ. In preparing such specimens for electron diffraction it is essential that the particle size be reduced to a value where the majority of the particles become at least partly transparent for electrons of the velocity used. The particles must then be mounted in such a way that they do not charge and that in the cross section of the beam there are transparent and properly oriented particles sufficient for the production of a smooth and complete pattern. The mounting must be such that there is either no preferred orientation of the specimen particles or an accurately known orientation. It is obvious that the electron microscope provides an ideal method of observing and controlling these factors. Figure 9 is an example of the effect of proper dispersion on an electron diffraction pattern.

It is unfortunate that the brevity of the preceding paragraph gives such a poor indication of the extreme importance of this aspect of the electron diffraction technique.

III. RESULTS

Using the principles and precautions described in the preceding pages a combination high resolving power electron diffraction camera and shadow type electron microscope has been constructed. Figure 10 is a photograph of the completed instrument. Since the construction of this strictly experimental unit follows the pattern of the experimental electron microscopes designed

in this laboratory only a few significant new features will be described in detail.

As can be seen from the photograph the instrument is mounted on a table-like cabinet in front of the control panel. The beam travels vertically upwards from the gun situated just below the table level and passes successively through the valve chamber, double magnetic lens system, and specimen chamber into the fluorescent screen and photographic chamber. The column is pumped by an oil diffusion pump backed by a mechanical pump. The former pumps through the liquid air trap and large manifold seen to the left of the column and just above the table. Both pumps are mounted below the table in the front part of the cabinet.

One of the most difficult of the problems encountered in the development of the camera was the designing of an electron gun which would give intense single-source illumination and yet at the same time would not be hopelessly critical of adjustment. Owing to the presence of the two small apertures in the lens system the criteria used in the adjustment of an electron microscope gun were not available. A gun satisfying the design requirements has now been developed. It consists of a conventional hair-pin tungsten filament axially situated behind, and insulated from, the focusing aperture. The beam current is fed to the filament from the high voltage supply through a high resistance. This arrangement produces a voltage drop which is applied to the focusing aperture. The voltage on the aperture is usually about 500 volts negative relative to the filament and very near the cut-off voltage for the system.

In operation, the filament temperature is set slightly above the value at which the beam current reaches saturation. The combined action of space charge and the dependence of the focusing aperture potential on the beam current serves to stabilize the beam current against small

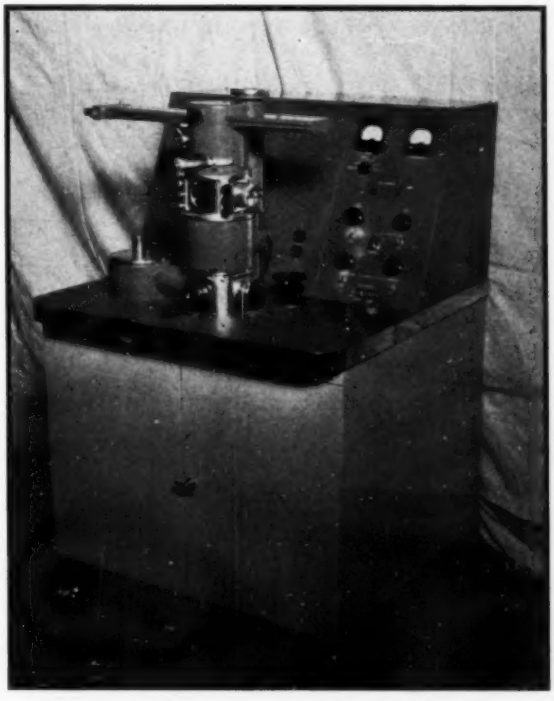

FIG. 10. Photograph of the experimental high resolution electron diffraction camera.

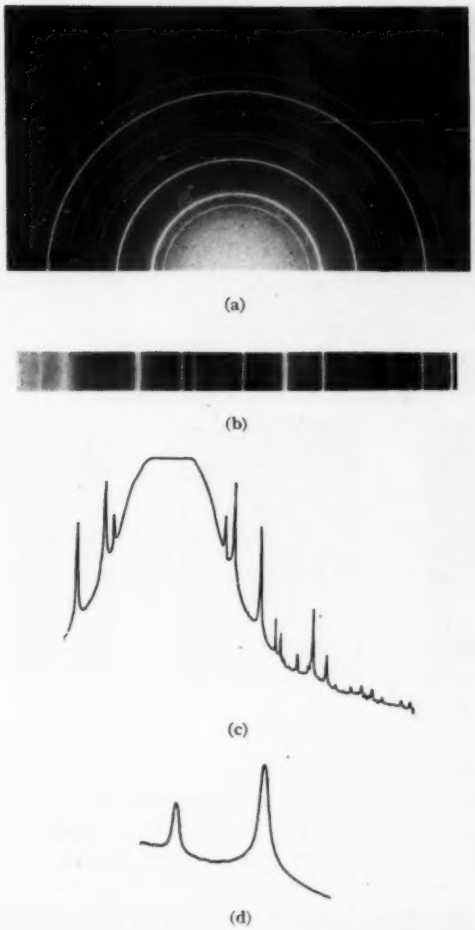

FIG. 11. (a) An electron diffraction pattern of sodium chloride sublimed in a vacuum onto a collodion membrane from a heated filament. (b) An enlargement of part of (a). (c) A microphotometer trace of the negative of the pattern shown in (a). (d) A microphotometer trace of the (111) (200) rings of sodium chloride. The abscissa scale has been magnified in order to show the intensity contours of the rings.

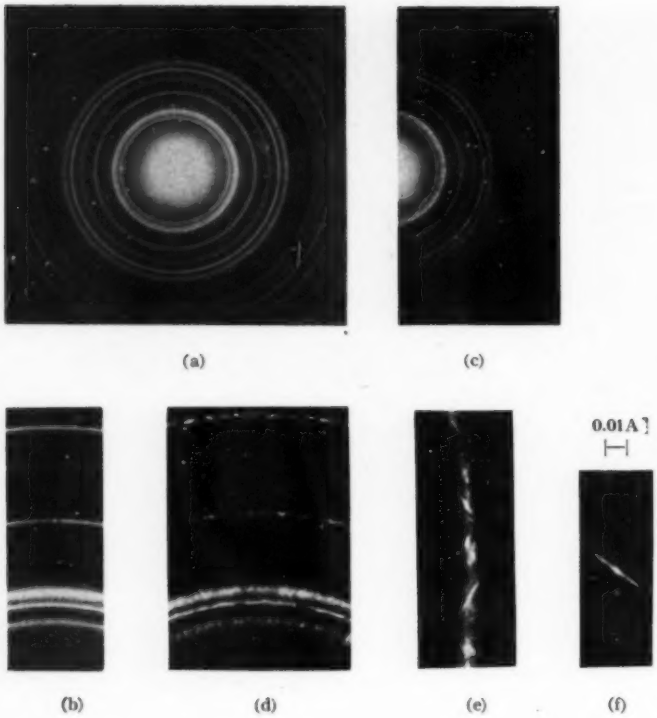

FIG. 12. (a) A normal powder pattern of zinc oxide smoke. (b) An enlargement of part of the pattern in (a). (c) Powder pattern slightly defocused. (d) An enlargement of part of the pattern in (c). The pattern has now become spotty due to the reduction in the irradiated area of the specimen and some of the spots are seen to be elongated due to the fact that they are now relatively low magnification images of the individual zinc oxide spikes. There is an interesting correlation of the individual spots and the line width in the focused pattern in (b). (e) and (f) Still further enlargements of the parts of the pattern in (c). The configuration seen in (f) may be due to a bending of an individual zinc oxide spike. It provides a good demonstration of the resolving power of the system as indicated by the attached scale.

filament current changes and *to center automatically the effective source relative to the focusing aperture*. The source produced is intense and small enough for the most critical electron microscope and diffraction work. The automatic centering of the source relative to the focusing aperture, even for off-center filaments, completely eliminates the necessity for translation and tilt

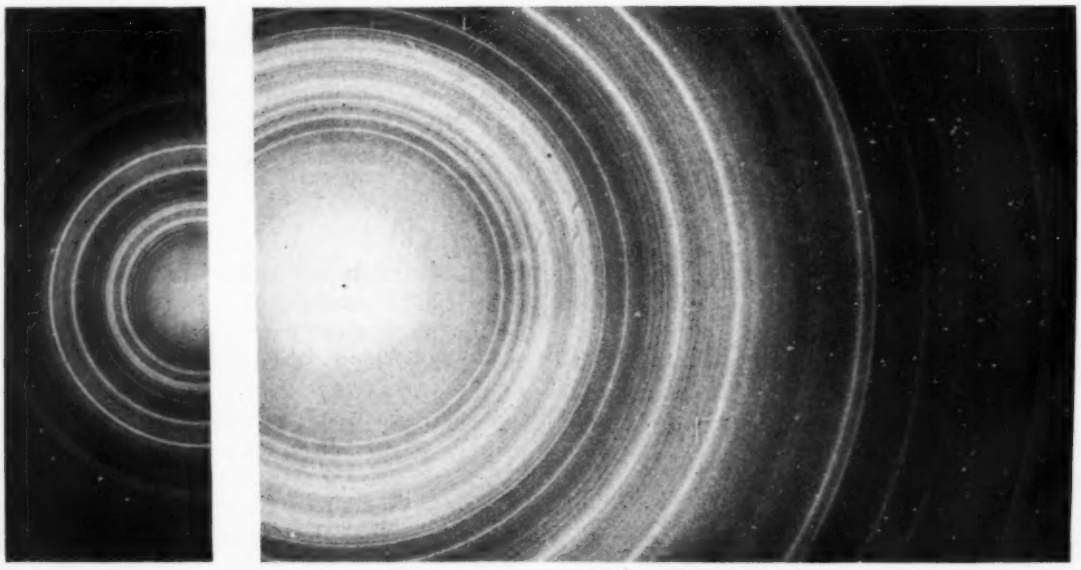

FIG. 13. (a) An electron diffraction pattern demonstrating the resolving power of the new system. The specimen was originally an evaporated film of silver floated from the surface of a rock salt crystal. It was allowed to stand in the atmosphere of the laboratory before the pattern was obtained. Rocksalt, silver, and silver sulphide rings have been identified. (b) An enlargement of (a).

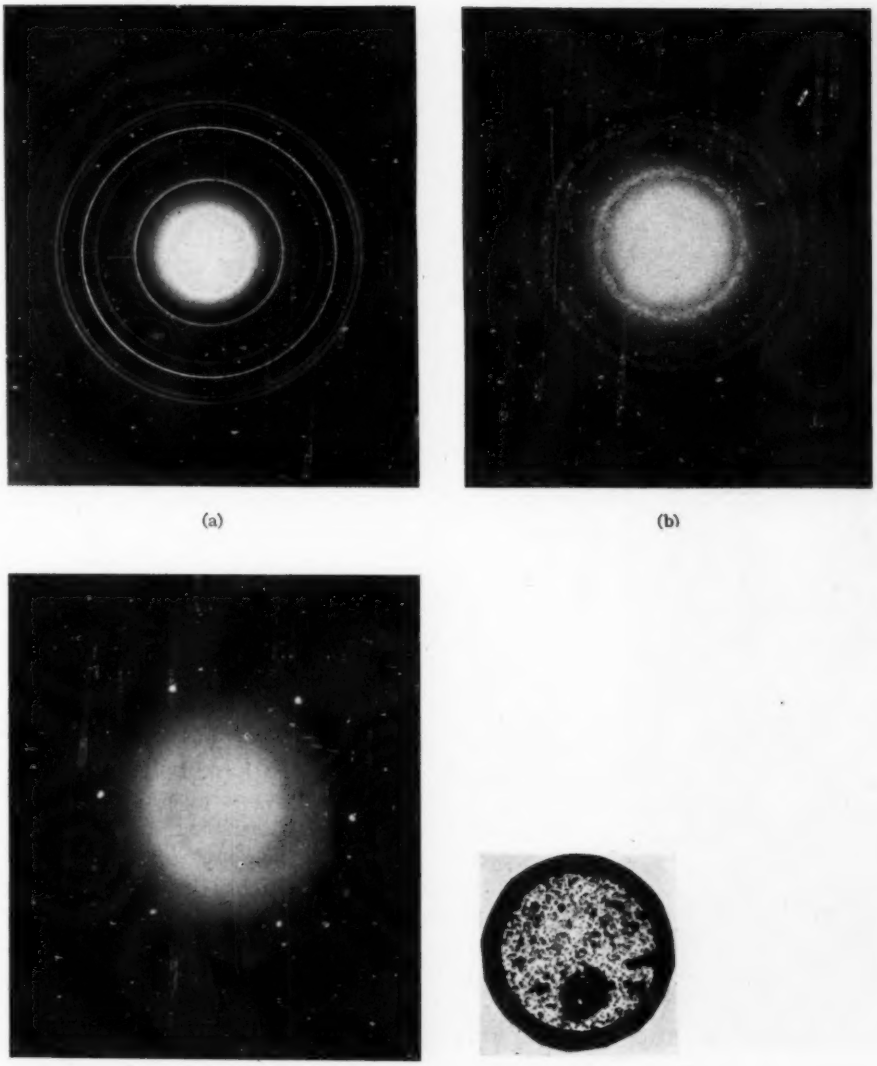

(a) (b) (c) (d)

FIG. 14. A series of pictures of clay showing the complete range of operation of the instrument. (a) A powder pattern. (b) A slightly defocused powder pattern. (c) In this case the instrument is approaching its operation as a shadow microscope. The area of irradiation of the specimen has been reduced until it covers one small group of crystals. At the same time the angular aperture of the irradiation of the specimen has increased so that a number of reflections from different planes are possible. The result is a complete hexagonal pattern. (d) Shadow micrograph of the same specimen.

adjustments on the gun. The saturation value of the beam current is determined by the axial separation of the filament tip from the plane of the focusing aperture.

The valve chamber situated between the gun and the lens coil has a valve of new design which when open introduces no obstruction or baffling of the main pumping path. This is accomplished by controlling the valve by a long thin rod sliding through a rubber packing type vacuum seal. When the valve is in the open position the packing can be tightened to prevent any possibility of leakage. Secondary valves are provided for letting air into the system and for by-passing the diffusion pump during prepumping. A large manifold running up the back of the instrument provides for high speed pumping of the upper sections of the instrument. This manifold is also provided with a liquid air trap.

The lens coil and pole pieces are similar to those used in electron microscopes except that the final lens pole pieces are made to produce an asymmetrical axial field distribution. With this system it is not necessary to introduce the specimen into the lens opening. The maximum dimensions of the specimen are then limited only by the size of the specimen chamber.

In the specimen chamber a serious attempt has been made to avoid contamination of the specimen with organic vapors from gasket materials and grease lubrication of the packing seals. It is essentially a double-walled chamber arranged so

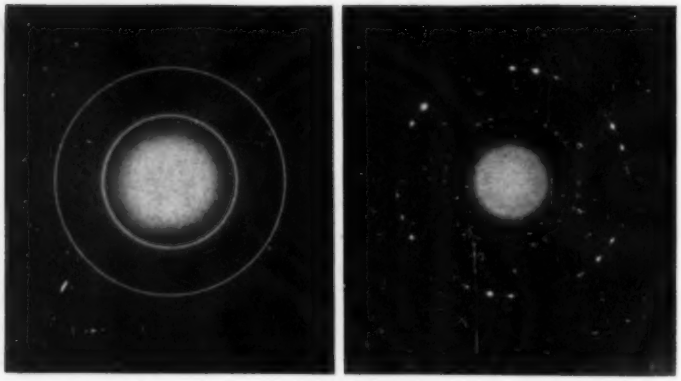

(a) (b)

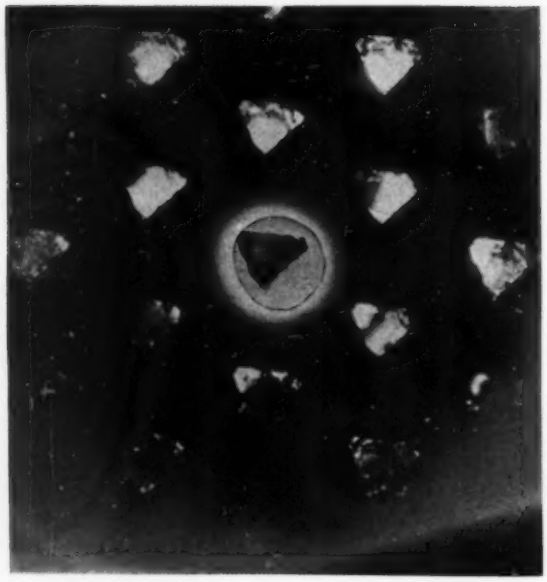

(c)

FIG. 15. A similar series of pictures of a graphite specimen. (a) Focused powder pattern. (b) Slightly defocused pattern. (c) A considerably defocused pattern in which a single flake was in the irradiation area. Superimposed on the center of this picture is the bright field shadow image of the flake producing the pattern. This image was observed in the instrument simultaneously with the diffraction pattern. It was necessary, however, to make two different exposures owing to the great difference in the intensity of the two types of images. (7000×)

that there is no direct open path between any gasket or packing seal and the inner chamber. Vapors leaving any of these sources of trouble must diffuse past the manifold liquid air trap before entering the actual specimen chamber.

The viewing system consists of a high resolution fluorescent screen fitted with a forty-five degree front surface mirror and a low-power compound microscope (30×). The fluorescent-screen mirror system is mounted on an arm permitting it to be pivoted out of the beam path when photographic records are made.

The photographic chamber uses the standard 2×10 in. plate size and is quite conventional except in that it is fitted with an engraved cassette holder, allowing the accurate positioning of the plate, and with a quick-acting adjustable opening shutter. These features have been introduced to permit the use of the instrument in sequential studies on the treatment of material which cannot be exposed to air during the experiment. They permit the obtaining of a large number of narrow strip diffraction patterns or micrographs. The power supplies which are quite conventional and which are mounted in the rear of the cabinet consist of a regulated coil current supply with appropriate adjustable shunts for setting the relative powers of the two lenses, a regulated high voltage supply which is adjustable from twenty to fifty kilovolts in five-kilovolt steps, a radiofrequency filament current supply, and the necessary vacuum gauge circuits. All circuits are operated from a line voltage regulator.

The electron optical performance of the system appears to be in good agreement with the predictions of the above mentioned formulae though the total effect of the specimen mounting and charging are by no means thoroughly understood. Some patterns obtained show resolving power exceeding anything in the literature by an order of magnitude. Whether this is a justifiable measure of the performance of the instrument will be better judged from the final appearance of the reproductions in this article. Figures 11 to 15 will serve to illustrate the resolving power of the instrument as a true diffraction camera and its versatility as a probe diffraction camera and shadow microscope.

The authors are greatly indebted to J. M. Morgan who did a large part of the mechanical and electrical design work involved in the development of this instrument.

Applications of Metallic Shadow-Casting to Microscopy[1,2]

ROBLEY C. WILLIAMS AND RALPH W. G. WYCKOFF
University of Michigan, Ann Arbor, Michigan

(Received July 3, 1945)

The factors which determine image contrast in optical and electron micrographs are discussed in relation to a new metal shadow-casting technique whereby the contrast of images is greatly increased by depositing obliquely a thin film of metal on the microscope preparations. Further advantages of the use of shadow-casting are described, and an estimate is made of the lower limit of size of objects which should be observable by shadow-casting. Examples are given and illustrations are shown of the applications of this technique to the electron micrography of particles of macromolecular dimensions, of replicas of such particles, and of surface replicas prepared in several ways.

INTRODUCTION

A GOOD micrograph gives clear and accurate information about the size, shape, and structure of the object from which it is derived. Whether one is dealing with microscopy involving light or electrons, the limit to what can be seen in a micrograph is in the end determined by the resolving power of the lens system and by the contrast between adjacent elementary regions of the object. Most of the contrast in the optical microscope results from differences in absorption of light within the preparation. Many important classes of objects, particularly those of biological origin, have in themselves little variation in absorption for visible light, but this restriction on microscopic examination, of course, has been in large measure eliminated through the development of elaborate methods of differential staining using dye-stuffs and other coloring agents, and to a lesser degree through the use of ultraviolet light. Under these circumstances the magnification, and the smallness of detail that can be observed with the optical microscope, are set by the attainable resolving power, i.e., by the wave-length of the light used.

Conditions are somewhat different in electron micrography at the present stage of its development. Contrast in an object illuminated by a beam of electrons is not due to differential absorption but rather to an unequal amount of scattering of electrons at different points in the preparation. The visibility of details of an object resulting from the contrast they introduce into an electron micrograph is thus determined largely by the amounts of matter contained in these details. Such amounts of matter may be so small that, especially for objects resting on a supporting membrane, insufficient contrast rather than inadequate resolving power of the microscope fixes the lower limit of visibility. The present paper is devoted to a discussion of some of these limitations arising from insufficient contrast, and to a description of a technique by which the contrast in specimens for microscopy can be greatly enhanced.

The image responsible for an electron micrograph is formed by focusing the electrons that penetrate the specimen and its substrate. The contrast in the final image is a result of failure of the lenses to focus accurately those electrons scattered through relatively large angles while passing through specimen and substrate. If these widely scattered electrons are allowed to strike the photographic plate they cause a generally distributed fogging. Maximum of contrast is therefore achieved by employing a small objective aperture which will exclude such widely deflected electrons and pass only those that can be focused with precision by the objective and projector lenses. All the electron micrographs described in this paper have been made with an RCA Type EMB instrument equipped with an objective aperture.

Simple considerations make evident the lower limit of size of biological and other objects of low density which can be recorded by direct photography with the electron microscope. One can, for example, scarcely expect to observe

[1] From the Department of Physics, University of Michigan.

[2] This research was supported in part by the Evaporated Metals Films Corporation, Ithaca, New York.

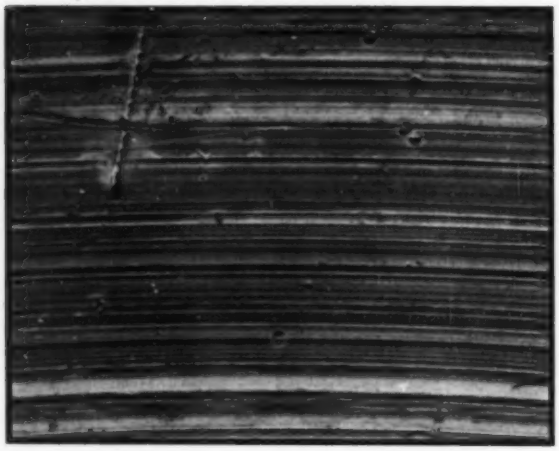

FIG. 1. An aluminized collodion replica of a machined brass surface. 10×

directly the details of surface structure on a bacterium. Such an organism will have a thickness of not less than several tenths of a micron and it will be supported on a film of collodion or Formvar[3] which supplies additional scattering matter. It is evident that surface details which provide variations in thickness of amounts less than, say, 0.02 micron will introduce totally imperceptible differences in scattering and contrast in micrographs. In the range of particles smaller than bacteria it is clear that none can be detected if its scattering is insignificant compared with that of the substrate on which it rests. All organic substances have about the same low scattering for electrons, and experience shows that under the most favorable conditions it is hard to detect the existence of particles supported by a substrate and having diameters less than about 0.01 micron. By the same reasoning it is impossible to form an accurate idea of the shapes of much bigger particles. Unless they are flat or are enclosed in thick membranes, the outlines of even relatively large organic objects must be diffuse on direct electron micrography, since at some point within their geometrical edge they will have thinned down to such an extent that the scattering is no longer considerable compared with that of the substrate.

The same kind of diffuseness of fine detail is observed in an electron micrograph of a collodion or Formvar[4] replica of an etched metal or other rough surface, and it has usually been concluded[5] from this that such replicas are not sharp. The work described in this paper shows that such simple replicas are faithful to the surface from which they are stripped and that their apparent lack of sharpness arises from the insufficient contrast introduced by their small scale variations in thickness and scattering. This conclusion has great practical importance because replicas made with polymers in solution are especially convenient to prepare, and can be stripped from many surfaces and materials that cannot be subjected to the high temperatures and pressures involved in making polystyrene[5] and other molded replicas.

THE SHADOW-CASTING TECHNIQUE

In a previous paper[6] we have described a technique for enhancing contrast in electron microscopic preparations which we have called shadow-casting. Briefly it consists in coating the specimen obliquely with a very thin film of metal prior to the microscopic examination. The coating is accomplished in an auxiliary vacuum chamber by means of a filament containing the metal to be deposited. The effect of the oblique deposition is to cause the higher elevations in the specimen to cast total or partial metallic "shadows" on the sides or slopes away from the filament. When the shadow-cast specimen is photographed, it yields a negative that shows light and dark areas whose degree of darkness, as a measure of the thickness of deposited metal, is a function of the angle between the tangent planes of the areas and the direction to the filament during evaporation. Such a negative, or negative print, of a shadow-cast specimen gives the same impression that is produced by a picture taken with light reflected from an obliquely illuminated landscape.

Any substance that does not exhibit structure of its own in thin films and does not migrate after deposition on the specimen could be used for shadow-casting, but it is clear that only the

[3] Formvar 15-95 is a polyvinyl formal supplied by the Shawinigan Products Corporation, New York, New York.

[4] V. J. Schaefer and D. Harker, J. App. Phys. **13**, 427 (1942).

[5] R. D. Heidenreich and V. G. Peck, J. App. Phys. **14**, 23 (1943); R. D. Heidenreich, *ibid.* **14**, 312 (1943).

[6] R. C. Williams and R. W. G. Wyckoff, J. App. Phys. **15**, 712 (1944).

heavier elements can provide the extremely thin films of great scattering power that are needed in electron microscopy. Very thin films are generally desirable since they cause a minimum of alteration in the geometrical outline of the specimen on which they are deposited. Chromium yields a notably structure-free film and is ideal for shadowing relatively large objects such as bacteria,[7] but the considerable thickness of the requisite film (*ca.* 70A) makes it unsuitable for delineating objects of macromolecular dimensions. For such smaller objects gold[8] in a computed thickness of *ca.* 8A on the plane of the substrate gives satisfactory results.

Shadow-casting has a number of desirable consequences, first of which is that the heights or thicknesses of discrete objects that are not wholly flat are readily estimated from the lengths of the shadows[9] they have cast. Relative heights can of course be obtained in other ways, for instance by stereoscopy,[10] but these other procedures are more laborious, and with them it is hard to be sure which areas are high and which are low. Shadow-casting brings out in great relief the surface contours of the specimen by enhancing the scattering power, or optical effectiveness, over the entire preparation and by causing this increase to vary with the contours and to concentrate in the surface layers of the specimen. The type of detail brought out by shadowing can be varied by altering the thickness of the evaporated layer; for example if it is so thick that its optical effectiveness exceeds that of the rest of the object, it will portray almost exclusively the details of the surface. Shadowing also affords contrast between areas whose elevations in the specimen are similar but whose slopes are different, or between areas whose slopes are the same but are separated by regions of different slopes. Furthermore it makes clearly evident objects so small or thin that by themselves they would not produce a minimum contrast against the background of the rest of the specimen. Experience indicates that an object even smaller than the lower limit of resolution of the electron microscope as it now exists can be made to cast a partial or total shadow at some highly oblique angle of illumination and that it can be detected by the existence of this shadow.

[7] R. C. Williams and R. W. G. Wyckoff, Proc. Soc. Exp. Biol. Med. **59**, 265 (1945).
[8] R. C. Williams and R. W. G. Wyckoff, Science **101**, 594 (1945).
[9] H. O. Müller, Kolloid Zeits. **99**, 6 (1942).
[10] See R. D. Heidenreich and L. A. Matheson, J. App. Phys. **15**, 423 (1944), for references.

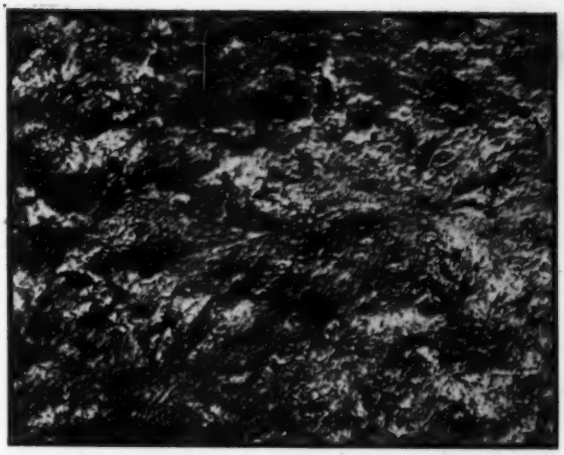

FIG. 2. An aluminized "Faxfilm" replica from an anodicly oxidized high speed drill. 500×.

SHADOW-CASTING FOR OPTICAL MICROSCOPY

Shadow-casting will increase the contrast on replicas which are to be studied and photographed with the optical microscope, as well as with the electron microscope. Lower magnifications will commonly be employed for examination with visible light, and the metallic film that produces the shadows need not be unusually fine grained. As a consequence of this freedom of choice of film, aluminum of such a thickness that it is partially opaque to visible light can be used as a convenient shadowing metal for such "visual" replicas. We have made satisfactory visual replicas starting with dissolved collodion or Formvar, or with the commercial replica film process known as "Faxfilm."[11] Figure 1 is a photograph of an aluminum-shadowed collodion replica of a machined brass surface, magnified ten times. Figure 2 shows an aluminized "Faxfilm" replica of an anodicly oxidized surface of a high speed drill, magnified 500 times. Shadowing brings out much fine detail in this "Faxfilm" replica that could not be seen otherwise. Figure 3 is an aluminized collodion replica

[11] Faxfilm, R. D. McDill, Cleveland, Ohio.

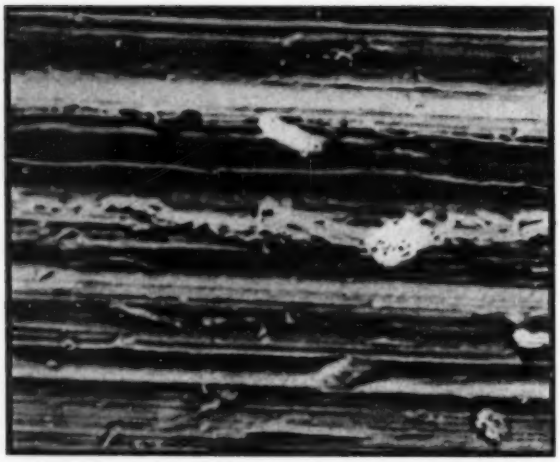

FIG. 3. An aluminized collodion replica of a machined steel surface. 1000×.

of a machined steel surface at a magnification of 1000 times. The contrast in such shadowed objects is so high that the condenser of the microscope can be employed at the full aperture necessary for maximum resolution.

SHADOW-CASTING FOR ELECTRON MICROSCOPY

1. Replicas of Surfaces

The electron microscope has proved to be especially useful in examining replicas of surfaces of many types of objects. Several methods of preparing these replicas have been described.[12] Two of them, however, are in greatest current use: the Formvar process, as developed by Schaefer and Harker, and the polystyrene-silica method of Heidenreich and Peck.

As stated above, a Formvar, or a collodion, stripping lacks sharpness when viewed at high magnification in the electron microscope, and this generally has been ascribed to its intrinsic lack of sharpness of outline and faithfulness to the surface from which it is drawn. We have found on the contrary that replicas of this sort appear geometrically sharp after being shadowed, and that their unsharpness when photographed before metal deposition must be ascribed to a lack of contrast between regions of nearly the same thickness.

[12] H. Mahl, Zeits. f. tech. Physik **21**, 17 (1940); *ibid.* **22**, 33 (1941); Metalwirtschaft **19**, 1082 (1940); V. K. Zworykin and E. G. Ramberg, J. App. Phys. **12**, 692 (1941); V. J. Schaefer and D. Harker, see reference 4; R. D. Heidenreich and V. G. Peck, see reference 5.

Polystyrene-silica replicas exhibit good contrast but probably not for the same reason that our obliquely metal-shadowed films do. Heidenreich has suggested[13] that silica deposits upon a polystyrene base in such a way as to form a layer of uniform thickness measured normal to the elements of the surface. Hence, as seen by the electron beam, regions of the silica film which are sharply tilted to the general plane of the replica will be effectively thicker than regions parallel to the plane. Highly tilted regions will consequently appear dark on positive pictures and flat regions will appear light. If this hypothesis is correct it makes detailed interpretation of the micrographs difficult, since only changes in elevation can be recognized. Stereoscopic photography can profitably be used in understanding these polystyrene-silica replicas, but it does not ordinarily resolve the fundamental ambiguity in them between what is high and what is low. This interpretation of the form of the silica film is supported indirectly by our observation that a replica film made by depositing a uniform film of chromium in a good vacuum at normal incidence upon a polystyrene replica cast, unlike a

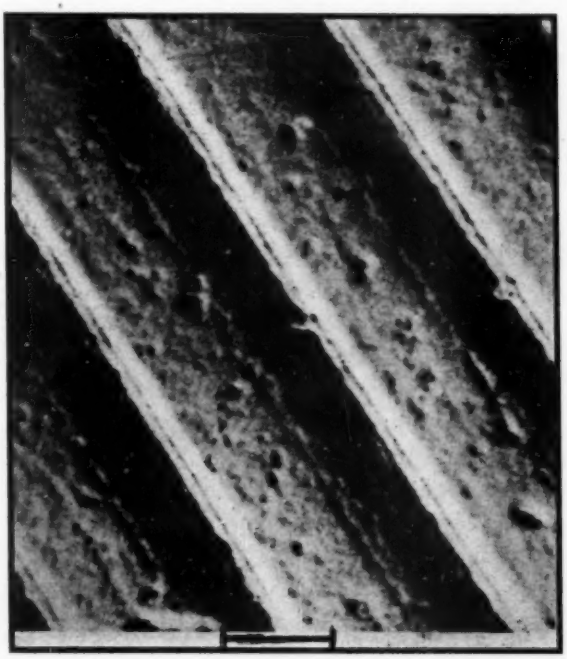

FIG. 4. An all-metal chromium-shadowed replica of a glass diffraction grating.

[13] R. D. Heidenreich, see reference 5.

deposited silica film, introduces no contrast in the micrographs made of it. In this case the metal, which does not migrate after deposition, can be expected to form a film varying in thickness over the contours of the surface according to the cosine law, thereby producing thinner films on highly tilted areas as measured normal to the area. As a result the effective thickness of the film as seen by the electron beam will be sensibly constant over the entire replica and the result will be an almost complete lack of contrast.

We have found a number of different procedures satisfactory for preparing replicas, depending on the surface to be reproduced and the use to which the replica and its photograph are to be put. At one stage or another, however, we invariably include a high vacuum deposition of a thin metallic film at a known oblique angle.

a. All-metal replicas can be made of glass and of many crystalline surfaces. One way to make them involves evaporation from three filaments. First there is deposited upon the original surface, at normal incidence, an extremely thin (*ca.* 20A) film of acid-, or water-, soluble material such as copper or NaCl. This is followed by a film of chromium 100A thick evaporated also at normal incidence to provide body to the replica. The third film, which introduces contrast, can be another 100A of chromium deposited obliquely.

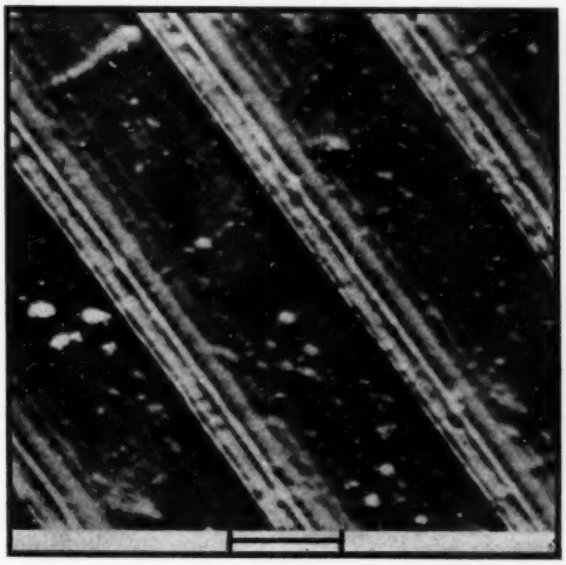

FIG. 5. A gold-shadowed collodion replica of the diffraction grating of Fig. 4.

FIG. 6. A chromium-shadowed collodion replica of a surface of a used roller bearing.

The specimen with its attached films is then immersed in dilute acid or in water in order to float off the coherent film of chromium, and this is then picked up on a microscope screen by "fishing." Figure 4 shows such an all-metal replica of a 15,000 line-per-inch glass diffraction grating.[14] The intermediate soluble layer has in our experience introduced minute pits that make this type of replica unsuitable for magnifications exceeding *ca.* 20,000 times. The all-metal replica is chiefly useful when, as for calibration of magnification, one wants a specimen that can be relied on not to expand or shrink perceptibly while being made, and that does not charge up and distort under the impact of the electron beam.

b. Shadow-cast collodion replicas[15] are especially easy to make and to use, and with a fast evaporating unit the time elapsed in passing

[14] All the electron micrographs of this paper are from negative prints of intermediate contact positives on lantern slide emulsion. The scale of magnification in each instance is indicated by the one micron scale underneath the photograph.

[15] L. Thomassen, R. C. Williams, and R. W. G. Wyckoff, Rev. Sci. Inst. 16, 155 (1945).

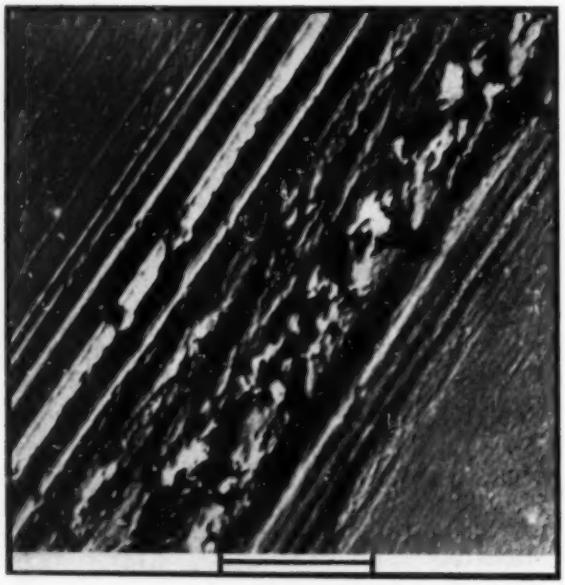

FIG. 7. A chromium-shadowed collodion replica of a scratched glass slide.

from the original specimen to the finished replica can be as short as 15 minutes. The average time required to make such a replica, or a corresponding one with Formvar in place of collodion, is further reduced since a great many strippings can be shadowed at one time. For the sake of comparison between the all-metal and the collodion-base processes, there is reproduced in Fig. 5 a collodion-gold (10A deposited at a four-to-one angle) replica of the same glass diffraction grating employed to make Fig. 4.

Figures 6 to 11 are additional examples of electron micrographs of replicas prepared by this collodion-metal process. All the collodion strippings for these replicas have been shadow-cast at angles of five-to-one (arctan 1/5) either with a film of chromium *ca.* 80A thick or with *ca.* 8A of gold.

Figure 6 is a chromium-shadowed replica of the inner surface of the outer cone of a used roller bearing. This picture illustrates a great advantage of the process: it can be employed with many kinds of intact objects whose shapes, sizes, and locations are such that molded replicas could not be drawn from them.

Figure 7 is a replica of an accidental scratch on a glass microscope slide. It shows the unusual smoothness of the undamaged glass surface as well as the large amount of small scale tearing and flowing in the scratch.

Figure 8 is a gold-shadowed replica of the surface of a diamond polished parallel to a (110) plane. The approximately circular areas about one micron across correspond to elevations on the polished surface, and in this field a sharp minute pit can be seen near the center of each elevation. The residual polish marks are clearly seen running parallel across the surface of the diamond; the depth of the smallest of these is *ca.* 50A.

Figures 9–11 are gold-shadowed collodion replicas of the polished and etched surfaces of pieces of steel, of 60-40 brass and of magnesium. They illustrate the ease with which determinations can be made of relative heights and depths in such specimens. This is particularly evident in Fig. 11 where four distinct levels can be seen on the surface of the replica. The center is a high triangular peak surrounded by a slightly raised region of roughly triangular shape; around this

FIG. 8. A gold-shadowed collodion replica of a polished diamond face.

is the general level of the replica surface which is partially covered with nearly circular pits.

c. Replicas can also be made by depositing first a metal film obliquely on the surface of the specimen. If the film is sufficiently thick and the specimen has an appropriate surface it can sometimes be stripped directly to yield a simple all-metal replica. Otherwise the film can often be backed up by forming on it a supporting collodion film and stripping the two together from the underlying specimen. This process does not appear to be applicable to most etched metallic surfaces but, as will be indicated at a later

FIG. 9. A gold-shadowed collodion replica of an etched steel surface.

point, it provides a very valuable way of studying macromolecules and other minute particles that can be deposited on a glass surface prior to being shadowed.

2. Specimens mounted on Substrates

The advantages of shadow-casting discussed earlier in this paper are all applicable to electron microscopic preparations in which the object of study is mounted for examination on a collodion or Formvar substrate. Figures 12 to 14, and the photograph on the cover of this Journal, have been chosen to illustrate the applications that

FIG. 10. A gold-shadowed collodion replica of an etched surface of 60-40 brass.

FIG. 11. A gold-shadowed collodion replica of a piece of magnesium etched with salt water.

FIG. 12. Chromium-shadowed typhoid bacilli.

have been made of shadow-casting to the observation of biological objects of very different sizes when mounted on collodion.

Bacteria can conveniently be used to demonstrate the kind of new information that can be brought out by shadow-casting relatively large objects. Figure 12 is a photograph of chromium-shadowed typhoid bacilli which have been given an exposure in the electron microscope just sufficient to show properly the collodion background and such small details on it as the bacterial flagella, both intact and fragmented. Though the organisms themselves are underexposed it is nevertheless possible to see something of their surface structure. Figure 13 contains a group of old cells from a culture of *Staphylococcus aureus*. They have been shadowed with chromium and exposed in the electron microscope long enough to bring out much surface detail that is not otherwise seen. The way in which shadow-casting supplements the direct electron micrography of large biological objects such as bacteria is evident from these pictures and others that have been published.[7] Since it concentrates scattering in the superficial layers of the object, it has necessarily the general effect of hiding any inner structural details that may exist. Hence, for the most complete photographic survey of such objects three kinds of photographs should be made: micrographs of the unshadowed preparation, brief exposures, and prolonged exposures of the preparation after shadowing. In this way one obtains information regarding inner structure, structure around the periphery and adjacent to the object, and details of its surface.

In photographs we have published elsewhere of influenza virus particles[16] and of tobacco mosaic virus fibrils[8,16] we have demonstrated the application of the shadow technique to biological entities too small to be seen by optical microscopy. We have also shown that the technique permits the unequivocal photography of the elementary molecular particles of such macromolecular substances as the hemocyanins.[17] Figure 14 is a gold-shadowed preparation (at ten-to-one angle) of a very dilute ultracentrifugally purified solution of the hemocyanin from the horseshoe crab, dried on a collodion sub-

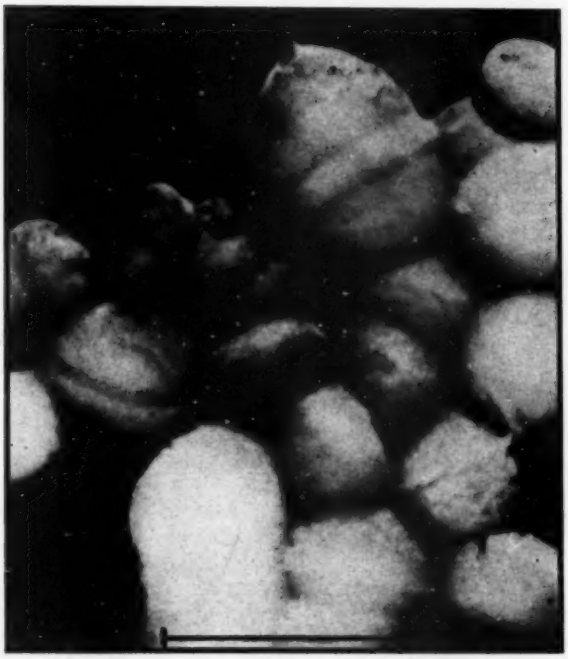

FIG. 13. Chromium-shadowed cells from an old culture of *Staphylococcus aureus*.

[16] R. C. Williams and R. W. G. Wyckoff, Proc. Soc. Exp. Biol. Med. **58**, 265 (1945).
[17] R. C. Williams and R. W. G. Wyckoff, Nature **156**, 68 (1945).

strate. A few molecules distributed singly and in small clusters can be seen lying on the sharply granular collodion background. These molecules, while clearly visible and casting well-defined shadows, are not much bigger than the individual collodion granules; and it would be hard to distinguish much smaller particles from the collodion on which they rest. In other words, the fine structure of the supporting collodion membrane itself sets a lower limit to the size of particles which can be mounted on it and investigated.

The picture on the cover of this Journal is another example of the photography of macromolecules supported on a collodion membrane and shadowed with gold (deposited at a five-to-one angle). The bushy stunt virus,[18] whose elementary particles are the small spherical bodies covering most of the field of the micrograph, is known to crystallize readily from purified solution, and this tendency of the molecules to form regular arrays is very apparent in this figure. Other photographs demonstrate how similarly oriented molecular layers pile one on top of another to produce the three-dimensional symmetrical arrangements of molecules that constitute a true crystal and are responsible for its distinctive properties.

FIG. 14. Gold-shadowed hemocyanin molecules on a collodion substrate.

FIG. 15. A gold replica of hemocyanin molecules on a glass surface. For comparison with Fig. 14.

3. Preshadowed Replicas

It is evident from a photograph such as Fig. 14 that, in order to investigate molecules the size of the granules seen in a collodion film, the molecules should be on a smoother substrate when shadowed. We have found[8,17] that one way to do this is to employ a technique which is essentially that mentioned above under 1*c*. A drop of the solution to be studied is first placed on a piece of clean, polished glass and allowed to evaporate to dryness. The glass with the desiccated material adhering to it is next shadowed obliquely with *ca.* 8A of gold. Since such a thin film is too fragile to be handled directly, it is backed by the usual thin film of collodion or Formvar. The polymer and the metal films are then stripped together from the glass and mounted on a specimen screen. Figure 15 shows a micrograph

[18] W. C. Price, R. C. Williams, and R. W. G. Wyckoff, Science 102, 277 (1945); Arch. Biochem. In press.

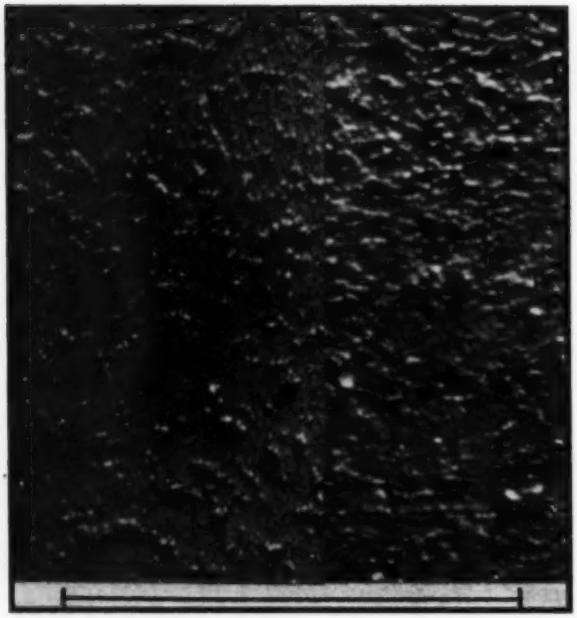

FIG. 16. A gold replica of the cellulose molecular fragments from collodion, on a glass surface.

of a preshadowed replica of limulus hemocyanin molecules for comparison with Fig. 14. The molecules themselves appear equally well defined and of the same size on both photographs, but since the collodion was not metal-shadowed in the replica preparation for Fig. 15, its granular fine structure is not brought out. Obviously, far smaller particles can be distinguished and photographed on the smooth background of Fig. 15 than on a pebbly one such as that of Fig. 14.

Examination of a photograph of this type immediately raises the question of whether or not the particles that are being studied are removed with the stripped films. When dealing with objects as large as bacteria we have found that they sometimes are retained in the replica and sometimes left on the glass; which is the case in any particular instance is obvious from the opacity of the image in the electron microscope. With very small particles like the molecules of hemocyanin it makes no practical difference which is true because the electron scattering power of the metal film greatly exceeds that of the particles themselves.

Preshadowing also makes it possible to study the intimate structure of collodion and of other highly polymerized substances which must be dissolved in organic solvents that would attack the materials ordinarily used as substrates. This application is illustrated in Figs. 16 and 17. Figure 16 shows the nitrated cellulose fragments that make up collodion, as photographed in this way. The object for the left half of Fig. 16 was collodion very greatly diluted with amyl acetate and spread on glass to dry. The molecular fragments are thread-like aggregates, of various lengths, of the same granules that cover the entire surface of Fig. 14. For the right half of Fig. 16 the collodion solution was not quite so dilute. It shows how, in the formation of a continuous film, these beaded threads pack together with their long axes parallel. At the top of this figure the cellulose threads are widely spaced; towards the bottom the film is nearly continuous.

A preshadowed gold replica (at a ten-to-one angle) of polystyrene dissolved in ethyl bromide has been photographed to yield Fig. 17. The fragments strewn over the glass background vary much more in size than do those seen in the collodion photographs and some of them are of an

FIG. 17. A gold replica of polystyrene molecular fragments on a glass surface.

exceedingly small cross section. Measurements of shadow lengths indicate that some are not more than 15A high. Though it may not be too apparent in the print, inspection of the original negatives shows that the large droplets on this and other photographs are aggregates of the smaller fragments such as those of Fig. 17. It is clear from our experience with many preshadowed replicas that the minimum of particle size which can be detected on them is now set by the smoothness and cleanliness of the glass surface employed. At least for the very small areas needed for this type of work, glass can be found and cleaned so as to be free from abrupt variations of surface elevation within an amount not exceeding five to 10A, as judged by observed shadow lengths, and hence it can be concluded that electron microscopy makes it feasible to detect the existence of sharply defined objects of this range of height.

The Electrical Resistance of Iron Wires and Permalloy Strips at Radiofrequencies

ALVA W. SMITH, J. H. GREGORY,* AND J. T. LYNN**
Mendenhall Laboratory of Physics, The Ohio State University, Columbus, Ohio
(Received September 22, 1945)

The ratio of a.c. to d.c. resistances of iron wires and permalloy strips has been measured in the frequency range 1.5–6.0 megacycles per sec. Empirical equations obtained are compared with existing theoretical equations derived on the assumption of constant permeability.

I. INTRODUCTION

WHEN an electric current flows through a cylindrical conductor in a direction parallel to the axis of the cylinder, magnetic flux lines are set up in circular paths concentric with the axis. If the current is alternating, the time variations of this magnetic flux induce voltages in closed paths in the radial planes of the cylinder. The direction of these induced voltages is such as to decrease the longitudinal current in cylindrical elements of small radii and increase it in elements of larger radii. Thus eddy currents cause the current density to be a maximum at the surface and to decrease as the distance from the surface is increased. As a result of the concentration of current near the surface of the conductor, the a.c. resistance of the conductor is greater than the d.c. resistance. The phenomena here described are usually referred to as skin effect. Since the induced voltages in the radial planes are proportional to the time-rate of change of magnetic flux and the eddy currents produced by these voltages are proportional to the conductivity of the conductor, skin effect phenomena become more pronounced with increase in frequency, magnetic permeability, and electrical conductivity. An increase in any or all of these factors results in a decrease in the depth of penetration of the current into the conductor and an increase in the ratio of a.c. to d.c. resistance. This statement applies also to conductors of rectangular sections or of other configurations.

Exact formulas for the a.c. to d.c. resistance ratio for straight conductors of circular cross section have been developed by Maxwell, Heaviside, Kelvin, and Rayleigh. By the application of Maxwell's field equations and Ohm's law, this ratio is expressed in terms of a zero-order Bessel function of an argument involving the square root of the product of frequency, permeability, and conductivity.[1] For values of this argument of ten or greater, the solution reduces to the approximate formula

$$R/R_0 = 0.25 + 1.57d(f\mu\sigma/10^8)^{\frac{1}{2}}, \qquad (1)$$

in which d is the diameter of the wire in cm; μ the

* Now at Massachusetts Institute of Technology, Cambridge, Massachusetts.
** Now at North Carolina State College of Agriculture and Engineering, Raleigh, North Carolina.

[1] N. W. McLachlan, *Bessel Functions for Engineers* (Oxford Press, New York, 1934), p. 135; August Hund, *High Frequency Measurements* (McGraw-Hill Book Company, Inc., New York, 1933), p. 263; S. Ramo and J. R. Whinnery, *Fields and Waves in Modern Radio* (John Wiley and Sons, New York, 1944), p. 213.

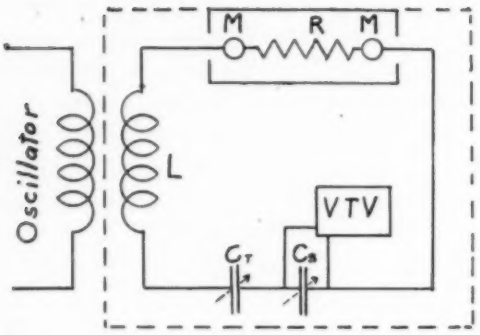

FIG. 1. Plan of the resonant measuring circuit.

magnetic permeability in gauss-oersted^{-1}; and σ the conductivity in mho cm^{-1}.

In the derivation of this formula, the permeability is assumed to be constant. For nonferromagnetic substances this assumption is valid; for ferromagnetic substances its validity is questionable.

The derivation of a similar formula for conductors of other than circular section has presented considerable mathematical difficulty. Strutt[2] has obtained a formula for conductors of constant permeability and with cylindrical cross section. His expression is

$$R/R_0 = A + Bf^{\frac{1}{2}}, \qquad (2)$$

where A and B are constants and f is the frequency. Cockcroft[3] has obtained a similar result for conductors of rectangular cross section.

In this paper we are reporting values of the skin-effect resistance ratio for iron wires and permalloy strips in the frequency range 1.5–6.0 megacycles per second.

II. METHOD

The substitution method was used in determining the resistance of each specimen at a given frequency by comparison with the resistances of a set of standards made of No. 28 B.S. constantan wire. Essential features of the apparatus, exclusive of power supplies, oscillator, and General Radio wave meter, type 724-A, are shown in Fig. 1. A Western Electric 305-A tube was used in a Hartley circuit to supply high frequency power through inductive coupling to the resonant circuit. Tests with the wave meter indicated that the output of the oscillator was essentially free from harmonics. The resonant circuit consisted of an interchangeable inductance L made of quarter-inch copper tubing, the two condensers C_s and C_T, the mercury cups M for receiving the removable resistance R, and the vacuum-tube voltmeter VTV. Fine adjustment of coupling between the oscillator and L was obtained by the use of a worm-drive to rotate L. Each part of the measuring circuit was shielded to prevent unwanted coupling between parts. Tuning was accomplished by means of the standard air condenser C_T, and resonance was indicated by the vacuum-tube voltmeter connected to the terminals of C_s. The circuit of the vacuum-tube voltmeter was of the conventional bridge type in which the vacuum tube acts as one of the bridge arms. In this circuit, a 6 C 6 tube was used as a biased detector.

During a series of measurements at a given frequency, the output of the oscillator, the coupling between it and the resonant circuit, and the setting of C_s were kept constant. The resistance standards and the test samples were connected one at a time to the circuit through the mercury cups to form the resistance R. Condenser C_T was varied until the vacuum-tube voltmeter indicated a maximum current in the circuit. The graph obtained by plotting voltmeter readings against the known resistances of the standards was a straight line. From this graph the values of the resistances of the test samples were obtained by interpolation. A similar procedure was used at each frequency at which measurements were made.

The d.c. resistances of test samples and standards were determined by means of a Mattiessen and Hockin bridge.

Corrections for variations of the resistances of the constantan standards with frequency, amounting to a maximum of 3 percent at 6 megacycles per sec., were applied.

III. DESCRIPTION OF STANDARDS AND TEST SPECIMENS

A set of standard resistances was constructed to cover the range of resistances of the test samples. Suitable lengths of No. 28 B.S. constantan wire were used in making the set. Each

[2] M. J. O. Strutt, *Electrotechmische Nachrechitentechnik* (1931), Vol. 8, p. 269.
[3] J. D. Cockcroft, Proc. Roy. Soc. [A], **122**, 533 (1929).

standard was made by soldering each end of the wire to a short section of quarter-inch copper tubing. This resistance element was placed in a straight glass tube and sealed in place at the ends with wax. The protruding ends of the copper tubing were bent to fit into the mercury cups and amalgamated. Lengths of wire in this set ranged from 1.6 to 17 cm.

The test specimens were similarly mounted. The iron wires were cut from chemically pure stock, and the lengths varied from 3.4 to 15.2 cm.

The permalloy samples were cut from a sheet of 78.5 permalloy, having a composition of 78.5 percent nickel and 21.5 percent iron. Samples designated as PA-1 and PA-2 were annealed by heating in a closed electric furnace to 1000°C and cooled with the furnace over an eight-hour period. Samples designated as PQ-1 and PQ-2 were heated to 1000°C, but were withdrawn to cool quickly in the air when the temperature of the furnace had dropped to 600°C. The sample marked PU was not given any heat treatment.

IV. RESULTS AND CONCLUSIONS

Figure 2 shows the a.c. to d.c. resistance ratio as a function of the square root of the frequency in megacycles per sec. for iron wires of the indicated diameters. The empirical equation of these curves is

$$R/R_0 = 0.4 + 1.57d(f\mu\sigma/10^3)^{\frac{1}{2}}, \qquad (3)$$

which agrees, within the limits of experimental error, with the theoretical Eq. (1) above. The electrical conductivities were determined from the dimensions and the d.c. resistances of the specimens. The values of magnetic permeabilities were then calculated from the empirical equation. Results are given in Table I.

TABLE I. Data and computed constants for iron wires.

Diam. cm	Length cm	R_0 ohm	σ ohm cm^{-1}	μ gauss-oersted^{-1}
0.1019	15.2	0.0204	9.2×10^4	83
0.0823	15.5	0.0311	9.3	77
0.0406	5.0	0.0482	8.0	82
0.0201	3.4	0.0956	11.2	80

The linearity of the curves in Fig. 2 indicates that, with small currents of a few milliamperes, the permeability of each specimen can be regarded as constant within this range of frequencies. Moreover, the deviations of the values of permeability of the individual wires from the mean value were within the limits of experimental error.

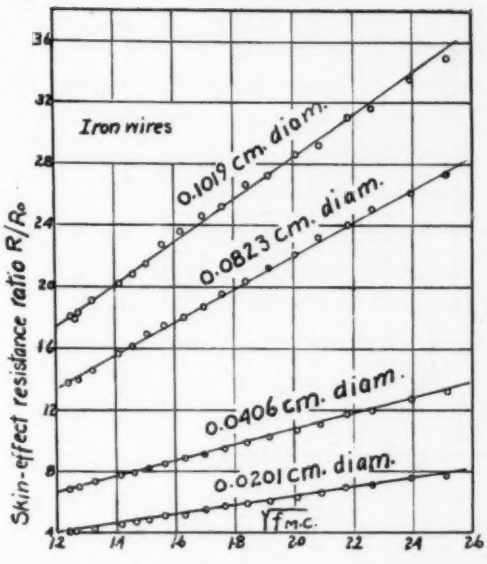

FIG. 2. Ratio of a.c. to d.c. resistance *versus* the square root of the frequency in megacycles per second.

The absence of maxima or minima from the curves of Fig. 2 indicates the absence of an anomaly in permeability at 100 meters wavelength reported by Mitiaev.[4] Our results are in agreement with those of Wait, Brickwedde, and Hall[5] and those of Strutt and Knoll[6] in that no such anomalies were found.

In Figs. 3 and 4, the a.c. to d.c. resistance

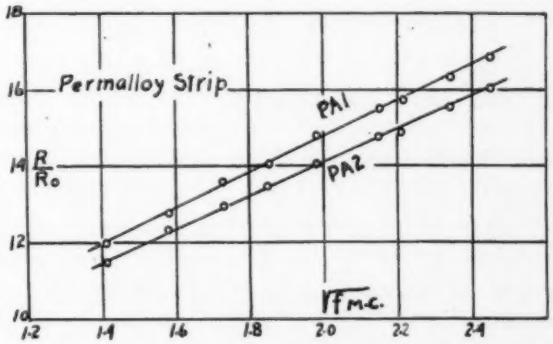

FIG. 3. Ratio of a.c. to d.c. resistance *versus* the square root of the frequency in megacycles per second. Annealed samples.

[4] W. K. Mitiaev, Zeits. f. Physik **38**, 716 (1926).
[5] G. R. Wait, F. G. Brickwedde, and E. L. Hall, Phys. Rev. **32**, 967 (1928).
[6] M. J. O. Strutt and K. S. Knoll, Physica [7] **2**, 145 (1940).

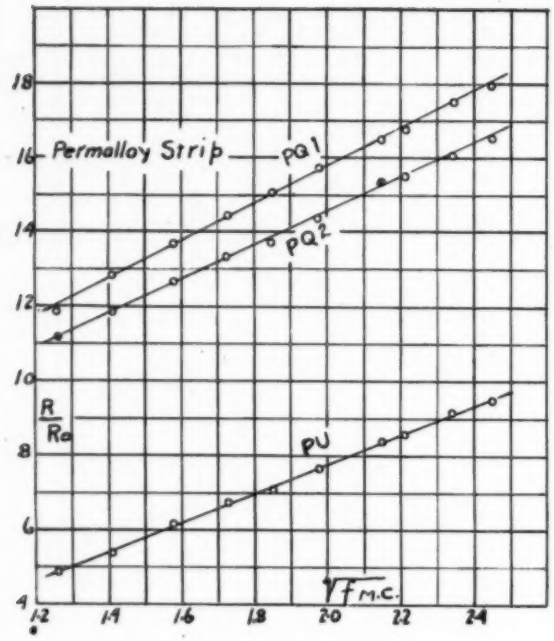

FIG. 4. Ratio of a.c. to d.c. resistance *versus* the square-root of the frequency in megacycles per second. PQ-1 and PQ-2 quenched samples; PU without heat treatment.

ratios for permalloy strips are plotted as ordinates and the square root of the frequencies, in megacycles per sec., as abscissas. The linearity of the curves indicates that for each specimen the permeability was essentially constant over this frequency range. The general form of equation to fit these data is that of Eq. (2). A more detailed equation in conformity with Cockcroft's theory is

$$R/R_0 = A + f\left(\frac{a}{b}\right)1.12\left(\frac{fab\sigma\mu}{10^3}\right)^{\frac{1}{2}}, \qquad (4)$$

in which A is an empirical constant for each specimen; f is the frequency in megacycles per sec.; σ is the conductivity in ohm cm^{-1}; μ is the magnetic permeability; a is the width and b the thickness of the strip in cm; and $f(a/b)$ is a function obtained from Cockcroft's theoretical curves. In attempting to check the agreement between the theoretical values of this function and empirical values for copper calculated from the limited data in the literature, Cockcroft found that the experimental values were a little over half the theoretical values. As a further check on this point, we made some supplementary measurements on two copper strips and obtained the data and results given in Table II.

TABLE II. Comparison of theroetical and experimental values of $f(a/b)$ for copper strips.

$f^{\frac{1}{2}}$	R/R_0	a	b	σ	$f(a/b)$ exp.	$f(a/b)$ theor.
2.4	1.45	0.15	0.0026	56×10^4		
1.4	1.20				0.48	0.72
2.4	1.525	0.11	0.0026	54		
1.4	1.235				0.66	0.79

The experimental values of $f(a/b)$ from these data are less than the theoretical values, but the disparity is somewhat less than that calculated by Cockcroft. Since the depth of penetration in our copper strip was greater than the half thickness of the strip, it is probable that we cannot come to a definite conclusion as to the reliability of the theoretical values of $f(a/b)$.

However, if we assume the theoretical values of this function to be correct, using Eq. (4), we can calculate from our measurements on permalloy the permeabilities of the strips. Data and computed values are recorded in Table III.

TABLE III. Data and computed constants for permalloy strips.

	a	b	σ	$f(a/b)$ theor.	μ	A
PA-1	0.15	0.040	5.2×10^4	1.52	24	5.4
PA-2	0.11	0.040	4.9	1.62	29	5.2
PQ-1	0.17	0.040	4.9	1.50	27	5.8
PQ-2	0.12	0.040	4.6	1.60	30	5.4
PU	0.10	0.042	4.0	1.66	34	−0.05

If Cockcroft's theoretical values of $f(a/b)$ for an infinite strip are used, the values of μ will be of the order of twice those in the table. Empirical values of the constant A are given in the table. The values of this constant do not show large variations among the heat-treated samples, but these vary widely from that of the untreated sample. No theoretical basis for predicting the value of this constant has been found. The relatively simple form of the empirical equation supports the hope that a definite physical meaning can be assigned to the constant A and Cockcroft's function $f(a/b)$.

Liquid Rise in a Capillary Tube

WESLEY E. BRITTIN
Department of Physics, University of Colorado, Boulder, Colorado

(Received August 20, 1945)

A theory of the dynamics of capillary rise is developed by making certain assumptions as to the nature of the motion of the liquid in the tube. The most important assumptions are that the same forces act on the liquid when it is in an accelerated state of motion as when it is in a steady state, that the surface tension is constant, that the angle of contact between the meniscus of the liquid and the tube wall is constant, and that the wetting of the tube is not a rate-determining factor of the motion. This theory leads to a second-order non-linear differential equation, the solution of which represents the motion of the liquid in the tube. A formal solution of the differential equation is obtained in the form of a double Dirichlet series. Approximations to the series are compared with experimental data, and it is concluded that the agreement between theory and experiment is satisfactory.

INTRODUCTION AND STATEMENT OF THE PROBLEM

C. DECHARME has investigated experimentally and theoretically the motion of a liquid in a capillary tube. The theory[1] of Decharme is somewhat unsatisfactory because of doubtful assumptions and analysis used, and because the final equation of the motion[2] has three empirical constants which must be evaluated before the equation can be used. An experiment must be performed before the theory can be applied, which defeats at least one purpose of the theory.

W. A. Rense[3] has used a stroboscope and motion picture camera to photograph the ascent of water in a capillary tube, and has derived a semi-empirical equation for the motion of the liquid in the tube. G. Pickett[4] has shown that the theory of Rense is incorrect, and has derived a differential equation for the motion of the liquid which takes into account most of the important forces acting on the liquid. Pickett expressed the solution of his differential equation in terms of an asymptotic relation valid as the time approaches zero, and a finite difference equation valid for the time greater than zero. In the present paper a differential equation for the motion of the liquid in the tube is set up, and a method of solution is discussed. The results of the theory are then compared with experiment. The problem may be stated as follows:

A capillary tube of radius r is touched to the surface of a liquid of density ρ, surface tension σ, and viscosity μ at time $t=0$. Let Z be the extent of rise of the surface of the liquid, measured to the bottom of the meniscus, at time $t \geqslant 0$, and α the angle that the axis of the tube makes with the horizontal. The problem is then to determine the extent of rise, Z, as a function of the time, t; $Z=Z(t)$.

THE DIFFERENTIAL EQUATION OF MOTION

An exact hydrodynamical theoretical treatment of the problem would be difficult and has not been attempted. Rather, simplifying assumptions are made in order to obtain an ordinary differential equation for the motion. It is assumed that the same forces act on the liquid when it is in an accelerated state as when it is in a steady state. The amount of liquid above the bottom of the meniscus is neglected which enables one to write $\pi r^2 \rho Z(dZ/dt)$ for the momentum of the liquid in the tube.

The Poiseuille viscous force for streamline flow is $-8\pi\mu Z(dZ/dt)$,[5] and the component of the weight along the tube is $-\pi r^2 \rho g Z \sin \alpha$, where g is the gravitational force per unit mass. The surface tension force which is responsible for the rise is given by $2\pi r\sigma \cos \vartheta$ where ϑ, the average angle of contact between the surface of the liquid and the wall of the tube, is assumed constant. The forces mentioned above were taken into account by Pickett.

The end of the tube, assumed flat, gives rise to some turbulent flow in the neighborhood of the opening which produces additional drag forces on the liquid. The end-effect drag will be taken to be

[1] C. Decharme, Ann. Chim. Phys. **23**, 228–242 (1872); **29**, 415–425, 564–569 (1873); **30**, 145–207, 318–342 (1874).
[2] C. Decharme, Ann. Chim. Phys. **39**, 318–342 (1874).
[3] W. A. Rense, J. App. Phys. **15**, 436–437 (1944).
[4] G. Pickett, J. App. Phys. **15**, 623 (1944).
[5] R. von Mises and K. O. Fredricks, *Fluid Dynamics* (Brown University, Providence, Rhode Island, 1941), p. 140.

of magnitude $\frac{1}{4}\pi r^2\rho(dZ/dt)^2$ for the fluid entering the tube.[6,7] The viscous force brought about by the motion of air in the upper part of the tube is neglected, since it depends upon the density of the air which is small. For extremely long tubes or if the velocity were high, the effect of air could not be neglected. It is further assumed that the rate of wetting of the tube is sufficiently rapid to be insignificant as a factor in the rate of rise of the liquid.

The assumption of streamline flow can be given justification by consideration of the maximum Reynolds number, $Re_{\max}$, for the flow. The Reynolds number, Re, for liquid flow in a tube is defined by

$$Re \equiv (2\rho r/\mu)(dZ/dt),$$

and if this dimensionless ratio is less than a certain critical value, $Re < Re_c \sim 2000$, streamline motion is the rule. The maximum velocity of the liquid is shown below to be

$$(dZ/dt)_{t\to 0} = [(8\sigma \cos\vartheta/5\rho r)]^{\frac{1}{2}},$$

making the maximum Reynolds number

$$Re_{\max} = [(32\rho r\sigma \cos\vartheta/5\mu^2)]^{\frac{1}{2}}.$$

Taking

$$r = 0.05 \text{ cm}, \quad \rho = 1 \text{ g cm}^{-3}, \quad \sigma\cos\vartheta = 75 \text{ dyne cm}^{-1}, \quad \text{and} \quad \mu = 0.005 \text{ poise},$$

$$Re_{\max} \sim 1000 < Re_c,$$

which shows that even for this extreme case the condition for streamline flow is satisfied.

Under the foregoing assumptions Newton's second law of motion yields the following differential equation for the motion of the liquid in the capillary tube:

$$Z\left(\frac{d^2Z}{dt^2}\right)+\frac{5}{4}\left(\frac{dZ}{dt}\right)^2+bZ\left(\frac{dZ}{dt}\right)+cZ+d=0, \quad t>0, \tag{1}$$

where

$$b \equiv \frac{8\mu}{\rho r^2}, \quad c \equiv g\sin\alpha, \quad \text{and} \quad d \equiv -\frac{2\sigma\cos\vartheta}{\rho r}.$$

THE FORMAL SOLUTION OF THE DIFFERENTIAL EQUATION OF MOTION

Assume that the solution of the differential Eq. (1) can be represented by the function series

$$Z=\sum_{i=0}^{\infty}\varphi_i(t)\lambda^i, \tag{2}$$

where λ is an arbitrary parameter independent of t, and the functions $\varphi_i(t)$ are to be determined.[8] When the series (2) is substituted into Eq. (1) there results

$$\sum_{i=0}^{\infty}\{\alpha_i+\tfrac{5}{4}\beta_i+b\gamma_i+c\varphi_i\}\lambda^i+d\doteq 0, \tag{3}$$

where

$$\alpha_i \equiv \sum_{k=0}^{i}\varphi_k\varphi''_{i-k}, \quad \beta_i \equiv \sum_{k=0}^{i}\varphi_k'\varphi'_{i-k}, \quad \gamma_i \equiv \sum_{k=0}^{i}\varphi_k\varphi'_{i-k},$$

and primes denote differentiation with respect to the independent variable time. By equating the coefficient of each λ^i to zero, one obtains the set of differential equations for the $\varphi_i(t)$,

$$\varphi_0\varphi_0''+\tfrac{5}{4}\varphi_0'^2+b\varphi_0\varphi_0'+c\varphi_0+d=0, \tag{4}$$

---

[6] W. H. McAdams, *Heat Transfer* (McGraw-Hill Book Company, Inc., New York, 1942), pp. 121–122.
[7] H. J. Hughes and A. T. Safford, *Hydraulics* (The Macmillan Company, New York, 1911), p. 298.
[8] The use of similar function series for the solution of non-linear equations is discussed by H. Bateman, *Partial Differential Equations of Mathematical Physics* (Dover Publications, New York, 1944), p. 497.

and

$$\alpha_i+\tfrac{5}{4}\beta_i+b\gamma_i+c\varphi_i=0, \quad i>0. \tag{5}$$

For the present, the case $c=0$ will be excluded, which restricts the motion to non-horizontal flow. For a solution of (4) take

$$\varphi_0=-d/c, \quad c\neq 0. \tag{6}$$

If the solution (6) is used for φ_0 in (5), it follows that the differential equation for φ_i, $i>0$, is

$$\varphi_i''+b\varphi_i'+\frac{c}{\varphi_0}\varphi_i=-\frac{1}{\varphi_0}\sum_{k=1}^{i-1}\{\varphi_k\varphi''_{i-k}+\tfrac{5}{4}\varphi_k'\varphi'_{i-k}+b\varphi_k\varphi'_{i-k}\}. \tag{7}$$

Put

$$F_i(t)\equiv-\frac{1}{\varphi_0}\sum_{k=1}^{i-1}\{\varphi_k\varphi''_{i-k}+\tfrac{5}{4}\varphi_k'\varphi'_{i-k}+b\varphi_k\varphi'_{i-k}\}, \quad i>1. \tag{8}$$

Then if the roots r_1 and r_2 of the quadratic equation

$$x^2+bx+c/\varphi_0=0 \tag{9}$$

are distinct, the general solution of (7) is

$$\varphi_i(t)=\int_0^t G(t-\tau)F_i(\tau)d\tau+C_i\exp(r_1t)+D_i\exp(r_2t), \tag{10}$$

where

$$G(t)\equiv\frac{1}{r_1-r_2}\{\exp(r_1t)-\exp(r_2t)\},$$

and C_i and D_i are arbitrary constants. The solution of the homogeneous part of (7) is the same for all $i>0$. Therefore without any loss of generality all of the C_i and D_i, $i>1$, may be set equal to zero,

$$C_i=D_i=0, \quad i>1.$$

Putting $\lambda=1$ in (2) there results

$$Z=\varphi_0+C_1\exp(r_1t)+D_1\exp(r_2t)+\sum_{i=2}^{\infty}\int_0^t G(t-\tau)F_i(\tau)d\tau, \tag{11}$$

which, if convergent, represents the general solution of (1). If the roots of Eq. (10) are equal $r_1=r_2\equiv r$, then the general solution of (7) is

$$\varphi_i(t)=\int_0^t H(t-\tau)F_i(\tau)d\tau+C_ie^{rt}+D_ite^{rt}, \tag{12}$$

where $H(t)\equiv te^{rt}$, and C_i and D_i are arbitrary constants. As before, all C_i and D_i with the exception of C_1 and D_1 are set equal to zero $C_i=D_i=0$, $i>1$. For equal roots then, putting $\lambda=1$ in (2) results

$$Z=\varphi_0+C_1e^{rt}+D_1te^{rt}+\sum_{i=2}^{\infty}\int_0^t H(t-\tau)F_i(\tau)d\tau, \tag{13}$$

which, if convergent, is the general solution of (1). It is very unlikely in practice that $r_1=r_2$, so the solution (11) will be the usual one, rather than (13).

The construction of the series (11) requires the evaluation of the integrals

$$\int_0^t G(t-\tau)F_i(\tau)d\tau$$

which are all elementary, but become more and more cumbersome as i increases. Since the only

terms which appear in the series are of the type $\alpha_{k,l}\exp(kr_1t)\exp(lr_2t)$ where $\alpha_{k,l}$ is a constant and k and l are integers, the Dirichlet series

$$Z=\sum_{m,n=0}^{\infty}\alpha_{m,n}\exp[(mr_1+nr_2)t] \tag{14}$$

can be used to represent the function series (11). To evaluate the coefficients $\alpha_{m,n}$, substitute the series (14) into the differential Eq. (1), whence

$$\sum_{m,n=0}^{\infty}\{\beta_{m,n}+\tfrac{5}{4}\gamma_{m,n}+b\delta_{m,n}+c\alpha_{m,n}\}\exp[(mr_1+nr_2)t]+d=0, \tag{15}$$

where

$$\beta_{m,n}\equiv\sum_{k,l=0}^{m,n}\alpha_{k,l}\alpha_{m-k,n-l}(kr_1+lr_2)^2,\quad \gamma_{m,n}\equiv\sum_{k,l=0}^{m,n}\alpha_{k,l}\alpha_{m-k,n-l}(kr_1+lr_2)\{(m-k)r_1+(n-l)r_2\},$$

and

$$\delta_{m,n}\equiv\sum_{k,l=0}^{m,n}\alpha_{k,l}\alpha_{m-k,n-l}(kr_1+lr_2).$$

Equation (1) will be satisfied formally if

$$\beta_{0,0}+\tfrac{5}{4}\gamma_{0,0}+b\delta_{0,0}+c\alpha_{0,0}+d=0, \tag{16}$$

and

$$\beta_{m,n}+\tfrac{5}{4}\gamma_{m,n}+b\delta_{m,n}+c\alpha_{m,n}=0,\quad \binom{m}{n}\neq\binom{0}{0}. \tag{17}$$

Therefore

$$\alpha_{0,0}=-d/c,\quad c\neq0, \tag{18}$$

$$\alpha_{1,0}\left(r_1^2+br_1+\frac{c}{\alpha_{0,0}}\right)=0, \tag{19}$$

$$\alpha_{0,1}\left(r_2^2+br_2+\frac{c}{\alpha_{0,0}}\right)=0, \tag{20}$$

and

$$\alpha_{m,n}=\frac{-1}{\alpha_{0,0}\{(mr_1+nr_2)^2+b(mr_1+nr_2)+c/\alpha_{0,0}\}}$$

$$\times\sum_{k,l=0}^{m,n}{}'\alpha_{k,l}\alpha_{m-k,n-l}\{-\tfrac{1}{4}(kr_1+lr_2)^2+(kr_1+lr_2)[\tfrac{5}{4}(mr_1+nr_2)+b]\},\quad \binom{m}{n}\neq\begin{cases}\binom{0}{0}\\ \binom{0}{1},\\ \binom{1}{0}\end{cases} \tag{21}$$

where $\sum'$ denotes summation omitting the term $\binom{k}{l}=\binom{m}{n}$. If $\alpha_{1,0}\neq0$, and $\alpha_{0,1}\neq0$, r_1 and r_2 must be the roots of the quadratic

$$x^2+bx+c/\alpha_{0,0}=0, \tag{22}$$

which was to be expected according to Eq. (9), since by (6) and (18) $\alpha_{0,0}=\varphi_0$. If the Dirichlet series (14) is convergent, it represents the general solution of (1) for the case of distinct roots, $r_1\neq r_2$. The

recurrence relation (21) gives all of the coefficients $\alpha_{m,n}$, in terms of the two arbitrary and independent constants $\alpha_{0,1}$, and $\alpha_{1,0}$.

The evaluation of the constants $\alpha_{0,1}$ and $\alpha_{1,0}$ is made possible by means of the initial conditions

$$Z(0)=0, \quad (dZ/dt)_0=V_0. \tag{23}$$

The initial velocity V_0 is assumed to be finite as it must be physically, and thus is obtained from the differential equation by setting $Z=0$,

$$V_0=(-\tfrac{4}{3}d)^{\frac{1}{3}}. \tag{24}$$

In an actual problem one must use an approximation to the series (14), and the character of the roots r_1 and r_2 determine to a great extent the number of terms required for a good approximation. The roots r_1 and r_2 will be real and negative if $b^2-4c/\alpha_{0,0}>0$, and a simple calculation shows that for most liquids r_1 and r_2 will be real and negative if the capillary tube has a radius in the neighborhood of 0.010 cm or less. The following treatment applies to real roots, and r_1 will be taken to be of smaller magnitude than r_2, $|r_1|<|r_2|$. If $|r_2|$ is large compared to $|r_1|$, a good approximation may be had by using only one term in r_2 and n terms in r_1,

$$Z\sim\alpha_{0,0}+\alpha_{0,1}\exp(r_2t)+\sum_{k=1}^{n}\alpha_{k,0}\exp(kr_1t), \tag{25}$$

where n is restricted by $n\leqslant|r_2/r_1|$. By Eq. (21), the coefficient $\alpha_{k,0}$ has a factor $(\alpha_{1,0})^k$, so for convenience define α_k by

$$\alpha_k\equiv\alpha_{k,0}/(\alpha_{1,0})^k \tag{26}$$

Equation (25) then becomes

$$Z\sim\alpha_{0,0}+\alpha_{0,1}\exp(r_2t)+\sum_{k=1}^{n}\alpha_k(\alpha_{1,0})^k\exp(kr_1t). \tag{27}$$

The evaluation of $\alpha_{0,1}$ and $\alpha_{1,0}$ is made by utilizing relations (23) and (24), from which it is evident that $\alpha_{0,1}$ and $\alpha_{1,0}$ must satisfy

$$\alpha_{0,0}+\alpha_{0,1}+\sum_{k=1}^{n}\alpha_k(\alpha_{1,0})^k=0, \tag{28}$$

and

$$r_2\alpha_{0,1}+\sum_{k=1}^{n}r_1k\alpha_k(\alpha_{1,0})^k=V_0. \tag{29}$$

The elimination of $\alpha_{0,1}$ between (28) and (29) gives rise to an algebraic equation of the nth degree in $\alpha_{1,0}$,

$$V_0+r_2\alpha_{0,0}=\sum_{k=1}^{n}(kr_1-r_2)\alpha_k(\alpha_{1,0})^k. \tag{30}$$

The real root of Eq. (30) having the smallest magnitude will be taken as $\alpha_{1,0}$, while the value of $\alpha_{0,1}$ will be obtained directly from (28). The α_k are given by

$$\alpha_k\equiv\frac{-1}{\alpha_{0,0}(k^2r_1^2+kr_1+c/\alpha_{0,0})}\sum_{i=0}^{k-1}\alpha_i\alpha_{k-i}r_1i(-\tfrac{1}{4}r_1i+\tfrac{5}{4}kr_1+b), \quad k>1. \tag{31}$$

Equations (28)–(30) will be subsequently applied to actual physical data.

It is interesting to note that the transformation $(dZ/dt)=1/W$ reduces the original differential Eq. (1) to the first-order equation

$$\left(\frac{dW}{dZ}\right)=-\frac{5}{4}\frac{W}{Z}+bW^2+cW^3+d\frac{W^3}{Z}. \tag{32}$$

The solution of (32) can be used to find t in terms of Z,

$$t=\int W(Z)dZ. \tag{33}$$

COMPARISON OF THEORY WITH EXPERIMENT

If the series (14) is to have any meaning as the solution of the differential equation, it must necessarily converge. The mathematical analysis of the convergence or divergence of the series is encumbered by the fact that the coefficients, $\alpha_{m,n}$, are not known as explicit functions of m and n, but are known only through the multiple-term recurrence relation (21). The difficulty of applying standard convergence tests to the double series (14) is thus apparent.

An indication, but certainly not a proof, of the convergence of the series (14) is obtained by taking an approximation to it using actual physical data, and then comparing the result with experiment. As one example, the data of Rense[3] are used, and the temperature is assumed to be 26°C. A five-term approximation from Eq. (25) is

$$Z\sim\alpha_{0,0}+\alpha_{0,1}\exp(r_2t)+\alpha_{1,0}\exp(r_1t)-\frac{\alpha_{1,0}^2}{\alpha_{0,0}}\left\{\frac{r_1^2+\frac{5}{4}r_1^2+br_1}{4r_1^2+2br_1+c/\alpha_{0,0}}\right\}\exp(2r_1t)$$
$$+\frac{\alpha_{1,0}^3}{\alpha_{0,0}^2}\left\{\frac{r_1^2+\frac{5}{4}r_1^2+br_1}{4r_1^2+2br_1+c/\alpha_{0,0}}\right\}\left\{\frac{5r_1^2+5r_1^2+3br_1}{9r_1^2+3br_1+c/\alpha_{0,0}}\right\}\exp(3r_1t). \tag{34}$$

Using relations (22)–(24), Eq. (34) becomes

$$Z\sim4.633-0.585e^{-66.84t}-2.187e^{-3.165t}-1.037e^{-6.33t}-0.787e^{-9.495t} \tag{35}$$

which is plotted in Fig. 1.

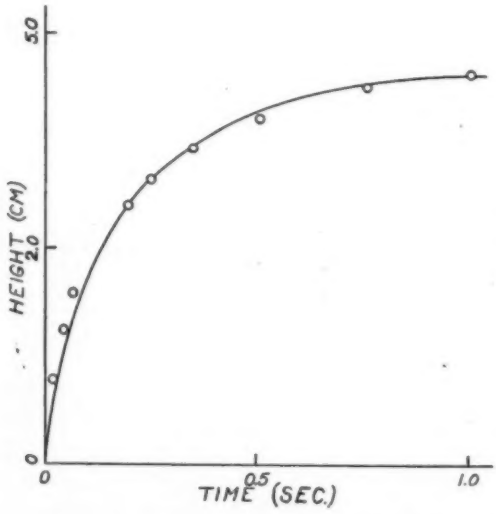

FIG. 1. Rise of water in a vertical tube. Circles represent data of Rense. Solid curve represents Eq. (36).

A further comparison is obtained from the results of Decharme[9] on water rising in a capillary tube inclined at an angle of 45°. The five-term approximation given by Eq. (25) is

$$Z\sim11.745-0.0682e^{-258.4t}-6.108e^{-0.23t}-3.137e^{-0.46t}-2.432e^{-0.69t}. \tag{36}$$

[9] C. Decharme, Ann. Chim. Phys. **30**, 162 (1874).

TABLE I. Rise of pure water in a capillary tube of radius 0.01777 cm, temperature of water 19.5°C, and angle of inclination of the tube 45°.

Time (sec.)	Z (cm) Eq. (36)	Z (cm) Eq. (37)	Z (cm) Eq. (38)	Z (cm) Eq. (39)	Z (cm) Decharme	Time (sec.)	Z (cm) Eq. (36)	Z (cm) Eq. (37)	Z (cm) Eq. (38)	Z (cm) Eq. (39)	Z (cm) Decharme
0	0.00	0.00	0.00	0.00	0.00	8				10.91	10.87
1	3.69	4.19	4.61	4.96	6.20	9				11.09	11.05
2	6.03	6.46	7.00	7.22	7.87	10				11.23	11.20
3	7.59	7.96	8.34	8.52	8.80	12				11.43	11.40
4	8.66	8.96	9.24	9.36	9.48	14				11.55	11.54
5	9.42	9.57	9.84	9.94	9.98	16				11.62	11.62
6	9.97	—	—	10.36	10.36	18				11.67	11.66
7				10.67	10.65	20				11.70	11.70

The six-term approximation is

$$Z\sim 11.745-0.085e^{-258.4t}-5.591e^{-0.23t}-2.629e^{-0.46t}-1.866e^{-0.69t}-1.574e^{-0.92t}. \tag{37}$$

The eight-term approximation is

$$Z\sim 11.745-0.077e^{-258.4t}-5.123e^{-0.23t}-2.207e^{-0.46t}$$
$$-1.435e^{-0.69t}-1.110e^{-0.92t}-0.944e^{-1.15t}-0.849e^{-1.38t}, \tag{38}$$

and finally the ten-term approximation is

$$Z\sim 11.745-0.100e^{-258.4t}-4.906e^{-0.23t}-2.024e^{-0.46t}-1.260e^{-0.69t}$$
$$-0.933e^{-0.92t}-0.761e^{-1.15t}-0.655e^{-1.38t}-0.561e^{-1.61t}-0.545e^{-1.84t}. \tag{39}$$

Table I gives the values of Z as a function of time for the approximations (36)–(39), and for the experimental values obtained by Decharme. It is to be noted that the agreement of the approximations with the experimental values does improve with the number of terms in the approximation.

HORIZONTAL FLOW

For horizontal flow, $\alpha=0$, and Eq. (1) becomes

$$ZZ''+\tfrac{5}{4}(Z')^2+bZZ'+d=0, \tag{40}$$

or

$$(ZZ')'+\tfrac{1}{4}(Z')^2+bZZ'+d=0. \tag{41}$$

If the tube is of small bore, $\frac{1}{4}(Z')^2$ can be neglected, which means that the end-effect drag is neglected, and Eq. (41) is linear in (ZZ'). The solution, neglecting $\frac{1}{4}(Z')^2$, is

$$ZZ'=-de^{-bt}\int e^{bt}dt=-\frac{d}{b}\{1+C_1e^{-bt}\}, \tag{42}$$

where C_1 is a constant of integration. When $t=0$, $(ZZ')=0$, and $C_1=-1$. Integrating (42) one obtanis

$$Z^2=-\frac{2d}{b^2}\{bt+e^{-bt}+C_2\}, \tag{43}$$

where C_2 is a constant of integration. When $t=0$, $Z=0$, and $C_2=-1$, which when substituted into (43) yields

$$Z^2=-\frac{2d}{b^2}\{bt+e^{-bt}-1\}. \tag{44}$$

Substituting $b\equiv 8\mu/\rho r^2$ and $d\equiv -2\sigma\cos\vartheta/\rho r$ into (44), one obtains the approximate solution for

horizontal flow,

$$Z^2=\frac{\rho\sigma r^3\cos\vartheta}{16\mu^2}\left\{\left(\frac{8\mu}{\rho r^2}\right)t+\exp\left[-\left(\frac{8\mu}{\rho r^2}\right)t\right]-1\right\}. \tag{45}$$

If liquid were forced through a capillary tube under pressure, a constant term would be added to d, and if conditions for streamline flow were not violated, the above theory should still be satisfactory. For large values of t, Z^2 is asymptotically linear in t according to Eq. (45), which is in qualitative, if not quantitative, agreement with experiment.[10,11]

[10] J. M. Bell and F. K. Cameron, J. Phys. Chem. **10**, 658–674 (1906).
[11] R. L. Peek and D. A. McLean, Ind. Eng. Chem. Anal. Ed. **6**, 85–90 (1934).

Shunt and Series Sections of Transmission Line for Impedance Matching

C. T. Tai
Cruft Laboratory, Harvard University, Cambridge, Massachusetts

(Received August 20, 1945)

The problem of using shunt and series sections of transmission line as matching devices is here investigated mathematically. By making use of hyperbolic functions the condition of match for both cases can be expressed in a very simple way. Both devices when used alone have a limited range with regard to the impedance to be matched. The exact range within which matching is possible is shown graphically. By using one additional matching network each device can be designed to match impedance of any value. The complete systems still preserve their simplicity in structure.

INTRODUCTION

PARALLEL lines or coaxial lines are often used to transmit power from a generator to a load. In practice, it is desirable to eliminate standing waves on these lines, that is, to make the lines non-resonant. Under this condition the efficiency of transmission along the line is a maximum. A line is non-resonant if it is terminated in an impedance equal to the characteristic impedance of the line. A load impedance not equal to the characteristic impedance of the line can be made to match the line by means of a matching device. This is illustrated in Fig. 1, where Z_s is the load

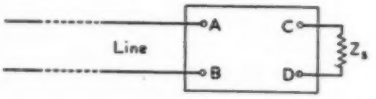

FIG. 1. Matching section for a transmission line.

impedance and $ABCD$ is a matching device. By a proper design of this device the input impedance looking from AB toward the load can be made equal to the characteristic impedance of the line. It is known that shunt sections and series sections when properly designed can be used as matching devices.[1,2] However, little has been published about the limitations of these two devices. The present paper discusses them in detail in two separate parts.

[1] Ronold King, "Transmission line theory and its application," J. App. Phys. **14**, 577 (November, 1943).
[2] Andrew Alford, "High frequency transmission-line network," Elec. Comm. **17**, No. 3, 301 (January, 1939).

PART I

Shunt Sections of Line

General Equations and Their Solutions

The structure of shunt sections of line is shown in Fig. 2. It consists of two sections of line of the same characteristic impedance R_c as the main line, and of length s_1 and s_2. Physically, either branch may be considered as an extension of the main line, with the other branch connected in shunt. It is assumed in the following analysis that radiation from all sections of line is negligible, and that the coupling between lines I and II is so loose that mutual impedance may be neglected. These two assumptions are legitimate if the separation of the wires forming each line is small

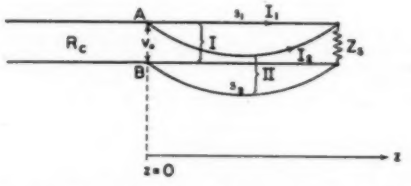

FIG. 2. Shunt section of transmission line for impedance matching.

compared with its length and if the two branches are not very close. Then the current and voltage of either of them, expressed in complex form, satisfy the following two differential equations:

$$dI/ds = -YV, \tag{1}$$

$$dV/ds = -ZI, \tag{2}$$

where Z and Y are complex line constants.

The solution of these two equations in terms of hyperbolic functions is

$$I = C_1 \cosh ks + C_2 \sinh ks, \tag{3}$$

$$V = -Z_c(C_1 \sinh ks + C_2 \cosh ks), \tag{4}$$

where k is the complex propagation constant and Z_c the characteristic impedance of the lines. They are related to Z and Y as follows:

$$k = \alpha + j\beta = (ZY)^{\frac{1}{2}}, \tag{5}$$

$$Z_c = R_c(1 - j\phi_d) = (Z/Y)^{\frac{1}{2}}. \tag{6}$$

It is assumed in the following analysis that attenuation along the two sections of lines is negligible so that the complex constant k is purely imaginary, being equal to $j\beta$, and Z_c is purely resistive, being equal to R_c.

If one defines the complex terminal functions,[1] $\theta = \rho + j\Phi$, for the terminal impedance Z_s, by setting

$$Z_s = R_c \coth \theta, \tag{7}$$

the input impedance looking from AB in Fig. 2 can be found to be

$$Z_{in} = R_c \frac{\cosh^2 \theta \cos \beta s_1 \cos \beta s_2 - \cosh (\theta + j\beta s_1) \cosh (\theta + j\beta s_2)}{\sinh 2\theta - \sinh (2\theta + j\beta(s_1 + s_2)) + j \cosh^2 \theta \sin \beta(s_1 + s_2)}. \tag{8}$$

The condition of match requires that Z_{in}/R_c be equal to unity. Setting Z_{in}/R_c in (8) equal to unity and separating the real and imaginary parts one obtains the following solutions for s_1 and s_2:

$$\tan \beta\left(\frac{s_1 + s_2}{2}\right) = \frac{\cos 2\Phi - e^{-2\rho}}{2 \sin 2\Phi}, \tag{9}$$

$$\tan \beta\left(\frac{s_1 - s_2}{2}\right) = \left[\frac{(5e^{-2\rho} + 3 \cos 2\Phi)(e^{-2\rho} - \cos 2\Phi)}{4(1 - e^{-4\rho})}\right]^{\frac{1}{2}}. \tag{10}$$

These two equations determine completely the length of the two sections for different values of ρ and Φ or different values of Z_s, provided the solutions for s_1 and s_2 are real and positive.

It is to be noted that there is no practical limitation upon the value of ρ and Φ in order to yield a real value of $s_1 + s_2$, since the right-side expression of (9) is always real. But in order that the value of $s_1 - s_2$ be also real, ρ and Φ have to satisfy the following condition,

$$\frac{(5e^{-2\rho} + 3 \cos 2\Phi)(e^{-2\rho} - \cos 2\Phi)}{1 - e^{-4\rho}} \geqslant 0. \tag{11}$$

As results from (7), for each given pair of values of R_s and X_s there is a corresponding pair of values of ρ and Φ, and *vice versa*. The inequality (11), therefore, implies that matching is possible only for those impedances of which the corresponding values of ρ and Φ satisfy this inequality.

In order to carry on the discussion in terms of the more familiar parameters R_s and X_s jointly, it is necessary to review briefly some of the analytical relations between ρ and Φ with R_s and X_s (for a fuller discussion the reader is referred to reference 1). The terminal functions ρ and Φ defined by (7) can be directly expressed in terms of R_s/R_c and X_s/R_c. They are

$$\rho = \tfrac{1}{2} \tanh^{-1}\left[\frac{2r_s}{r_s^2 + x_s^2 + 1}\right], \tag{12}$$

$$\Phi = \tfrac{1}{2} \tan^{-1}\left[\frac{-2x_s}{r_s^2 + x_s^2 - 1}\right], \tag{13}$$

where r_s and x_s are defined for a low-loss line by

$$r_s = \frac{R_s}{R_c}, \quad x_s = \frac{X_s}{R_c}. \tag{14}$$

The values of ρ and Φ may also be determined graphically with sufficient accuracy from a "circle diagram" as discussed in reference 1. This diagram is reproduced in Fig. 3.

The condition of match as expressed by (11) can now be used to find the region in the $r_s - x_s$ plane within which matching is possible. Substituting the values of ρ and Φ given by (12) and (13) into the left side of (11) and setting the resulting expression equal to zero, one obtains the

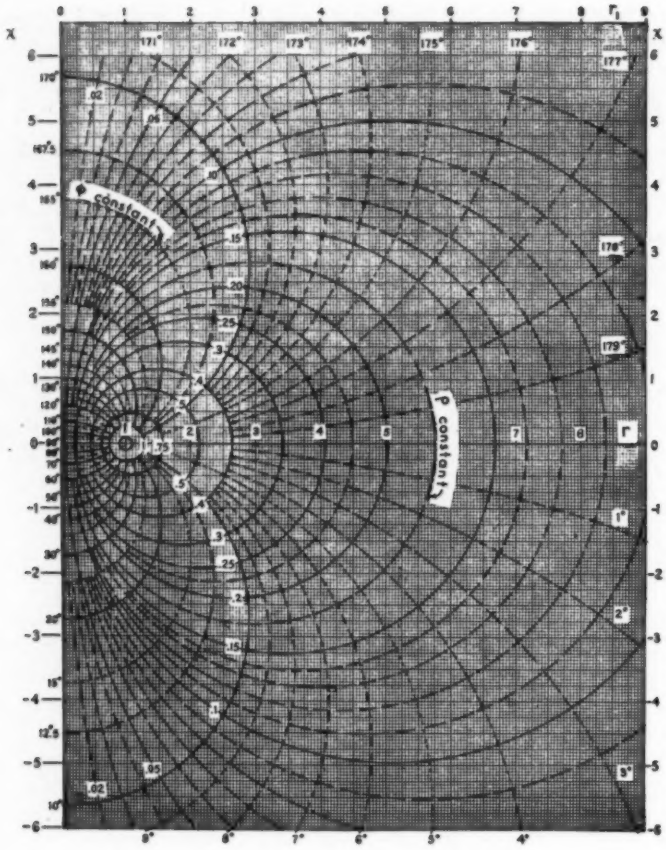

FIG. 3. Circle diagram (from reference 1).

following two equations:

$$r_s = 1, \tag{15}$$

$$4(r_s^2 + x_s^2) - 5r_s + 1 = 0. \tag{16}$$

Equation (15) is the equation of a vertical straight line passing through $r_s = 1$, and (16) is that of a circle with center at $(\frac{5}{8}, 0)$ and of radius equal to $\frac{3}{8}$. These two curves are plotted in Fig. 4. They define two distinct zones in the plane of $r_s - x_s$. Matching is *possible* only for those values if r_s and x_s lie to the *left of the line* $r_s = 1$, *with the region enclosed by the circle* C_{sh} *excluded*. On the other hand, matching is *not possible* by using shunt sections alone if the values of r_s and x_s lie to the *right of the line or inside the circle* C_{sh}.

Shunt Sections with Additional Section of Line

The above analysis deals with shunt sections only and the restrictions thus found are inherent to this type of network. It is obvious, however, that if a simple additional impedance-transforming network be added such that any impedance can be transformed into a value which satisfies the matching condition of the shunt sections, then the limitation no longer exists. The simplest way of doing this is to insert an additional section of line of the same characteristic impedance between the shunt sections and the load, as shown in Fig. 5. It is to be added here that an analysis of this system applying the theorem of conjugate impedance is given in reference 2, where the system is called "re-entrant

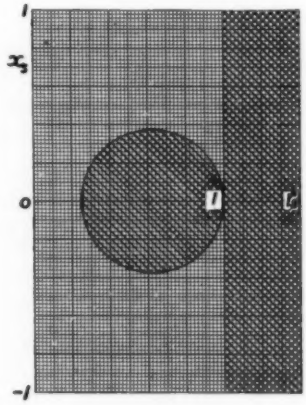

FIG. 4. Loci of match for shunt sections.

lines." But because of the close similarity between the shunt sections and the series section, which will appear in Part II, a more specific term is used in this paper.

Referring to reference 1 it is seen that the values of ρ and Φ corresponding to the impedance looking from CD in Fig. 5 to the right are

$$\begin{cases} \rho_{in} = \rho + \alpha s_3, \\ \Phi_{in} = \Phi + \beta s_3, \end{cases} \tag{17}$$

where s_3 denotes the length of Section III. Since α is assumed to be small, (17) can practically be written as

$$\begin{cases} \rho_{in} = \rho, \\ \Phi_{in} = \Phi + \beta s_3. \end{cases} \tag{18}$$

The only modification of ρ and Φ due to the presence of Section III is therefore a change in Φ only.

Referring back to Figs. 3 and 4, suppose a pair of values of ρ and Φ to be given that corresponds to a point lying outside the region where matching is possible, say, $\rho = 0.5$ and $\Phi = 15°$. Ordinarily, that is, without the insertion of Section III, matching would be impossible. By inserting an additional section of line of electrical length, say, 30°, a shift is made to a new point where $\rho = 0.5$ and $\Phi = 45°$. This new point is well within the domain where matching is possible. It is to be noted that as far as matching is concerned the exact value of s_3 is not critical. But with s_3 so fixed there is only one pair of values s_1 and s_2 that makes the main line non-resonant. Since all the constant-ρ circles have some part of them included in the matching region, it is always possible to shift any given pair of values of ρ and Φ into this region by the insertion of an additional section of line. Any given load Z_s can in this way be matched to a given line.

Graphical Representation of Solutions

For practical purposes, the values of s_1/λ and s_2/λ can be solved for in terms of ρ and Φ from (9) and (10). They are

$$s_1/\lambda = \frac{1}{2\pi}[\tan^{-1} A + \tan^{-1} B], \tag{19a}$$

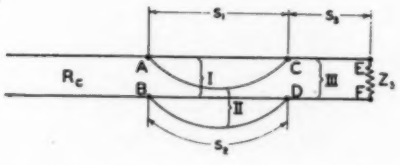

FIG. 5. Shunt sections with additional section of line.

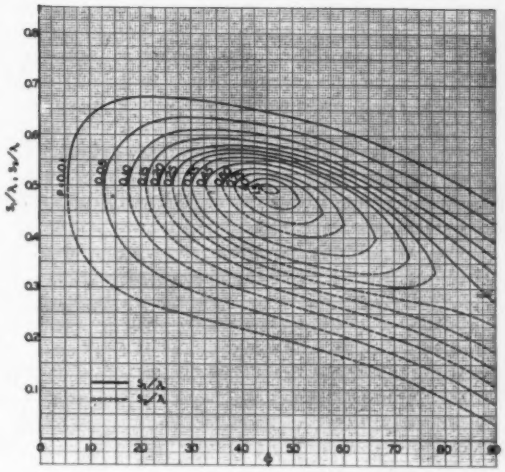

FIG. 6. s_1/λ and s_2/λ *vs.* ρ and Φ.

$$s_2/\lambda = \frac{1}{2\pi}[\tan^{-1} A - \tan^{-1} B], \tag{19b}$$

where A and B are defined by the following equations:

$$A = \frac{\cos 2\Phi - e^{-2\rho}}{2 \sin 2\Phi}; \tag{20a}$$

$$B = \left[\frac{(5e^{-2\rho} + 3\cos 2\Phi)(e^{-2\rho} - \cos 2\Phi)}{4(1 - e^{-4\rho})}\right]^{\frac{1}{2}}. \tag{20b}$$

The values of s_1/λ and s_2/λ are plotted in Fig. 6 for different values of ρ and Φ. The mirror part corresponding to $90° < \Phi < 180°$ is omitted. When ρ and Φ are known s_1 and s_2 can be readily determined from these curves. Numerical examples concerning the design of shunt sections will be given at the end of the paper.

PART II

Series Section of Line

General Solution

It is well known that lines of different characteristic impedance may also be used for matching. This arrangement is usually called a series transformer. From the point of view of its structure and also as a counterpart of the shunt sections described above, the name "series section" will be used. Its structure is shown diagrammatically in Fig. 7, where R_c' and R_c denote, respectively, the characteristic impedance of the line to be matched and that of the line used for matching. It has been derived in reference 1 that if the

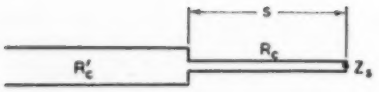

FIG. 7. Series section of transmission line for impedance matching.

attenuation along the line R_c is negligible, the general condition for match is

$$R_c' > R_c \begin{cases} R_c' = R_c \coth \rho, & (21) \\ \beta s = n\pi - \Phi, & (22) \end{cases}$$

$$R_c' < R_c \begin{cases} R_c' = R_c \tanh \rho, & (23) \\ \beta s = \left(\frac{2n+1}{2}\right)\pi - \Phi, & (24) \end{cases}$$

where ρ and Φ denote the terminal functions of the load impedance defined in terms of R_s, X_s, and the characteristic impedance R_c which is the unknown. They are given by (12) and (13). In case of resistive termination both (21–22) and (23–24) with $n=1$ and 0, respectively, reduce to

$$\begin{cases} R_c = (R_c' R_s)^{\frac{1}{2}}, & (25) \\ \beta s = \dfrac{\pi}{2}. & (26) \end{cases}$$

This shows that any purely resistive load can be matched theoretically by choosing a proper value of R_c for the matching line of length $\lambda/4$. A more general case will now be treated in which the load impedance includes reactance as well as resistance. The question is whether it is always possible for any given values of Z_s to find values for R_c and s such that the main line with characteristic impedance R_c' can be made non-resonant.

The explicit solution for R_c in (21) or (23) is

$$R_c = \left[\frac{R_c'(R_s^2 + X_s^2) - R_s R_c'}{R_s - R_c'}\right]^{\frac{1}{2}}. \quad (27)$$

In order for R_c to be real, the following conditions must be satisfied

$$R_s > R_c', \quad R_s^2 + X_s^2 > R_s R_c', \quad (28)$$

$$R_c < R_c', \quad R_s^2 + X_s^2 < R_s R_c'. \quad (29)$$

Condition (28) is always true, while (29) shows that the values of R_s and X_s must lie within certain definite domains for a given value of R_c'. As in the discussion of shunt sections, it is possible to find the regions in the $r_s' - x_s'$ plane within which matching is possible. These regions are bounded by the following curves:

$$r_s' = 1, \quad (30)$$

$$r_s'^2 + x_s'^2 - r_s' = 0, \quad (31)$$

where r_s' and x_s' denote, respectively, R_s/R_c' and X_s/R_c'. Equation (30) is the equation of a vertical straight line passing through $r_s' = 1$ and (31) is that of a circle with center at $(\frac{1}{2}, 0)$ and of radius equal to $\frac{1}{2}$. They are plotted in Fig. 8. As in the shunt case, the curves defined again two distinct zones. Matching is *possible* only for those values of r_s' and x_s' that lie *to the right of the line* $r_s' = 1$, *or within the circle* C_s. On the other hand, matching is *not possible*, using series section alone, if the values of r_s' and x_s' lie *outside the circle and to the left of the line* $r_s' = 1$.

The condition of match for the series section, insofar as R_c is concerned, has been discussed in terms of r_s' and x_s'; the solution for R_c, (27), is also expressed in terms of R_s, X_s, and R_c'. The solutions for s, (22) and (24), however, are still expressed in terms of Φ which is itself a function of R_s, X_s, and R_c. To avoid confusion, it is desirable to obtain an expression for s in terms of R_s, X_s, and R_c' directly. By making use of formula (13), one obtains the following expression of Φ,

$$\Phi = \tfrac{1}{2} \tan^{-1}\left[\frac{-2(X_s/R_c)}{(R_s/R_c)^2 + (X_s/R_c)^2 - 1}\right] = \tfrac{1}{2} \tan^{-1}\left[\frac{-2mx_s'}{r_s'^2 + x_s'^2 - m^2}\right], \quad (32)$$

where m denotes the ratio R_c/R_c' which is given by (27), i.e.,

$$m = \frac{R_c}{R_c'} = \left[\frac{r_s'^2 + x_s'^2 - r_s'}{r_s' - 1}\right]^{\frac{1}{2}}. \quad (33)$$

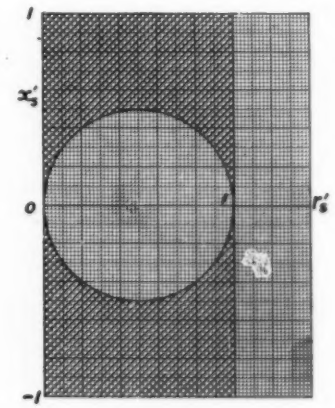

FIG. 8. Loci of match for series section.

The complete solution for R_c and s can then be written as follows,

$$R_c = mR_c' = R_c'\left(\frac{r_s'^2 + x_s'^2 - r_s'}{r_s' - 1}\right)^{\frac{1}{2}}. \tag{34}$$

$$m<1 \quad \left\{\beta s = n\pi - \tfrac{1}{2}\tan^{-1}\left[\frac{-2mx_s'}{r_s'^2 + x_s'^2 - m^2}\right] = n\pi - \Phi, \right. \tag{35}$$

$$m>1 \quad \left\{\beta s = \frac{(2n+1)}{2}\pi - \tfrac{1}{2}\tan^{-1}\left[\frac{-2mx_s'}{r_s'^2 + x_s'^2 - m^2}\right] = \left(\frac{2n+1}{2}\right)\pi - \Phi. \right. \tag{36}$$

The form of solution for s in terms of Φ has been preserved, for it is more convenient as will be apparent in the illustrative example given later.

Series Section with Additional Section of Line

As in the case of shunt sections, the series section also is limited in its application if it is used alone. But here, as before, it is possible to shift the values of ρ' and Φ' (where ρ' and Φ' are the equivalent of r_s' and x_s' so they are defined in terms of R_s, X_s, and R_c', not R_c), practically of Φ' only, by connecting an additional section of line between the series section and the load. The complete system then has the structure shown in Fig. 9. It is evident from Fig. 8 and Fig. 3 that the length of this additional section of line need not be longer than $\lambda/4$.

Graphical Solution

Instead of plotting the values of R_c and s against r_s' and x_s', it is simpler in this case to use a graphical construction. If one treats m as a parameter, (33) defines a family of circles which are plotted in Fig. 10. Besides the point (1, 0) each circle crosses the r_s'-axis at $(m^2, 0)$. This diagram enables one to determine R_c/R_c' quite rapidly. If one enters the diagram at a point where there is no available circle, instead of using interpolation, one can determine m by constructing the line AB as shown in Fig. 10 and another line BC perpendicular to it. The square root of OC then gives the value of m. Once m has been determined, one can make use of the circle

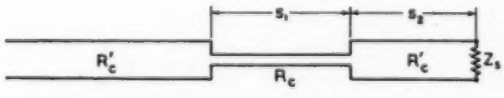

FIG. 9. Series section with additional section of line.

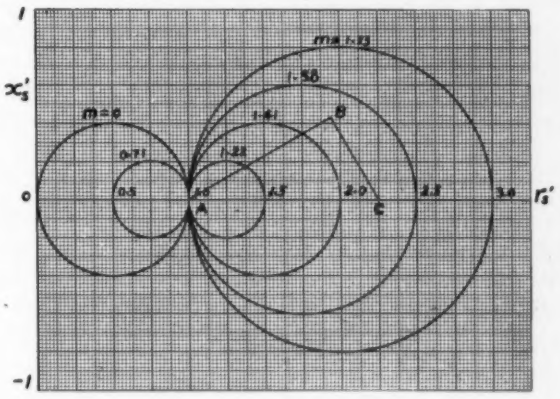

FIG. 10. Constant m circles.

diagram to determine the value of Φ, and hence the value of s by (35) or (36).

Numerical Examples

Four examples illustrating the practical design of typical shunt and series sections are given below.

Shunt sections:

Case 1.—Shunt section alone, i.e., terminated directly in the load.

Suppose $R_c = 400$ ohms, $Z_s = 200 - j400$ ohms. This corresponds to $r_s = 0.5$ and $x_s = -1$. Referring to Fig. 4, this point lies inside the matching region. From the circle diagram one finds that the values of ρ and Φ corresponding to the given values of r_s and x_s are 0.24 nepers and 41.5°, respectively. From Fig. 6 one finds $s_1/\lambda = 0.572$ and $s_2/\lambda = 0.350$.

Case 2.—Shunt sections with additional section of line.

Suppose $R_c = 400$ ohms, $Z_s = 800 + j0$ ohms. This corresponds to $\rho = 0.55$ and $\Phi = 0$. It is seen from Fig. 4 that this pair of values of r_s and x_s lies outside the matching region. Let an additional section of line of length $s_3 = \lambda/8$, or $\beta s_3 = 45°$ be

inserted. Then the effective value of Φ changes to 45° while ρ remains unchanged. This new pair of values of ρ and Φ now lies well inside the matching region. From Fig. 6 the values of s_1/λ and s_2/λ are found to be 0.535 and 0.414, respectively.

Series sections:

Case 3.—Series section alone.

Suppose $R_c' = 400$ ohms, and $Z_s = 800 - j40$ ohms. This corresponds to $r_s' = 2$ and $x_s' = -0.1$. Referring to Fig. 8, this point lies inside the matching region. The value of $m = R_c/R_c'$ determined from Fig. 10 is 1.42; so $R_c = 568$ ohms. With this value of R_c one finds $r_s = 1.41$, $x_s = -0.0705$. The corresponding value of Φ as determined from the circle diagram is 5°. Using (36), with $n = 0$, one obtains $s/\lambda = 0.236$.

Case 4.—Series section with additional section of line

Suppose $R_c' = 400$ ohms, and $Z_s = 200 + j500$ ohms. The given point lies outside the matching region in Fig. 8. The corresponding values of ρ' and Φ' are 0.186 nepers and 144°. Suppose Φ' is increased by 36° by inserting an additional length section of line of length s_2 equal to 0.1λ. The effective Φ' then shifts to 180° while ρ' remains unchanged. From Fig. 10 one finds $m = 2.33$ for this new point, hence $R_c = 930$ ohms. The length of the section s_1 is $\lambda/4$.

CONCLUSION

The preceding analysis shows that a close similarity exists between the use of shunt and series sections of line. When used alone, both are limited to a certain range of impedances. But there is a marked difference regarding the ranges which each one covers. In general, the series section permits matching a much wider range of impedances than the shunt section. It is interesting to note that the shunt sections are useful precisely in the range in which the series section cannot yield a match. If an additional section of line is included, both systems can be designed to match any impedance. With regard to the method used it is seen that the introduction of the terminal functions ρ and Φ leads to great mathematical simplicity at several points. In particular, the effect of the introduction of an additional section of line would not be so obvious if these two terminal functions were not used.

The writer wishes to acknowledge his indebtedness to Professor Ronold King for suggesting this problem and guiding his work. He also wishes to express his appreciation of the helpful suggestions and criticisms of Dr. P. LeCorbeiller and of Dr. A. H. Wing, Jr. Acknowledgment is also due his friend Mr. C. M. Liang who helped to prepare most of the figures.

On the Proportion of Crystalline and Amorphous Components in Stretched Vulcanized Rubber*

A. J. WILDSCHUT
Rubber Foundation, Delft, Holland
(Received September 28, 1945)

Determinations of the tension-temperature relation of strêtched vulcanized rubber can provide us with data about the proportion of crystalline and amorphous components. The amount of crystalline material appears to be 30–32 percent at 600 percent elongation and at 20°C. An expression is derived relating percentage crystalline material and temperature. The results are in close agreement to those of x-ray measurements carried out by Goppel but diverge largely from those obtained by Field. The cause of this difference is not yet quite clear. Stretched vulcanized rubber consists of a predominating amorphous phase with crystallites embedded in it. On stretching orientation occurs and a systematical addition of secondary valency forces is possible. This is the main cause of the existence of a certain tensile strength. Crystallization, though important as an indication on orientation, is more or less an incidental phenomenon. The distance function of the secondary forces may be of equal importance with the orientation.

1. INTRODUCTION

SINCE Katz[1] recognized the crystalline structure in stretched rubber, x-ray analysis has improved our knowledge about high polymeric elastic substances to a considerable extent. The influence of temperature on the deportment of the rubber crystallites was studied on raw as well as on vulcanized rubber. Various influences of mixing and vulcanization on the x-ray pattern were investigated. The fibrous character of stretched rubber was definitely established, which contributed considerably to the important new theories about high elasticity.

Long before the crystallinity of stretched and of "frozen" rubber was proved by the x-ray diagram, it was understood that physical properties such as specific weight, hardness, light-transmission showed transition points when their courses with temperature were determined. It was known for a long time that stored raw rubber could become hard and opaque, while the original suppleness could be restored by heating or even by repeated bending and stretching. Bunschoten[2] pointed out that the specific gravity of "frozen" raw rubber decreases considerably after heating and increases again after the rubber is kept for a certain time at a relatively low temperature. Though the possibility of a phase-change was considered, the "freezing" of rubber was not yet then explained by presuming a partial crystallization. In later years analogous experiments, though over a much longer range of temperature, were done by Bekkedahl,[3] who found several transition points in the specific volume-temperature curve.

Many other investigations could be mentioned in this connection, but those two suffice in pointing out that x-ray analysis need not be the only way in which the crystallization of rubber can be studied. After recognizing the importance of crystallization on the plastic properties of vulcanized rubber,[4] the author made a study of the relation between elastic tension and temperature, which relation appeared also to be influenced by crystallization to a considerable extent. Though originally meant for a different purpose, this study proved to be valuable also for a *quantitative* investigation of the crystallization. It appeared possible to calculate the percentage of crystalline material in stretched vulcanized rubber from tension-temperature relations as determined for thermodynamical investigations.

* Communication number 51 of the Rubber Foundation, Delft, Holland.

[1] J. R. Katz, "Ueber die Aenderungen des Röntgenspektrums bei der Dehnung," Kolloid Zeits. **36**, 300 (1925).

[2] E. Bunschoten, "Eenige waarnemingen betreffende het soortelijk gewicht van ruwe en gevulcaniseerde rubber," Versl. en Meded. Afd. Handel Dep. van Landb., Nijverh. en Handel (1921) No. 6.

[3] N. Bekkedahl, "Forms of rubber as indicated by temperature-volume relationship," J. Research Bur. Stand. **13** (September, 1934).

[4] See A. J. Wildschut, "Pseudo-plastic phenomena with vulcanized rubber," Physica **10**, 571 (1943). "Les phénomènes pseudo-plastiques dans le caoutchouc vulcanisé," Rev. Gén. du Caoutchouc **21**, 9 (1944).

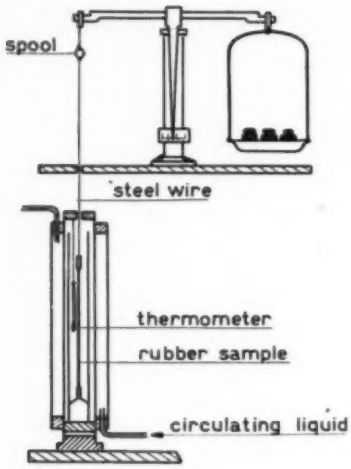

FIG. 1. Apparatus for determining the tension-temperature relation.

It is not the author's intention to deal with these latter investigations[5] in full, as this is quite a different subject. Only the side path, leading to a new method of quantitative determination of the degree of crystallization, will be treated here.

2. THE TENSION-TEMPERATURE RELATION

The well-known thermodynamical formula

$$\sigma=(\partial U/\partial L)_T+T(\partial\sigma/\partial T)_L, \qquad (1)$$

where σ is the elastic tension, U the internal energy, L the length, and T the absolute temperature, used already by Wiegand and Snyder,[6] denotes a linear relation between the tension σ and the temperature T. The scope of the $\sigma-T$ line fixes $(\partial\sigma/\partial T)_L$, while the point of intersection with the ordinate gives the value for $(\partial U/\partial L)_T$.

This formula is valid provided the process is reversible. Therefore the rubber sample under investigation must be sufficiently elastic so that plastic flow during the measurements may be neglected. With a normal vulcanized pure gum mixture from natural rubber it is comparatively easy to meet this requirement. If such a rubber is stretched, heated for some time at, for example, 70°C till the rate of relaxation is sufficiently small, cooled down to room temperature, and heated again to 70°C, as has been done by Meyer and Ferri,[7] the original tension is reached again or is so nearly approximated that the difference may be neglected. As the process is reversible, Eq. (1) is valid and the relation found between tension and temperature must be linear. Up to a certain extent the experimental data are in accordance with the thermodynamical theory, but for a complete explanation of all experimental facts it appeared necessary to consider a possible partial crystallization of the rubber investigated. This crystallization is influenced also by the velocity with which the experiments are carried out.

3. METHOD OF DETERMINING THE TENSION-TEMPERATURE RELATION

The apparatus (see Fig. 1) comprises a part regulating the temperature of the test piece and a part by means of which the elastic tension can be measured at constant elongation. As it was believed desirable to heat the rubber in air, a double-walled glass-mantle, through which a liquid could be pumped, was constructed around the test piece, while the tension was measured by means of an ordinary balance from which one of the scales had been removed. The elongation was determined and controlled by measuring the distance of two marks on the rubber by means of two calibrated glass plates, acting as cathetometer.

The stretched rubber was even more sensitive to slight fluctuations in temperature than the precision-thermometer used. By means of two water baths, however, one for heating and cooling and the other for measuring at constant temperature, the temperature inside the mantle could be kept sufficiently constant.

Small variations in elongation of the part of the test piece between the marks could occur, as this part was not always elongated in the same way as the rest of the test piece. This could then be corrected by means of a small spool in the steel wire connecting the sample with the balance.

The cross section of the test pieces used was mostly about 0.5 mm² (e.g., 0.3×1.4 mm); the loads varied up to about 200 grams and could be measured with an accuracy of 0.1 gram.

[5] A survey is given in: A. J. Wildschut, *Technological and Physical Investigations of Natural and Synthetic Rubbers* (Elsevier, Amsterdam, 1945). (In press).

[6] W. B. Wiegand and J. W. Snyder, "The rubber pendulum, the Joule-effect and the dynamic stress-strain curve," Trans. I.R.I. **10**, 234 (1934).

[7] K. H. Meyer and C. Ferri, "Sur l'élasticité du caoutchouc," Helv. Chim. Acta **18**, 570 (1935).

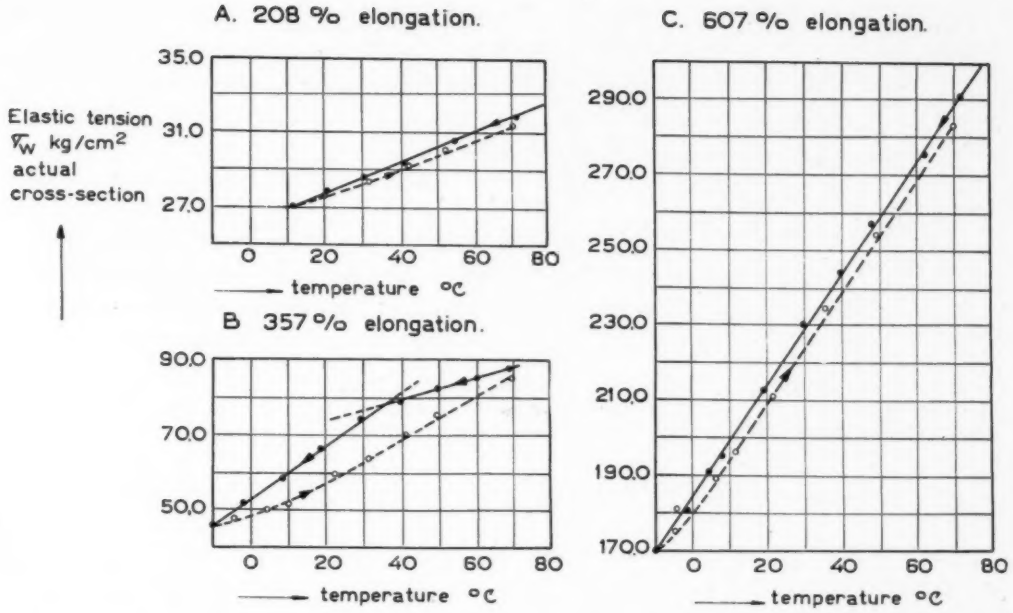

FIG. 2. Tension-temperature diagrams of vulcanized natural rubber (see reference *a* of Table I) at different elongations.

Originally the experiments were carried out over a range from room temperature to 70°C, but in the course of the investigations it proved to be necessary to extend this range up to 100°C and down to −10°C. For temperatures below room temperature, alcohol, cooled in a mixture of solid carbon dioxide and acetone, was pumped through the glass mantle.

Most experiments were carried out after heating the stretched rubber at 70°C during 4 hours. The sample was then cooled down in steps of about 10 degrees Celsius. At each temperature the rubber was kept for about 10 minutes.

If the sample was heated to temperatures above 70°C, the time of relaxation, at least in the cases of higher elongations, had to be shorter than 4 hours, as otherwise breaks might occur. As the rate of relaxation increases strongly with increasing temperature, no difficulties were presented by this.

4. INFLUENCE OF CRYSTALLIZATION

If stretched and heated vulcanized rubber is cooled down again, three cases can be distinguished, dependent on elongation and rate of cooling. Examples of these cases are given in Fig. 2.

First case, Fig. 2A. Low elongation (208 percent). There is but little crystallization, and after having been kept at 70°C during 4 hours, the rubber is certainly amorphous. On cooling, the amorphous state can be maintained and in that case the tension-temperature relation is straight, in accordance with Eq. (1). On heating, the initial point is reached again, proving that relaxation during the cycle may be neglected.

Second case, Fig. 2B. Medium elongation (357 percent). The rubber crystallizes on stretching, but after 4 hours at 70°C the sample may be considered amorphous. On cooling, the tension decreases linearly with temperature till the transition point of 36°C. Then partial crystallization sets in, causing a marked increase in the slope of the tension-temperature line, which, however, remains straight.

Third case, Fig. 2C. High elongation (607 percent). The stretched sample is partly crystallized and 70°C is too low to melt the crystallites under these circumstances. On cooling, a straight line without a transition point is obtained, as over the whole range the sample is already (partly) crystallized. The increase in degree of crystallization, which certainly takes place on cooling, will increase the slope of the line but apparently does

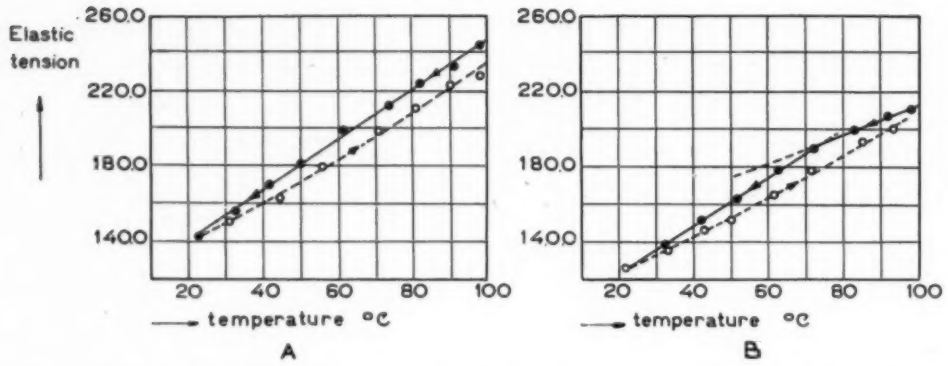

FIG. 3. The tension-temperature relation at 600 percent elongation. Influence of the time of heating. Natural rubber pure-gum vulcanizate (see reference *a* of Table I). *A*. Heated 15 min. at 100°C. *B*. Heated 60 min. at 100°C.

not influence the linear course of the tension-temperature relation.

From Fig. 2B it can be seen clearly that the tension of partly crystallized rubber is lower than it would be if no crystallization had taken place. This latter situation can easily be realized if the rubber is cooled down comparatively rapidly, as has been done by Meyer and Ferri,[7] who had their test pieces in direct contact with the cooling medium, water. This is the reason why these investigators could not observe a transition point.

On heating again a retardation in the melting of the crystallites occurs, with the effect that partial crystallization still exists even in the range above the melting point. The observed lower tensions are a consequence of this retardation as they cannot be caused by relaxation. Ultimately the initial tension is practically reached again, which gives proof that relaxation may be neglected.

At higher elongations very little retardation appears to occur (Fig. 2C). The reason for this phenomenon is not clear as yet. Also in this case the initial tension is approximated sufficiently to justify neglect of relaxation.

5. THE "MELTING POINT" OF THE CRYSTALLITES

It was learned from measurements at medium elongations that the transition point in the $\sigma - T$ curve was displaced to higher temperatures when higher elongations were used. Therefore it was logical to search for the missing transition points at higher elongations by measuring over a wider range of temperature. For this purpose the initial point was raised to 90°C, later even to 100°C. At elongations of about 600 percent breaks often occurred, but sufficient relaxation was obtained in a short time, e.g., 15 minutes. Although the initial tension is not quite reached again (see Fig. 3A), the influence of relaxation during the cooling may still be neglected, as at lower temperatures the rate of relaxation decreases strongly.

As the curve of Fig. 3A shows no transition point, heating for 15 minutes at 100°C is not sufficient to melt a noticeable part of the crystallites. After heating during 60 minutes, however, the transition point appears at about 74°C (Fig. 3B). From further contemplations it can be derived that in this case by heating at 100°C during 60 minutes about 60 percent of the crystalline phase is melted.

So it is quite clear that at higher elongations not only a high temperature, but also a comparatively long time is needed to melt the crystallites. On cooling, crystallization sets in on a fairly definite point; there is only a small range of temperature during which the crystallization begins. After that range has been passed, the percentage crystalline material appears to increase in inverse proportion to temperature (see Section 6). The rather sharp solidification point may be caused by the existence of crystallization nuclei or small crystallites acting as nuclei.

As the melting of the crystallites appears to depend so strongly on circumstances, it is not astonishing that no distinct relation between transition points and elongation could be derived from the experimental data. Yet, when the

results of 26 measurements are plotted on squared paper, as has been done in Fig. 4, it is quite clear that a certain relation is present.

An increase in elongation from 300 to 600 percent corresponds with a displacement of the transition-point from about 40 to about 65°C.

These measurements provide us with a qualitative picture of the influence of crystallization on the tension-temperature relation. The most important conclusion is that the linear course of this relation is not disturbed by increasing partial crystallization.

6. DETERMINATION OF THE DEGREE OF CRYSTALLIZATION

In Fig. 5 the course of tension with temperature at medium elongation, as given already in Fig. 2B, is pictured again.

The rubber has been stretched, heated for 4 hours at 70°C, and then cooled down comparatively slowly. The stretch AB corresponds with wholly amorphous rubber (see below) and is thus in accordance with Eq. (1). Below the transition point at B partial crystallization occurs. The stretch BC therefore corresponds to partial crystallized rubber *with increasing amount of crystalline material*. The slope of this part of the curve is caused by the combination of the decrease according to form, (1), known to be linear, and the decrease, caused by the growing amount of crystalline material. The result is a linear

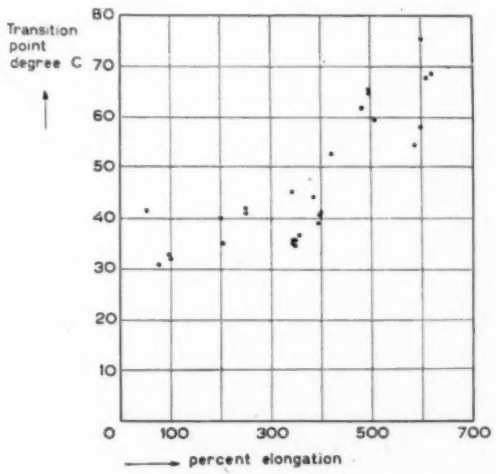

FIG. 4. Transition-points in the $\sigma-T$ relation as a function of the elongation. Natural rubber pure-gum vulcanizate (see reference *a* of Table I).

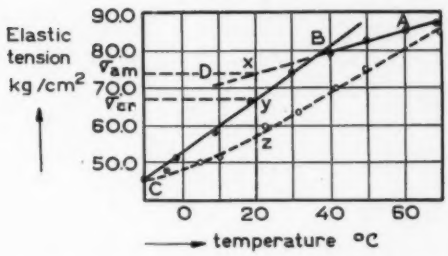

FIG. 5. Calculating the degree of crystallization from the tension-temperature relation. (Natural rubber pure-gum vulcanizate (see reference *a* of Table I) at 357 percent elongation.)

decrease of tension with temperature; therefore the decrease, caused by the crystallization-effect, must also be linear.

Now this decrease is caused by the fact that decreasing temperature causes an increasing amount of crystalline material, while more crystallization involves a lower tension. As the combination of these two functions is linear, it is very likely that both of them are linear also. If that is so, the conclusion would be reached that *the elastic tension decreases in inverse proportion to the amount of crystalline material.*

Presuming this conclusion valid, the calculation of the degree of crystallization in stretched vulcanized rubber from measurements as given in Fig. 5 is very simple.

If no crystallization had taken place, the tension-temperature relation would have followed the course BD and at 20°C the point X would be passed, corresponding with an "amorphous tension," σ_{am}^{20}, of 73.7 kg/cm². As, however, the rubber is partly crystallized, at 20°C the point Y is reached, corresponding with a "crystalline tension," σ_{cr}^{20}, of 66.9 kg/cm². This tension is 9.2 percent lower than the "amorphous tension," which denotes that 9.2 percent of the rubber molecules have been eliminated by crystallization.

In general, the percentage crystalline material K is given by:

$$K=\frac{\sigma_{am}-\sigma_{cr}}{\sigma_{am}}100. \qquad (2)$$

The tension in stretched rubber is thus caused by the amorphous phase only. Only these molecules have a possibility to return to their most

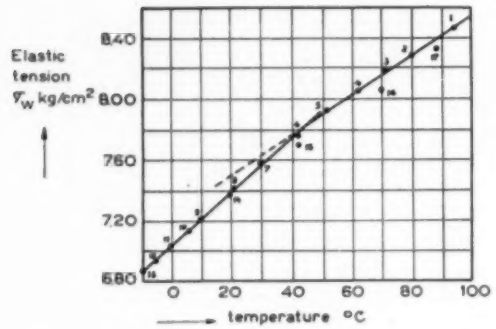

FIG. 6. Existence of crystallization in stretched vulcanized rubber (see reference *a* of Table I) at 55 percent elongation.

probable position; as soon as they have entered a crystal lattice, this possibility no longer exists.

If the test piece, after cooling to −10°C, is heated again, the tension at 20°C corresponds to that of the point *Z* (see Fig. 5). On passing *Z*, a higher degree of crystallization still exists, but this situation is not stable and is therefore left out of account. It denotes, however, *the necessity to consider always the history of a given piece of rubber if its crystallization is to be measured.*

Only if it is certain that at the initial point *A* the rubber is wholly amorphous, exact data about the degree of crystallization are obtained, for the transition point may appear also when at higher temperatures the rubber is still partly crystallized. In those cases only an increase in degree of crystallization is found and the total amount of crystalline material may be higher.

It is, however, rather simple to prove the presence of the wholly amorphous state above the transition point. If the rate of cooling is augmented, the "crystalline part" of the tension-temperature line becomes curved—for crystallization takes time—while the "amorphous part," if wholly amorphous, remains straight. In this way it has been proved that, in cases as pictured in Fig. 5, the test piece must have been wholly amorphous at 70°C.

Theoretically the "crystalline part" of the tension-temperature curve cannot be straight, as crystallization is dependent on time, but as this relation is logarithmical, it suffices to measure with the velocity described in Section 3 to get a line that cannot be distinguished from a straight one.

With x-ray measurements below 300 percent elongation, no crystallization is observed in natural rubber pure gum mixtures. By means of the method described above, however, the existence of crystallization effects can be shown, and the amount of crystalline material can be calculated at elongations as low as 50 percent. The degree of crystallization is then naturally very small, about 1 percent, but the effect is unmistakable, as is shown in Fig. 6.

As yet it has not been possible to control all factors influencing crystallization at lower elongations. Sometimes crystallization occurs, but in other cases it may not happen at the same or even higher elongations. An example of this has already been given in Fig. 2A. The degree of crystallization found varies also in separate cases. But this is not considered essential at this stage of the investigations. Stress can be laid on the conclusion that at these low elongations a distinct, though very small, crystallization effect occurs. Whether at 50 percent elongation an exact degree of crystallization can be determined at all is not certain, as it is possible that this degree varies according to circumstances, and factors depending on the laws of probability may also play a part.

The degrees of crystallization, calculated from 25 measurements on a natural rubber pure gum mixture (different vulcanizates, but always the same mixture and cure), are given in Fig. 7 as well as in Table I.

As soon as the rubber is elongated, crystallization sets in, but up to 250 percent not more than

TABLE I. Percentage crystalline material in stretched vulcanized rubber[a] at increasing elongation. 20°C.

Percent elongation	Percent crystalline material	Percent elongation	Percent crystalline material
50	1.4	347	8.6
55	1.3	350	9.5
97	0.5	357	9.2
100	0.5	385	19.6
120	0.9	390	12.6
200	0.9	392	17.7
205	0.8	397	19.3
250	2.0	400	16.0
300	4.3	420	23.8
342	9.7	480	27.4
342	8.3	492	24.5
345	10.4	495	22.8
345	7.5		

[a] Composition: Crepe rubber 100, diphenylguanidine 0.5, mercaptobenzothiazole 0.8, sulphur 1.75, zinc oxide 5.0, stearic acid 1.0, aldol α naphtylamine 1.0. Cure 20 minutes at 142°C in a press.

2 percent is crystallized. Above 300 percent elongation the crystallization increases rapidly, till at 500 percent a maximum of about 27 percent crystalline material is reached. By extrapolating the curve of Fig. 7 to 600 percent elongation, the maximum degree of crystallization can be estimated to be about 30–32 percent. So even in that case the amorphous phase predominates.

Presuming that at 600 percent elongation, 30 percent of the stretched rubber is crystallized, it is possible to gain complete insight in Fig. 3B. When passing at 20°C from the extrapolated upper part of the curve to the lower part, the tension decreases from 148.4 to 122.7 kg/cm², that is, with 17.4 percent. If the upper part had represented the wholly amorphous state, the decrease would have been 30 percent. So $17.4 \cdot 100/30.0 = 58$ percent of the crystalline phase was melted by heating at 100°C during an hour.

Of course in such a calculation this exactness has no sense, but the conclusion may be drawn that rather more than half of the crystalline phase will be melted in an hour and that it will take at least another hour to reach the wholly amorphous state. Unfortunately most samples cannot stand this, so 600 percent is about the natural limit for this sort of investigation. Perhaps an improvement can be made by heating the unstretched sample at 100°C and then elongating it; these experiments will be done in due course.

7. INFLUENCE OF TEMPERATURE ON DEGREE OF CRYSTALLIZATION

As the relation between tension and temperature is linear, a tension coefficient at constant elongation, $(\partial\sigma/\partial T)_L$, can be calculated from these measurements. As long as the rubber is amorphous, the value of this tension coefficient depends on the elongation only. Below the transition point the tension coefficient increases, for the increasing degree of crystallization causes an additional decrease in tension. The "crystalline tension coefficient" is therefore dependent on time in the same way as the crystallization itself.[4]

The degree of crystallization can be calculated from the tension coefficients and the transition temperature as follows:

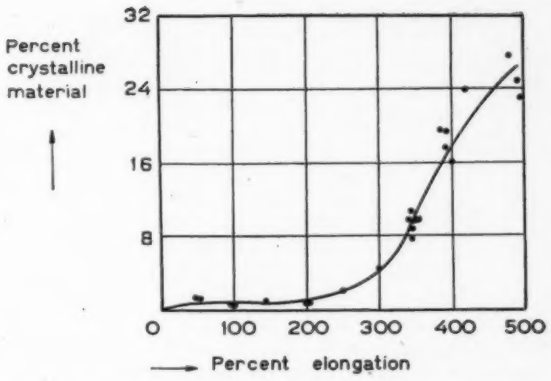

FIG. 7. Percentage crystalline material in stretched vulcanized natural rubber (see reference *a* of Table I) at 20°C.

From Fig. 5 it can be seen that the tension of the transition point, σ_{T_s}, is given by:

$$\sigma_{T_s} = \sigma_{T,\mathrm{am}} + (\partial\sigma_{\mathrm{am}}/\partial T)_L (T_s - T), \qquad (3)$$

as well as by:

$$\sigma_{T_s} = \sigma_{T,\mathrm{cr}} + (\partial\sigma_{\mathrm{cr}}/\partial T)_L (T_s - T), \qquad (4)$$

where $\sigma_{T,\mathrm{am}}$ and $\sigma_{T,\mathrm{cr}}$ are, respectively, "amorphous" and "crystalline" tensions at a temperature T and $(\partial\sigma_{\mathrm{am}}/\partial T)_L$ and $(\partial\sigma_{\mathrm{cr}}/\partial T)_L$ are the tension-coefficients for the wholly amorphous and partially crystallized rubber, respectively.

If the values for $\sigma_{T,\mathrm{am}}$ and $\sigma_{T,\mathrm{cr}}$, derived from Eqs. (3) and (4), are substituted in Eq. (2), we get:

$$K_T = \frac{[(\partial\sigma_{\mathrm{cr}}/\partial T)_L - (\partial\sigma_{\mathrm{am}}/\partial T)_L](T_s - T)}{\sigma_{T_s} - (\partial\sigma_{\mathrm{am}}/\partial T)_L (T_s - T)} 100, \qquad (5)$$

from which the percentage crystalline material K_T can be calculated at any temperature T. Equation (5) can be written $xy + ax + by - c = 0$, which is an equation of a hyperbola. As can be seen from Fig. 8, in practice the relation between K_T and T is approximately linear, as long as short ranges are considered.

The amounts of crystalline material have been calculated for the elongations 357 (the case represented in Fig. 5) and 492 percent; the results are given in Fig. 8.

The straightness of the tension-temperature curve has been proved down to −10°C. Below this temperature, calculation of K_T from Eq. (5) will have little or no physical meaning. In the first place the rate of crystallization diminishes

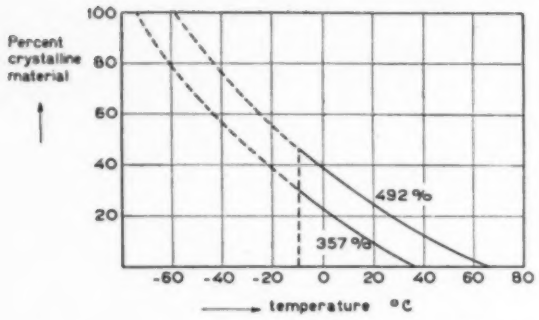

FIG. 8. Percentage crystalline material as a function of temperature. Natural rubber pure-gum vulcanizate (see reference *a* of Table I).

at decreasing temperature so strongly that for this reason alone it is doubtful whether the percentages represented by the dotted part of the curve will ever be reached at all. Secondly Eq. (5) is only valid as long as the "crystalline part" of the $\sigma - T$ curve remains straight as well as continuous. Any change in modification will cause a break in the $\sigma - T$ curve. This makes an extrapolation below the temperatures of the measurements without physical significance.

The degree of crystallization appears to be strongly dependent on temperature. While at room temperature (20°C) the maximum percentage crystalline material may be estimated to be about 30 percent, at zero degrees this maximum may be 45 percent and at -10°C even as high as 50 percent. The highest temperature at which crystallization in stretched rubber exists appears to be about 80°C, a conclusion that can be derived also from Fig. 4. Above 60°C the amount of crystalline material remains below 10 percent, provided the situation is stable. Of course, if stretched rubber is heated rather rapidly, higher degrees may temporarily occur, but then the system is not in equilibrium.

8. COMPARISON WITH X-RAY MEASUREMENTS

Quantitative measurements of the crystallization in stretched vulcanized rubber by means of the x-ray method have been done by Field[8] and by Goppel.[9] Both investigators compared the intensities of the diffuse rings in the diagrams of amorphous and partly crystallized rubber, while also measurements of the intensities of the diffraction spots were done.

It lies beyond the scope of this paper to discuss these investigations in full. As it happens, however, the results of Field and of Goppel show a large difference: while the former finds at 500 percent elongation and at room temperature a degree of crystallization of 65–70 percent, the latter measures 25–30 percent, which is in accordance with the results of the thermodynamical method described above.

The work of Goppel was carried out independently of that of the author and most of it at an earlier date. His results as given in Fig. 9 are obtained on the same mixture on which the thermodynamical measurements have been done, but also various other pure-gum mixtures have been investigated,[10] and it appeared that the differences between them were small.

Results of both x-ray investigations, as well as the results obtained with the thermodynamical method, have been collected in Fig. 9.

There is a close agreement between the results of Goppel and those of the author, while the data given by Field diverge very considerably. It is most unlikely that this is caused by the comparatively small differences in mixture and cure, but it is not yet possible to state the exact cause of this phenomenon.

Various arguments can be advanced for the existence of not more than a moderate amount of crystalline material in stretched vulcanized rubber. It is unlikely that an entangled knot, with primary valency bonds between the molecules, can be stretched in such a way that a great amount of regularity is gained. As soon as certain parts of the chains have entered into crystal lattices, other parts are hindered in their movements and less able to do the same. The primary valency bonds caused by the vulcanization arise while the rubber is unstretched; by stretching some of these bonds may break,

[8] J. E. Field, "An x-ray study of the proportion of crystalline and amorphous components in stretched rubber," J. App. Phys. 12, 23 (1941).

[9] J. M. Goppel, "Quantitatieve Röntgenografische Onderzoekingen aan Rubber," Thesis, Delft, 1945. (In press).

[10] The results of Goppel and of the author have been obtained on the vulcanizate, defined in note *a* of Table I. The data of Field have been derived from his Figs. 10 and 11. Compound *B*: smoked sheet 100, zinc oxide 2, sulphur 2, P.P.D. 2, cure 10 minutes at 260°F (127°C). Compound *C*: smoked sheet 100, zinc oxide 1, sulphur 2, zimate 1, cure 20 minutes at 260°F.

but others will not. It is in contravention of probability that the irregular network can be transferred in a system of crystal lattices; so crystallites can be formed only to a limited amount.

The thermodynamical measurements can only be compared with the two x-ray investigations mentioned. One is in close agreement with them, the other diverges largely. A third, if possible independent, measurement of the degree of crystallization will be required to make certain where the truth lies.

9. GENERAL PICTURE OF STRETCHED VULCANIZED RUBBER

The author is inclined to believe that the lower figures for the amount of crystalline material in rubber are right. This leads to the assumption that stretched vulcanized rubber is composed of an amorphous phase with up to a third part crystallized material. The existence of crystallization is important as an indication on regularity, *but it is doubtful whether crystallization, in itself, is of paramount importance for the tensile strength of rubber.*

Immediately after the elongation begins, orientation of the rubber molecules occurs. This orientation will be one of the main causes of the formation of a high mechanical firmness

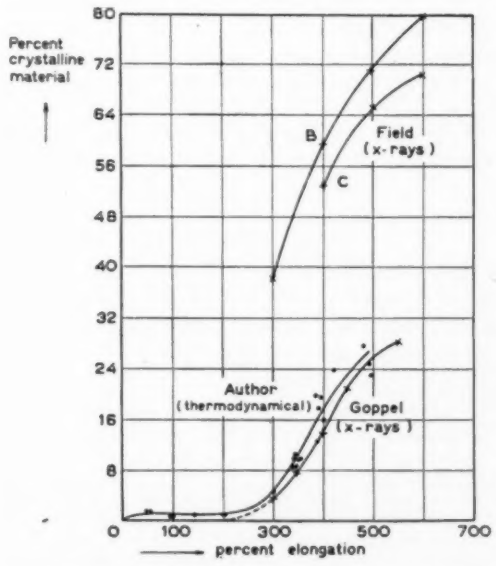

FIG. 9. Crystallization in stretched vulcanized rubber (see reference 10) according to three investigations.

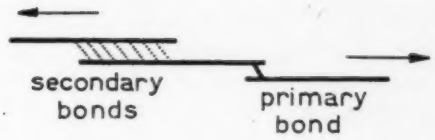

FIG. 10. On the mechanism of break.

during the elongation. Crystallization, though directly important for certain other properties, is only an incidental phenomenon and it is not even certain whether the existence of crystallites adds to the tensile strength or not. At any rate a high tensile strength is very easily possible without any crystallites playing a role, also in pure-gum vulcanizates. At temperatures up to 100–140°C vulcanized rubber keeps its tensile strength completely,[11,12] while certainly under these circumstances no crystallization is present.

Of equal importance with regard to the tensile strength may be the way the secondary forces between the molecules decrease at increasing mutual distance. If this function is favorable, a high tensile strength may occur even at medium orientation.

It is not likely that the primary valency bonds in vulcanized rubber are decisive for the tensile strength. They are, of course, important with regard to plastic flow, but it is unlikely that, on stretching, they are responsible for equal parts of the tension. So in the region shortly before break these primary bonds may be broken one after another, if the combined secondary energies between two chain-parts, drawn parallel, are higher than the energy of the primary bond concerned. (Compare Fig. 10.)

The tensile strength will be caused mainly by secondary forces, added systematically along the chains. This addition is possible for secondary forces only.[13] The crystallites may exert additional forces on the surrounding amorphous phase and thus add to modulus and tensile strength, in the same way as carbon black in

[11] A. van Rossem and H. van der Meijden, "Studies on the physical properties of rubber. I. Influence of high temperature on the stress-strain curve of vulcanized rubber," J. Soc. Chem. Ind. **45**, 67T (1926).

[12] A. A. Somerville and W. F. Russell, "Effect of temperature on tensile properties of vulcanized rubber," Ind. Eng. Chem. **25**, 1096 (1933).

[13] See also G. Briegleb, Zwischenmolekulare Kräfte und Molekülstruktur. Sammlung chemischer und chemisch-technischer Vorträge, New edition, No. 37 (1937).

Perbunan does, but it is equally possible that this effect—if it exists at all—is overcompensated by the partial elimination of rubber molecules by the crystallization (which causes, as has been shown above, a decrease in elastic tension). Of course the crystallites in themselves are firmly bound together, but this is of no importance to the tensile strength, as they are embedded in amorphous material. This may be the most important conclusion from our measurements about the degree of crystallization: when determining the tensile strength *the forces are applied on an amorphous phase* and not on a bundle of crystals.

This vision on the situation in stretched vulcanized rubber is strengthened by various phenomena, observed on synthetic rubbers,[5] with and without carbon black. Synthetic rubbers with very weak pure-gum mixtures show a normal high tensile strength when carbon black is added: secondary forces must play a role. Lightly swollen rubber[14] has lost most of its mechanical firmness; after evaporation of the swelling liquid the original tensile strength is completely restored. This phenomenon can only be explained by presuming secondary forces to be responsible for the tensile strength.

More could be said about this, but that would carry us much too far. It does not lie within the scope of this article to discuss all physico-chemical aspects of the rubber molecule, but only to draw attention to the fact that a relatively low degree of crystallization is likely to exist and leads to an essentially different picture of stretched rubber from that of a high degree. The picture, corresponding with a low degree of crystallization, agrees better with phenomena observed on synthetic rubbers.

[14] A swelling of 5–10 volume percent will be enough.

Letters to the Editor

On Plane Rotations in n Dimensions

PETER T. LANDSBERG
London, England
October 11, 1945

THIS note is intended as a contribution to the discussion of the "Representation of Rigid Rotations" which has recently been taking place in this journal.[1] The main formula (Eq. (1) below) derived by Professor Benedikt is an operational equation and will be shown in this note to be a three-dimensional statement of equations known to hold in n dimensions. Use will be made of the concepts and nomenclature of modern algebra.[2]

Consider a linear space γ_n of finite dimensionality n ($\geqslant 3$) and defined over a non-modula field $\mathfrak{F}$. Elements of γ_n, i.e., vectors, will be denoted by small Greek letters (θ is reserved to denote a variable angle), operators by capital Latin letters, and elements of $\mathfrak{F}$ by small Latin letters. In γ_3 the ordinary vector product (x) of two vectors is assumed to be defined.

Let any vector α_0 be rotated through a variable angle θ, yielding a vector α_θ, subject to the requirement that α_0 and all α_θ's are co-planar. Let the point about which α_0 is rotated be specified by a radius vector ρ relative to a fixed origin 0. The end points of α_0 and α_θ may then be specified relative to 0 by radius vectors

$$\rho_0=\rho+\alpha_0, \quad \rho_\theta=\rho+\alpha_\theta,$$

respectively. Further, let ρ be perpendicular to the plane defined by the α_θ's. Then Professor Benedikt has shown that for $n=3$

$$\rho_\theta=e^{\theta\eta x}\rho_0, \tag{1}$$

η being the unit vector parallel to ρ and in a positive direction relative to the rotation.

Consider now any linear space γ_n. Let an orthogonal normalized basis $\{\epsilon_{j0}\}$ be given in γ_n such that α_0 may be expressed in terms of ϵ_{10} and ϵ_{20}, ρ in terms of $\{\epsilon_{k0}\}(k=3, 4, \cdots, n)$. The n dimensional analog of Eq. (1) may then be obtained by assuming α_0 to be fixed but re-expressing it in terms of a new basis $\{\epsilon_{j\theta}\}$ obtained by rotating ϵ_{10}, ϵ_{20} through $(-\theta)$. The expression for α_0 in terms of $\{\epsilon_{j\theta}\}$ will obviously be the same as the expression for α_θ in terms of $\{\epsilon_{j0}\}$. If θ is continuously variable and $\mathfrak{F}$ the field of all complex numbers, a group of unitary operators $U(\theta)$ (these reduce to real orthogonal operators in the case of the real field) may be supposed to induce the transformation $\{\epsilon_{j0}\}\rightarrow\{\epsilon_{j\theta}\}$. If Y be an anti-symmetric operator, $U(\theta)$ may be represented in the form $e^{\theta Y}$, the latter expression being defined by the exponential series.[3]

[1] E. Benedikt, J. App. Phys. 15, 613 and 802 (1944).
[2] See, for instance, A. A. Albert, *Introduction to Algebraic Theories* (Chicago, 1941).

[3] It is not necessary to invoke this property of unitary matrices if *some* equation of the type $\epsilon_{j\theta}=U(\theta)\epsilon_{j0}$ is assumed possible. For it then follows from the nature of the problem that the $U(\theta)$'s have the property

$$U(\theta_1)\cdot U(\theta_2)=U(\theta_1+\theta_2),$$
$$U(0)=U(2\pi)=\text{identity operator},$$

whence $U(\theta)$ has an exponential representation. This is in fact merely a discussion of the representations of a one-parameter continuous Abelian group.

Hence

$$\epsilon_{j\theta}=e^{\theta Y}\epsilon_{j0}(j=1, 2, \cdots, n); \quad \epsilon_{k\theta}=\epsilon_{k0}(k=3, 4, \cdots, n);$$

whence

$$\alpha_\theta=e^{\theta Y}\alpha_0,$$
$$\rho=e^{\theta Y}\rho.$$

Therefore,

$$\rho_\theta=e^{\theta Y}\rho_0. \tag{2}$$

Defining

$$\lim_{\delta\theta\to 0}\frac{\rho_{\theta+\delta\theta}-\rho_\theta}{\delta\theta}\equiv\frac{d\rho_\theta}{d\theta},$$

we also have

$$\frac{d\rho_\theta}{d\theta}=Y\rho_\theta. \tag{3}$$

Equations (2) and (3) hold in n dimensions. In γ_3, Y is easily identified from (3) as the operator ηx so that (2) reduces to (1) in this case.

Letter to the Editor

GERALD PICKETT
Kansas State College, Manhattan, Kansas
October 5, 1945

THE purpose of this letter is to call attention to the trend of many contemporary writers to regard surface tension as something not quite real, and to present a few arguments against this view. For example, in discussing properties of liquid surfaces Glasstone[1] states "The tendency for a liquid to contract may be regarded as a consequence of its possession of free energy, . . . As a result of the tendency to contract a surface behaves as if it were in a state of tension." Adam[2] is more positive that surface tension does not really exist, that it only serves as a mathematical device. He says, "The essential mechanism, . . . of the production of the free surface energy, is the perpendicular inward attraction, exerted on the surface molecules by the underlying ones, there is no need to speculate how this can be transformed into a surface tension parallel to the surface, for the surface tension does not exist as a physical reality, and is only the mathematical equivalent of free surface energy."

The writer believes that surface tension is real, as real as any stress that may exist in a solid, liquid, or gas, and is concerned that progress in research may be hampered by the contrary view. A few arguments in favor of the writer's view follow.

For simplicity, consider only the surface tension of liquids at liquid-gas interfaces. For surface tension to exist points within the surface layer must have unequal principal stresses. Of course it is well known that at any point within a homogeneous liquid or gas at rest, the three principal stresses are equal. But a vapor-liquid interface is not a homogeneous phase, and, as a consequence, the principal stress normal to the interface may differ from the other two stresses.

Surface tension γ may be defined as

$$\gamma=\int(\sigma_t-\sigma_z)dz, \tag{1}$$

where σ_t and σ_z are the tangential and normal stresses, respectively, and the integration is taken over the thickness of the transition layer.

From a consideration of the equilibrium of a portion of the transition layer, the following well-known formula is readily obtained,

$$\gamma[(1/r_1)+(1/r_2)]=p, \tag{2}$$

where r_1 and r_2 are the principal radii of curvature of the interface, and p is the difference in the normal stress on the two sides of the interface.

The validity of Eq. (2) is not questioned by those who deny the reality of surface tension; they merely derive it from consideration of energy (see page 13 of reference 2) rather than from the equilibrium of a free body.

The writer will agree that for many if not most problems of interfaces the concept of surface energy will lead more directly to a solution than will the concept of surface tension just as many problems in mechanics are more simply solved by considering energy relations than by analysis of free bodies. For example, the lateral vibration of a bar could be studied by either energy methods or by methods based on free-body considerations. It might be argued (falsely) that there was no real longitudinal stress in the vibrating bar, since the motion and consequently the inertia forces are in a lateral direction. It is only from free-body analysis that one finds that longitudinal stress must accompany the lateral vibration of a bar. And from a free-body analysis of the transition layer between vapor and liquid, however thin that layer may be, one must accept the reality of surface tension.

Not only is surface tension in the transition layer between the homogeneous liquid and vapor phases real, but by making simplifying assumptions in regard to inter-particle forces; i.e., treat all forces as though they were Van der Waals forces between non-polar molecules, the thickness of the transition layer and the distribution of stress within it can be theoretically determined. An approach in this direction was made by Hulshof[3] who showed that to a first approximation

$$\sigma_t-\sigma_z=\frac{C}{2}\left(\frac{\partial\rho}{\partial z}\right)^2-\frac{C\rho}{2}\frac{\partial^2\rho}{\partial z^2}, \tag{3}$$

where ρ is density and

$$C=\int_0^\infty z^2\psi(z)dz,$$

where $\psi(z)$ is the attraction between a semi-infinite body of the material of unit density and a body of the material of unit mass located z distance from the semi-infinite body.

[1] Glasstone, *Textbook of Physical Chemistry* (D. Van Nostrand Company, New York, 1940), p. 473.
[2] Adam, *Physics and Chemistry of Surfaces* (Oxford Press, New York, 1930), p. 6. (See also second edition, 1938 and third edition, 1941).
[3] Hulshof, "Ueber die Oberflachenspannung." Ann. d. Physik [4] 4, 165 (1901).

On a Novel Form of Refrigerator

JENNY E. ROSENTHAL
Long Branch, New Jersey
October 30, 1945

THE September, 1945 issue of the *Journal of Applied Physics* contains a letter by Moody[1] criticizing "A Novel Form of Refrigerator" by Roebuck.[2] In addition to showing the flaws in analysis and design of the apparatus, the letter brings up several other points, which it is proposed to try to clarify in the following remarks.

As shown by Moody, Roebuck's machine is of awkward construction and cannot possibly make use of high speeds of rotation. In a subsequent publication it will be shown how a device can be designed so as to overcome these difficulties. For the present it will be assumed without proof that proper design makes it possible to raise the peripheral speed of rotation of the centrifuge at least to the value of 1300 ft./sec. given by Stodola.[3]

According to Kapitza[4] the efficiency of a turbine-like cooling device rests on the fact that the gas enters the cooling chamber at high density. If the compressor is external to the turbine, then it is impractical to attain the high density by high pressure, hence Kapitza has to introduce the gas into the turbine at a low temperature. In a centrifuge, where a compressor and cooling expansion chamber can constitute a single rotor unit, it is practical to introduce the gas into the rotor at moderate pressures and hence into the expansion chamber at high pressure with accompanying high density. However, this high pressure can only be attained by rotating the centrifuge near the limit set by Stodola. Hence the need for a good mechanical design mentioned above.

While unsatisfactory mechanically, Roebuck's device is nevertheless based on a sound underlying principle, which is different from that utilized in the Nernst gas turbine or in the device patented by Kapitza. Roebuck's reference to an article by Beams[5] reveals a fundamental fallacy in his conception of the operation of his cycle. Beams refers to an altogether different cooling effect, namely the cooling action of air jets external to the rotor.

As pointed out by Kapitza,[4] the gas expansion turbine proposed by Nernst is ineffective because no provision is made to introduce the gas into the device at high density. When gas at high density is used in a properly designed device constructed on the same principle as Roebuck's, the device functions as both a gas expansion and a hydraulic turbine, which makes use of centrifugal force. As mentioned before, Kapitza's device requires the introduction of a gas at a low temperature, a requirement which limits the range of usefulness of the device; although very efficient as a single stage unit, Kapitza's device is not constructed to give a large temperature change. Also, as pointed out by Moody, a single stage centrifugal unit cannot achieve a large temperature drop even if it runs at peripheral speeds near the limit set by Stodola, because the gas must expand under a pressure differential added to that attained through centrifugal force. This additional pressure differential is achieved by introducing the gas into the rotor at a different pressure from that existing at the exhaust.

[1] A. M. G. Moody, J. App. Phys. **16**, 551 (1945).
[2] J. R. Roebuck, J. App. Phys. **16**, 285 (1945).
[3] A. Stodola, *Steam and Gas Turbines* (McGraw-Hill Book Company, Inc., New York, 1927), p. 405.
[4] P. Kapitza, U. S. patent 2 280 585.
[5] J. Beams, *Science in Progress* (Yale University Press, New Haven, 1940), Second Series, p. 246.

Erratum: Secondary Emission of Pyrex Glass

[J. App. Phys. **16**, 453 (1945)]

C. W. MUELLER

George Eastman Laboratories of Physics, Massachusetts Institute of Technology, Cambridge, Massachusetts

TABLE I erroneously gave a very early composition of Pyrex brand glass. The composition tested was:

TABLE I.

SiO_2	80.5			Na_2O	3.8
B_2O_3	12.9			K_2O	0.4
		Al_2O_3	2.2		

Elastic Limit for Dynamic Loading

V. BARGMANN
School of Mathematics, The Institute for Advanced Study, Princeton, New Jersey

AND

H. F. LUDLOFF
Department of Aeronautical Engineering, New York University, New York, New York

November 25, 1945

IN dealing with dynamic processes, one is often confronted with the problem whether the elastic limit of materials can be characterized by a critical stress value, such as exists for static loading. In the case of transversal impact of a mass, striking upon the center of a simply supported beam, there are definite theoretical indications that the elastic limit is rather determined by a critical impulse, $\int_0^t F(t_1)dt_1$, where $F(t)$ is the contact force between striking mass and beam. $F(t)$ itself as well as local stresses may for short instants rise far beyond values that are permissible in statics.

Recent experiments yield precise time records of the center deflection $y_c(t)$ of a beam under impact loading. If the deflection of the beam is considered as forced vibration, it is evident that there must be a unique relation between the deflection of the beam and the contact force producing it. While the derivation of $y_c(t)$ from a known $F(t)$ is a routine calculation, the inverse problem involves Laplace transforms and "convolution" of functions. To provide a rigorous method for the experimental determination of $F(t)$-curves, we have solved the following problem:

Assume as experimentally known the center deflection of a simply supported beam with mass M and fundamental frequency ω:

$$y(t)=\frac{1}{M\omega}\sum_{n=1,3}^{\infty}\int_0^t F(t_1)\frac{\sin n^2\omega(t-t_1)}{n^2}dt_1.$$

What is the contact force between striking mass and beam $F(t)$?

Solution:

(1) Put

$$\sum_{n\ \text{odd}}\frac{\sin n^2\omega t}{n^2}=K(t),$$

then

$$y(t)=\frac{1}{M\omega}\int_0^t F(t_1)\cdot K(t-t_1)dt_1.$$

Let

$$\Phi(s)=\int_0^\infty e^{-st}\cdot\frac{F(t)}{M\omega}dt,\quad L(s)=\int_0^\infty e^{-st}\cdot K(t)dt,$$
$$\eta(s)=\int_0^\infty e^{-st}\cdot y(t)dt;$$

then:

$$\eta(s)=L(s)\cdot\Phi(s),\quad \text{i.e.,}\ \Phi(s)=\eta(s)/L(s).$$

Hence

$$F(t)=\frac{M\omega}{2\pi i}\int_{c-i\infty}^{c+i\infty}ds\cdot e^{ts}\cdot\Phi(s)=\frac{M\omega}{2\pi i}\int_{c-i\infty}^{c+i\infty}ds\cdot e^{ts}\cdot\frac{\eta(s)}{L(s)}$$

can be evaluated by complex integration, if the zeros of $L(s)$ are known.

(2) One can show that

$$L(s)=\frac{\pi^4}{16\omega\zeta^3}\left[\frac{\sinh\zeta-\sin\zeta}{\cosh\zeta+\cos\zeta}\right],$$

where $\zeta=\pi(s/2\omega)^{\frac{1}{4}}$.

The zeros of $L(s)$ can be computed from simple transcendental equations with any required accuracy; the asymptotic values are $s_k\sim\pm i\omega(2k+\frac{1}{2})^2$, for integer $k\geq 1$. The asymptotic expression for s_k yields sufficiently accurate values, even for s_1.

(3) Since at the start of the impact $F(t)=0$, we may assume $y(0)=y'(0)=y''(0)$; but $y'''\neq 0$. Then

$$\eta(s)=\int_0^\infty e^{-st}\cdot y(t)dt=\frac{1}{s^3}\int_0^\infty e^{-st}\cdot y'''(t)dt,$$

and

$$F(t)=\frac{M\omega}{2\pi i}\int_{c-i\infty}^{c+i\infty}ds\frac{e^{st}}{s^3\cdot L(s)}\left[\int_0^\infty e^{-st_1}\cdot y'''(t_1)dt_1\right].$$

After exchanging integrations and upon evaluating the residues according to standard methods, one obtains:

$$F(t)=M\omega\left\{\frac{96\omega}{\pi^4}y(t)+\frac{32}{\pi^2}\cdot\sum_{n_k^*}(1+\epsilon_{n_k^*})\times\int_0^t\sin\left[\omega n_k^{*2}(t-t_1)\right]y''(t_1)dt_1\right\},$$

which solves our problem. For all practical purposes: $\epsilon_{n_k^*}=0$; $n_k^*=(2k+\frac{1}{2})$, $k\geq 1$. The series converges, as can be seen by partial integration, at least as $\Sigma\frac{1}{n^{*2}}$.

(4) We are particularly interested in the transmitted impulse:

$$\int_0^t F(t_1)dt_1\sim M\omega\left\{\frac{96\omega}{\pi^4}\int_0^t y(t_1)dt_1+\frac{32}{\pi^2}\sum_{n_k^*}\int_0^t\sin\left[\omega n_k^{*2}t_1\right]y'(t_1)dt_1\right\}.$$

Also here the series converges, at least, as $\Sigma\frac{1}{n^{*2}}$; more over $y'(t)$ and $\int_0^t y(t_1)dt_1$, respectively, can be obtained more accurately from records than $y''(t)$ and $y(t)$, respectively.

Example: For a contact force $F(t)=t$, we have the deflection:

$$y(t)=\frac{1}{M\omega}\sum_{n\ \text{odd}}\frac{1}{n^4\omega}\left\{t-\frac{1}{n^2\omega}\sin n^2\omega t\right\}.$$

Inserting this in our inversion formula, we get:

$$F(t)=\frac{96}{\pi^4}\cdot t\cdot\sum_{n\ \text{odd}}\frac{1}{n^4},$$

which equals t.

Here and There

New Appointments

Dr. Ivan A. Getting has been appointed associate professor in the department of electrical engineering of the Massachusetts Institute of Technology. During the war he was head of a division of the Radiation Laboratory at the Institute and directed research and development in the general field of the applications of radar to gunnery and associated problems.

Dr. Ira S. Bowen, professor of physics at the California Institute of Technology, has been appointed director of the Mount Wilson Observatory. He succeeds Dr. Walter S. Adams, who retired January 1, 1946, after serving as director since 1923.

Chester A. Snell, until recently associated with the Chemical Development Division, Aluminum Company of America, has joined the staff of Foster D. Snell, Inc., consulting chemists and engineers, Brooklyn, New York.

Paul D. Zottu of Newton Centre, Massachusetts, formerly chief engineer of Thermex Division, the Girdler Corporation, Louisville, Kentucky, has entered the field of consulting industrial electronic engineering.

The British Columbia Industrial and Scientific Research Council has announced the appointment of three physicists to its staff. Dr. S. E. Maddigan, formerly head of the Division of Physics and Electro-chemistry at the Chase Brass and Copper Company, has been appointed Director of the Council. Dr. A. C. Young, who was with the Physics Section of the National Research Council of Canada during the war, has been appointed head of the Council's Physics Division, and Dr. H. F. Batho, recently assistant professor of physics at the University of Manitoba, has been appointed Associate Research Physicist.

A. C. Menzies has been appointed Controller of Research and Development for the firm of Adam Hilger, Ltd., optical instrument makers of London.

Guggenheim Awards

Among the 36 recipients of fellowship awards announced in October by the John Simon Guggenheim Memorial Foundation were the following: Dr. Harold F. Blum, Principal Biophysicist, Naval Medical Research Institute, Bethesda, Maryland; Dr. Roy Overstreet, Assistant Soil Chemist, Division of Soils, University of California; Walter H. Pitts, staff member, Radiation Laboratory, Massachusetts Institute of Technology; Dr. Charles Kittel, Supervisor, Submarine Operations Research Group, U. S. Navy; Dr. Lindsay Helmholz, Assistant Professor of Chemistry, Dartmouth College.

National Research Council Fellowships

Science reports the announcement of the National Research Council that fellowships in mathematics, astronomy, physics, chemistry, geology, paleontology, physical geography, zoology, botany, agriculture, forestry, anthropology, and psychology will be available for the year 1946–1947. These fellowships are awarded as a rule to persons under 35 years of age who are citizens of the United States or Canada, and who have met all the requirements for the doctor's degree. Applications must be filed on or before December 31 on forms obtainable from the Secretary of the Fellowship Board in the Natural Sciences, National Research Council, 2101 Constitution Avenue, Washington 25, D. C. A handbook describing the fellowships (stipends, conditions, and tenure) will be furnished upon request.

Dr. Jeffries Honored

Dr. Zay Jeffries of the General Electric Company has been awarded the 1946 John Fritz Medal for "leadership in the solution of problems affecting the production, conservation, substitution, and scientific appraisal of metals and alloys."

Annual Meeting of A.S.H.V.E.

The Council of the American Society of Heating and Ventilating Engineers has announced that the fifty-second annual meeting of the Society will be held January 28–30 at the Hotel Commodore in New York City.

Activities at Polytechnic Institute of Brooklyn

A symposium on "The Application of Polymer Chemistry of Textile Fibers" was held at the Polytechnic Institute of Brooklyn on November 24 under the chairmanship of Dr. Milton Harris. A series of eight seminars on "Recent Progress in Biochemistry," beginning in November, 1945, is being held at the Institute during the current academic year, and a series of fifteen seminars on alternate Saturdays, also beginning in November, is dealing with the newest developments in the scientific investigation of the chemistry of high polymers and the recent practical applications of polymers in the plastics industry.

Material Handling Society Organized

In Pittsburgh on October 8 a group of men interested in material handling voted to form a Society. Objectives for the Society include: furthering the application of good material handling practices; encouragement of an interchange of ideas among the members; promotion of education and training in the science and practice of practical coordinated material handling; arranging for the collection and dissemination of information relating to all phases of material handling. Temporary Chairman is T. O. English, Aluminum Company of America. Temporary Secretary is Richard Rimbach of Materials Publishing Company. Further information may be obtained from Mr. Rimbach at 1117 Wolfendale Street, Pittsburgh 12, Pennsylvania.

Organization of Applied Spectroscopy Society

The Society for Applied Spectroscopy has been formed by a group of practicing spectroscopists working in the New York metropolitan area. Meetings are held the first Tuesday evening of each month and consist of either a

lecture by some prominent speaker or a symposium on a general topic. At its first two meetings the Society heard lectures by Dr. O. S. Duffendack of the North American Philips Company and Dr. G. H. Dieke of Johns Hopkins University. Among the topics to be covered in symposia at coming meetings are: types of excitation, types of equipment, measurement of radiant energy, absorption spectra, and spectroscopic nomenclature. Membership in the Society is open to anyone having an interest in applied spectroscopy. Those interested can obtain more information from the Secretary, Charles L. Guettel, Driver-Harris Company, Harrison, New Jersey.

Meeting of Optical Society

The winter meeting of the Optical Society of America will be held at the Hotel Statler in Cleveland, Ohio, on March 7–9, 1946.

Industrial Research Institute at Chattanooga

The Industrial Research Institute has been established at the University of Chattanooga "to provide the following contract services on a non-profit basis to Chattanooga, the South, and the Nation: research for industry; fundamental studies in pure and applied science; the training of scientists and skilled workers; the maintenance of an up-to-date science library with reference service." Director of the new Institute is Dr. Raymond B. Seymour.

Columbia University Honored for Atomic Research

Science reports the recent presentation by the War Department to Columbia University of a scroll in recognition of its contribution to research on the atomic bomb. It was accepted for the university by Dr. George Pegram, chairman of the University Committee on War Research and dean of the graduate faculties. Dr. Nicholas Murray Butler, president emeritus of the university, gave the closing address at the ceremony. He singled out for special commendation Dean Pegram; Dr. Harold Clayton Urey, professor of chemistry; Dr. Enrico Fermi, professor of physics; and Dr. John R. Dunning, professor of physics.

Technical Translations

The R. T. P.'s translations listed below are available from the Durand Reprinting Committee in care of California Institute of Technology, Pasadena 4, California.

These were selected for reprinting from the British Ministry of Aircraft Production R. T. P. List No. 123.

2503	*The Lorin Nozzle for Aircraft Propulsion* (Focke-Wulff Flugzeugbau. O.m.b.H. Bremen). (40 pages)
2506 Sedow, L. I.	*Planing on a Water Surface* (T.W.F. No. 4–5, 1940). (28 pages)
2507 E. L.	*Piezo-Electric Microphone of Small Dimensions* (Z.V.D.I. Vol. 87, No. 25/26, June 26, 1943, p. 406). (1 page)
2508 Heilbing, F.	*Development of the Weibel Welding Process for Aircraft Construction* (Junkers. Nachtrichten. Vol. 14, No. 7/8 July–Aug., 1943, pp. 53–59). (8 pages)
2511 Busemann, A.	*Laval Nozzles for Uniform Super-Sonic Flow* (Z.V.D.I. Vol. 84, No. 45, 9.11.40. pp. 857–862). (9 pages)
2516	*German De-Icing Technique* (Reports on development, devices, etc.). (8 pages)
2517 Fischer, H.	*The Role of Inhibitors in the Electrolytic Percipitation of Metals* (Part II–Part I, see R.T.P. Trans. 2213). (Kolloid-Zeitschrift, Vol. 106, No. 1—Jan, 1944, pp. 50–62). (16 pages)
2518 Zeerleder, A.	*Testing of Aluminum Castings* (Die Giesserei, 9.1.42. pp. 7–10). (6 pages)
2519 Poschl, Th.	*On the Increase of Stress in a Plate with Circular Holes and Under Tension* (5 pages)
2523 Roos, H.	*New Equipment of the Junkers Research Station* (Luftfahrtforschung. Vol. 13, No. 2, pp. 67–70, 20.2.1936). (7 pages)

New Booklets

Interchemical Review, summer issue, 1945, features an article on oriental lacquer work and a discussion of scientific research by Vannevar Bush. Published quarterly by the Research Laboratories of Interchemical Corporation, 432 West 45th Street, New York 19, New York.

North American Philips Company, 100 East 42nd Street, New York 17, New York, has issued a new 8-page booklet entitled *Fine Wire of Special Materials*. It brings the reader up to date on manufacturing methods and problems connected with wires 0.002" to 0.0007" diameter and smaller.

Crystal Research Laboratories, Inc., 29 Allyn Street, Hartford, Connecticut, has published a new catalog describing various types of crystals manufactured by the Laboratories, and their possible usages, both in the communication and industrial fields. 8 pages.

Industrial Research Institute, Inc., 60 East 42nd Street, New York 17, New York, has released for distribution outside the membership of the Institute a monograph on *Organization of Technical Research in Industry*. 16 pages. Copies may be obtained without charge from the Institute.

ELECTRON MICROSCOPE SOCIETY OF AMERICA

THE Electron Microscope Society of America held its third annual meeting November 30–December 1 at the Frick Chemical Laboratory of Princeton University. Over two hundred people attended. In addition to the announced program of papers, abstracts of which are printed below, the following papers were presented in discussion:

H. C. HICKLE AND H. S. DAVIDSON, *Imperial Paper and Color Corporation*, **Dispersion Methods**

S. F. KERN, *Celanese Corporation of America*, **Silica Replica Techniques Applied to Fibers**

N. DAVIDSON AND R. F. BAKER, *RCA Laboratories*, **Shadow Casting Technique in Electron Microscopy**

JAMES HILLIER, *RCA Laboratories*, **Further Improvements in the Resolving Power of the Electron Microscope**

The following officers were elected:

President, David Harker, General Electric Research Laboratory
Vice President, L. Marton, Stanford University
Secretary-Treasurer, John Turkevich, Princeton University
Director, James Hillier, RCA Laboratories
Director, Ralph W. G. Wyckoff, National Institute of Health

1. Formal Opening of Meeting. JAMES HILLIER, *President.*

2. Welcoming Remarks. HUGH S. TAYLOR, *Dean of Graduate School, Princeton University.*

3. A Brightness Meter for Use on Electron Microscopes. F. W. CUCKOW, *National Physical Laboratory, Teddington, Great Britain.* (Time: 10 min.)—High contrast plates are normally used on electron microscopes and a brightness meter was first used simply as an exposure meter to ensure consistent results. The "reduced beam angle" technique leads to improved picture sharpness and involves visual focusing at a high screen intensity followed by a slight reduction of objective lens current and then exposure at the lower intensity consequent on reduction of beam angle. It has been shown that this procedure can be reduced to a routine giving consistently good results provided that the high and low intensities are both set by reference to the brightness meter and that the objective lens current is reduced by a pre-determined amount.

4. Measurements on Image Distortion in the RCA Type EMU Microscope. ROBERT G. PICARD, *RCA Victor Division, Camden, New Jersey.* (Time: 15 min.)—A discussion of the lens system of the type EMU microscope. The magnification range and distortion studies and measurements throughout the range will be shown.

5. A Study of Distortion in Electron Microscope Projection Lenses. JAMES HILLIER, *RCA Laboratories, Princeton, New Jersey.* (Time: 15 min.)—The "first-order" theory of distortion in electron microscope projection lenses is presented and is shown to agree with experiment to within the experimental error. It is shown to be possible to obtain a high degree of correction of distortion by the proper combination of two electron lenses. An experimental double-gap pole-piece for a magnetic projection lens and the distortion patterns obtained with it are also described.

6. New Accessories for Electron Microscopes. PERRY C. SMITH, *RCA Victor Division, Camden, New Jersey.* (Time: 15 min.)—A new design of vacuum unit wherein various materials may be evaporated or sputtered; a new design of vacuum gauge wherein pressures from atmospheric to better than 10^{-4} mm Hg may be measured; an electron spray device for replenishing electrons to specific materials while under electron bombardment in diffraction studies; and a mechanical film spreader for frabricating films for supporting electron microscope specimens will be described.

7. The Preparation of Powdered Materials for Electron Microscopy. MARY C. SCHUSTER AND E. F. FULLAM,* *Interchemical Corporation, New York, New York.* (Time: 15 min.)—The basic problems involved in the preparation of powdered materials for electron microscopy are discussed, with special reference to effecting and maintaining an adequate dispersion of ultimate particles. Various tested methods are described for forming thin films of clear resins, and for mounting dispersed powders on these films. Procedures are also given for dispersing and mounting powders suspended in resin solutions. The properties and applications of various resins and solvents are described, and electron micrographs are shown of several types of mounts.

8. Specimen Mounting Techniques for Inorganic Chemicals. JAMES HILLIER, *RCA Laboratories, Princeton, New Jersey.* (Time: 15 min.)—The mounting of inorganic chemicals for observation in the electron microscope is discussed and a number of techniques are described.

9. A High Speed Microtome for the Electron Microscope, ERNEST F. FULLAM* AND ALBERT E. GESSLER, *Interchemical Corporation, New York.* (Time: 20 min.)—Recognizing the need of a relatively simple method for making thin cross sections suitable for the electron microscope, a high speed microtome was designed after the one built by O'Brien and McKinley. The knife, a piece of razor blade mounted on a wheel rotating at 57,000 r.p.m. moves at speeds up to 1100 feet per second. It is able to make cross sections from (0.1 to 1 micron thick) suitable for stereoscopic electron micrographs of animal tissue, rubber, rayon, Lucite, Nylon, and other materials. A number of sectioning techniques were developed for use with the instrument. One of these employed the use of volatile solid embedding material and their eutectic mixtures to support the sample while being cut and the sections during their collection. Such materials have the advantage that they require no solvent extraction from

* At present at General Electric Company, Schenectady, New York.

the sections with the resulting solvent removal difficulties. A number of cross sections of different materials are shown indicating the possibilities of the apparatus in many fields.

10. The Form of Particles of Nickel Produced by the Carbonyl Process. F. W. CUCKOW, *National Physical Laboratory, Teddington, Middlesex, Great Britain.* (Time: 10 min.)—Electron microscopical examination of (carbonyl) nickel powders consisting of particles a few microns in diameter has revealed two types of powder consisting respectively of (a) a mixture of irregularly shaped and cube shaped particles, each with rough surfaces, and (b) characteristically shaped particles with smooth surfaces. The form of the smooth surfaced particles could not be determined until evidence from the electron microscope was combined with evidence from the light microscope. It was then inferred that the smooth surfaced particles were single crystals in the form of icositetrahedra, probable indices of faces (544).

11. Metal Shadowing of Preparations for Electron Micrography. ROBLEY C. WILLIAMS AND RALPH W. G. WYCKOFF, *University of Michigan, Ann Arbor, Michigan.* (Time: 20 min.)—A technique is described for preparing objects for electron micrography by depositing obliquely onto them a thin film of metal. This procedure, which can be thought of as a form of surface staining, makes evident many details that cannot otherwise be clearly seen and also gives the resulting micrographs a definite three-dimensional quality. Examples will be shown of photographs of such "shadowed" objects as purified viruses and other particles of macromolecular dimensions, replicas of such particles and replicas of surfaces of glass, crystals, and preparations of metallographic interest.

12. A Shadow-Casting Adapter for the Electron Microscope. THOMAS F. ANDERSON, *Johnson Foundation, University of Pennsylvania, Philadelphia, Pennsylvania.* (Time: 10 min.)—A device fitting on the specimen chamber door seat is described which permits the evaporation of metal onto the specimen in the high vacuum of the electron microscope itself. The specimen can be observed during the shadow-casting process to insure that proper thicknesses of metal are obtained. Results are illustrated with bacteria and bacterial viruses.

13. Metal Shadowing with Virus. D. GORDON SHARP, *School of Medicine, Duke University, Durham, North Carolina.* (Time: 15 min.)—Electron pictures showing marked three-dimensional properties have been obtained with virus by the method of metal shadowing.[1] Metal molecules deposited in vacuum by evaporation on the surface of electron microscope preparations are made to cast shadows of the virus particles. These preparations are then photographed in the electron microscope by transmitted electrons in the usual way. Examples of the work done in this way will be shown together with conventional electron micrographs of the same materials.

[1] R. C. Williams and R. W. G. Wyckoff, Proc. Soc. Exp. Biol. and Med. **58**, 265 (1945).

14. Report of the Committee on Resolving Power. (Time: 45 min.)

15. Recent Developments in the Field of Electron Microscopy (Invited paper). RALPH W. G. WYCKOFF, *National Institute of Health, Bethesda, Maryland.*

16. A Study of Oxide Films Formed on Metals and Alloys by Electron Microscopy and Diffraction. R. T. PHELPS AND EARL A. GULBRANSEN, *Westinghouse Research Laboratories, Pittsburgh, Pennsylvania.* (Time: 20 min.)—Highly polished samples of metals and alloys are oxidized at controlled conditions of temperature and time in a furnace attached to a diffraction camera. Diffraction patterns by the reflection technique are obtained on the samples before and after oxidation at the temperature of oxidation, also at room temperature after cooling. The thin oxide films, 100 to 400A thick, are stripped from the oxidized metal by chemical or electrochemical means for examination by transmission electron microscopy and diffraction. Electron micrographs reveal the following information concerning the oxide film: (1) particle size, (2) particle size distribution, (3) particle shape, (4) uniformity of film thickness, and (5) type of micrograph. Diffraction patterns are used to identify the composition of the films and to indicate approximate particle sizes. Complete agreement between reflection and transmission diffraction patterns is not expected in the films containing more than one metal or more than one oxidation state of a metal. Inherently the two methods sample the film differently.

17. An Electron Diffraction Study of Oxide Film Formation on Metals and Alloys. EARL A. GULBRANSEN AND J. W. HICKMAN, *Westinghouse Research Laboratories, East Pittsburgh, Pennsylvania.* (Time: 20 min.)—The reflection method is applied to the study of the oxidation reaction of metals with air or oxygen atmospheres. The experiments are carried out "in situ" over the temperature range of 200 to 700°C and over a wide time range. Existence charts of the oxides formed are plotted as a function of time and temperature of the oxidation reaction. These charts are used to correlate the structure with the protective nature of the oxide film. The factors influencing the formation of a particular oxide are briefly discussed.

18. Investigation of Etched Metallic Surfaces by Electron Diffraction and the Electron Microscope. R. D. HEIDENREICH,* L. STURKEY AND H. L. WOODS, *The Dow Chemical Company, Midland, Michigan.* (Time: 20 min.)—A method of rinsing metal surfaces immediately after etching is described which produces surfaces that are "clean" as far as electron diffraction is concerned. Examples of the method are presented including magnesium alloys, steel and copper alloys. The combined technique of electron microscopy and electron diffraction proves to be very sensitive to minute amounts of secondary phases and

* Now at Bell Telephone Laboratories, Inc., Murray Hill, New Jersey.

impurities in etched metals. The decomposition of martensite at 200°C is shown to produce a colloidal mixture the slow etching component of which is Fe_3N. At 400°C the slow etching component is the usual Fe_3C. The nitride formed at 200°C can be converted to the carbide by further heating at 350°C. The position of these results relative to the earlier x-ray diffraction work is discussed. In the case of an aluminum-copper alloy, the usual etchants are not satisfactory due to the re-deposition of the copper on the etched surface as polycrystalline metal. Pure aluminum can be etched to produce clean surfaces. Difficulty with small amounts of impurities in copper alloys is illustrated by β-brass containing 0.0005–0.001 percent Ag. When etched in an acetic-nitric acid reagent, the silver impurity is dissolved and then precipitated onto the etched surface in the form of spherical particles about 1000A in diameter. Electron micrographs and electron diffraction reflection patterns for beryllium copper are shown although a systematic study of this system has not been completed. The possibilities for research on metals using these techniques are discussed not only from the standpoint of metallurgical structures but from that of studying the formation of surface films in various atmospheres.

19. The Application of the Electron Microscope to the Study of Metals (Invited Paper). DAVID HARKER, *Research Laboratory, General Electric Company, Schenectady, New York.* (Time: 60 min.)

20. An Application of the Electron Microscope to the Study of Animal Cells (Invited Paper). KEITH R. PORTER, *The Rockefeller Institute for Medical Research, New York, New York.* (Time: 60 min.)

21. Micrographs of Insect Wings. E. F. BURTON, *Department of Physics, University of Toronto, Toronto, Ontario, Canada.* (Time: 10 min.)

22. An Investigation of Transverse Striations and Myosin Filaments in Muscle. C. E. HALL, M. A. JAKUS AND F. O. SCHMITT, *Massachusetts Institute of Technology, Cambridge, Massachusetts.* (Time: 20 min.)—Electron microscope specimens of striated muscle were obtained by fragmenting fixed muscles in a blender. This treatment tends to split the fibre bundles into their constituent fibrils (myofibrils) along natural cleavage boundaries. Electron microscope examination of such fibrils permits a more detailed description of the transverse striations previously observed with the light microscope and provides additional information on other structures below light microscope resolution. The fibrils consist chiefly of parallel myosin filaments ranging in width from 50 to 250A. The filaments extend continuously through the anisotropic and isotropic bands and pursue a straight course in both extended and contracted states. Electron micrographs were also made of myosin filaments obtained by extracting fresh muscle in weakly alkaline salt solutions after the method of Edsall. Statistical measurements were made of lengths and widths of filaments from rabbit, frog, lobster, scallop, and clam. Lengths vary from 500 to 20,000A and show significant variations from one animal form to the next. Widths range from 50 to 250A and show relatively little variation between forms.

23. The Structure of the Trichocysts of Paramecium. MARIE A. JAKUS, *Massachusetts Institute of Technology, Cambridge, Massachusetts.* (Time: 15 min.)—The minute size of trichocysts makes them a suitable object for electron microscope investigation. Extruded trichocysts can be readily obtained by stimulating electrically a natant paramecium on an electron microscope specimen grid. Each trichocyst is found to consist of a dense pointed tip and an elongated shaft which appears cross-striated in electron micrographs. It is suggested that the shaft consists chiefly of thin cylindrical membrane formed by the close packing of longitudinal fibrils, in phase with respect to a periodic axial pattern. The structure and chemical properties of this membrane are discussed.

24. Electron Microscope Studies of the Structure of Chloroplasts, Chromoplasts, Leucoplasts Showing their Relationship to "Cellulose Particles," Carotin "Crystals" and Colloidal Carbon. EDITH A. ROBERTS, *Vassar College, Poughkeepsie, New York.* (Time: 10 min.)—The photographs taken with the electron microscope would indicate that the granules of which the chloroplasts, chromoplasts, and leucoplasts are composed are the same as the "cellulose particles" of which cell walls are built, the bodies of which carotin "crystals" are composed and the same as those found in colloidal carbon. All these granules are made up of similar primary (0.5 μ); secondary (0.25 μ); tertiary (0.15 μ); quarternary (0.05 μ); quintary (0.02 μ); and senary (0.01 μ) units.

25. Electron Microscope Studies of the Structure of Starch, Showing its Relationship to Plastid Structure. MILDRED D. SOUTHWICK, *Vassar College, Poughkeepsie, New York.* (Time: 10 min.)—Studies are made of the structural organization of starch grains from several genera of plants using the electron microscope. These starch grains are taken from varied storage organs—seed, fruit, root, or tuber. The structure of the starch grain is compared with that of the chloroplast and the starch bodies which appear in the chloroplasts of the same plant.